Finanziato dall'Unione europea NextGenerationEU | Ministero dell'Università e della Ricerca | Italiadomani PIANO NAZIONALE DI RIPRESA E RESILIENZA

multi-Risk sciEnce for resilienT commUnities undeR a changiNgclimate

Codice progetto MUR: **PE00000005** – CUP Lead Partner: F83C22001180002

Deliverable title: Report on habitat vulnerabilities

Deliverable ID: DV 4.2.3

Due date: 15/02/2026

Submission date: 27/01/2026

AUTHORS

Andrea Bottacin-Busolin (UNIPD), Federica Paola Cassetti (UNIPA), Giovanna Cilluffo (UNIPA), Laura Drago (UNIPD), Marta Greco (UNIPA), Andrea Marion (UNIPD), Sara Pacchini (UNIPD), Gianfranco Santovito (UNIPD), Gabriele Rizzuto (UNIPA), Geraldina Signa (UNIPA), Agostino Tomasello (UNIPA), Cecilia D. Tramati (UNIPA), Salvatrice Vizzini (UNIPA)

1 Technical references

Project Acronym	RETURN
Project Title	multi-Risk sciEnce for resilienT commUnities undeR a changiNg climate
Project Coordinator	Domenico Calcaterra UNIVERSITA DEGLI STUDI DI NAPOLI FEDERICO II domcalca@unina.it
Project Duration	December 2022 – November 2025 (36 months)

Deliverable No.	DV 4.2.3
Dissemination level*	CO
Work Package	WP 4.2 – Setting the scene on environmental degradation stressors in terrestrial and marine environment
Task	T 4.2.3 - Habitats vulnerabilities, resilience and adaptation of valuable ecosystems to environmental degradation and potential socio-economic relevance. Identification of hot spot, relevant emerging pollutant and stressors
Lead beneficiary	UNIPA
Contributing beneficiary/ies	UNIPD

* PU = Public

PP = Restricted to other programme participants (including the Commission Services)

RE = Restricted to a group specified by the consortium (including the Commission Services)

CO = Confidential, only for members of the consortium (including the Commission Services)

1.1 Document history

Version	Date	Lead contributor	Description
0.1	27/01/2025	Salvatrice Vizzini (UNIPA)	Final version

2 ABSTRACT

Habitat vulnerability refers to the risk of degradation of critical ecosystems due to external pressures (Gauthier, 2013). Climate change is a major driver of habitat vulnerability, as it alters key physical and biological processes through rising sea temperature and the increasing frequency of extreme weather events.

Among marine habitats, seagrass meadows play a fundamental ecological role by providing essential ecosystem services, including carbon sequestration, sediment stabilization, coastal protection, and nursery habitats. Nevertheless, significant declines have been reported, particularly in areas characterized by elevated temperature and salinity (Stipcich et al., 2022; Litsi-Mizan, 2023). Understanding seagrass vulnerability is therefore crucial for anticipating ecological shifts and supporting effective conservation and management strategies. The first research section focused on *Posidonia oceanica*, a seagrass species endemic to the Mediterranean Sea, investigating the individual and combined effects of increased temperature and salinity on plant performance. A mesocosm experiment was conducted using plants collected inside and outside a lagoon-like coastal basin (Stagnone di Marsala, western Sicily), a climate change hotspot due to its shallowness and limited water exchange with the open sea. Results showed that combined stressors significantly reduced photosynthetic efficiency, pigment content, and phenolic compounds. Plants originating from the lagoon exhibited partial adaptive responses, suggesting a certain degree of resilience, although growth was consistently reduced under combined stress conditions. In addition to experimental work, we investigated *P. oceanica* barrier reefs, long-lived biogenic structures formed by the accretion of matte in very shallow environments. Three reefs located in Sicily (Maragani, Solanto, and Marsala) were analysed using radiocarbon dating, $\delta^{13}C$ signatures, and lepidochronology. These structures developed over centuries (approximately 600–1200 years), with site-specific growth histories and carbon dynamics shaped by local environmental conditions. Older and more sheltered reefs showed divergent sedimentation rates and growth trajectories, challenging the assumption that reef age alone predicts vitality. In contrast, the younger and more exposed Marsala reef displayed steadier growth and productivity, suggesting lower vulnerability to current climatic stressors. Furthermore, the discovery of stranded matte blocks along the southern Sicilian coast suggests that extreme storm events can cause collective uprooting from shallow depths (Tomasello et al., 2025), highlighting the increasing vulnerability of these ecosystems under future climate change scenarios.

Freshwater habitats are of great ecological importance due to their strong interactions with terrestrial ecosystems, but they are also the aquatic environments most directly exposed to anthropogenic pollution, with severe consequences for biodiversity. Our research focused on contaminants of emerging concern, particularly per- and polyfluoroalkyl substances (PFAS), synthetic surfactants produced since the 1950s (Baran, 2001). PFAS are characterized by a partially or totally fluorinated aliphatic chain (–CnF2n+1–) and a functional group, typically carboxylic or sulfonic, whose structural variability has promoted widespread industrial use and uncontrolled environmental release (Buck et al., 2011). We investigated the effects of chronic PFAS exposure on freshwater fish fauna using the common chub (*Squalius cephalus*), a generalist species with high ecological plasticity (Balestrieri et al., 2006) and a valuable bioindicator of aquatic ecosystem vulnerability (Nyeste et al., 2019). The study was conducted in rivers of the Veneto region (Italy), one of the most emblematic PFAS contamination hotspots in Europe, affected since 1964 by emissions from a fluorochemical plant and extending over approximately 190 km² across the provinces of Vicenza, Padua, and Verona (Pitter et al., 2020). Physiological responses to chronic PFAS exposure were analysed in the liver and kidney, primary targets for PFAS accumulation and detoxification (Cui et al., 2009; Butenhoff et al., 2004). We focused on the antioxidant defence system, as PFAS exposure increases reactive oxygen species (ROS) production, leading to oxidative stress and macromolecular damage (Bonato et al., 2020; Juan et al., 2021). Gene characterization and expression analyses revealed the activation of multiple antioxidant pathways. Glutathione peroxidase (GPx) emerged as a first-line defence, catalase (CAT) activity increased under higher oxidative stress, and the down-regulation of peroxiredoxin 4 (Prdx4) appeared to promote lipid accumulation and cellular protection (Solé et al., 2021; Piva et al., 2022; Pacchini et al., 2025). Complementary experiments on the Louisiana crawfish (*Procambarus clarkii*) exposed to GenX showed oxidative protein damage only at the highest concentration tested, while lower doses were counteracted by GPx up-regulation. Overall, these results indicate that tolerance to PFAS-induced stress may favour invasive or resilient species, potentially increasing the vulnerability of native freshwater communities and leading to broader ecological imbalances.

3 Table of contents

3.1 List of Tables

3.2 List of Figures

Structure of the Deliverable

This deliverable is organised to provide a comprehensive assessment of habitat vulnerabilities across both marine and freshwater ecosystems. Following the technical references and methodological framework, the document is structured into two main sections. Section 4 examines marine coastal habitats, with a focus on the responses of *Posidonia oceanica* to climate-driven stressors and the long-term stability of biogenic barrier reefs. Section 5 addresses freshwater ecosystems, evaluating the effects of emerging contaminants - particularly PFAS - on physiological, molecular, and biochemical responses in selected indicator species, *Squalius cephalus* and *Procambarus clarkii*. All chapters included in both sections include an introduction, detailed methodological descriptions, results, and discussion.

4 Marine coastal habitat vulnerability

4.1 *Posidonia oceanica* vulnerability to increasing temperature and salinity

Vulnerability describes the degree to which an ecosystem is susceptible to, and unable to cope with, adverse effects of environmental change (IPCC, 2019). It reflects the combined influence of a system's exposure, sensitivity, and adaptive capacity, determining how ecological functions respond to climatic and anthropogenic stressors. As global temperatures rise and extreme events intensify, many ecosystems face accelerated degradation, with cascading effects on biodiversity, productivity, and the provision of essential services. Marine ecosystems are particularly at risk, given their direct dependence on stable physical and chemical conditions (Guo et al. 2022; Tittensor et al. 2021). Seagrasses are among the marine ecosystems at the highest risk. Despite their vulnerability, they play a crucial role in supporting biodiversity, stabilizing sediments, and storing large amounts of carbon, often exceeding terrestrial forests (Duarte et al. 2025; Krause et al. 2025). Among seagrass ecosystems, the Mediterranean *Posidonia oceanica* meadows stand out as both vital and vulnerable: they can store up to 4,100 tons of CO_2 per hectare (IUCN, 2021), yet extreme climatic events can rapidly erode centuries of accumulated growth, leading to sudden and catastrophic losses in shallow areas (Gera et al., 2014; Tomasello et al., 2025). Furthermore, marine heatwaves and hyperosmotic stress can impair photosynthesis and trigger shoot mortality (Rinaldi et al., 2023; Blanco-Murillo et al., 2024), underscoring the fragility of these ecosystems in a changing Mediterranean Sea

4.1.1 Introduction

In the Mediterranean, *Posidonia oceanica* is a keystone seagrass species facing severe decline (Marbà et al. 2014; Pergent-Martini et al. 2022). Endemic to this semi-enclosed sea, it thrives only within narrow thermal and salinity ranges but is highly sensitive to extreme events such as marine heatwaves and hyperosmotic conditions, which impair photosynthesis and can trigger shoot mortality (Rinaldi et al. 2023; Blanco-Murillo et al. 2024). While many aspects of its response to environmental change have been studied, little is known about the combined effects of heat and salinity stress. To address this gap, two populations of *P. oceanica* from contrasting sites in the Stagnone di Marsala lagoon (Sicily, Italy) were tested under controlled mesocosm conditions, examining their resistance to simultaneous thermal and osmotic stress.

4.1.2 Materials and methods

Posidonia oceanica shoots were collected from two contrasting habitats within the Stagnone di Marsala lagoon (Sicily, Italy): the inner lagoon, characterized by extreme summer conditions (temperatures up to 30 °C and salinity up to 48 PSU), and the open sea, where environmental conditions are more stable (Figure 4.1.2.1). The samples were transferred to the laboratory on 29 April 2024 and placed in six 250 L experimental tanks (Figure 4.1.2.12). Each tank was equipped with a self-pump system including mechanical filters, rocks, and a circulation pump to ensure continuous water movement. Two color-coded baskets were placed in each tank to distinguish plant origin (pink = Lagoon; blue = Open). Twelve shoots were placed in each basket, resulting in a total of 144 shoots (12 shoots × 2 baskets × 6 tanks). The room temperature was maintained at 16 °C via air conditioning, and a 10-hour light cycle (10:00 – 22:00) provided consistent illumination.

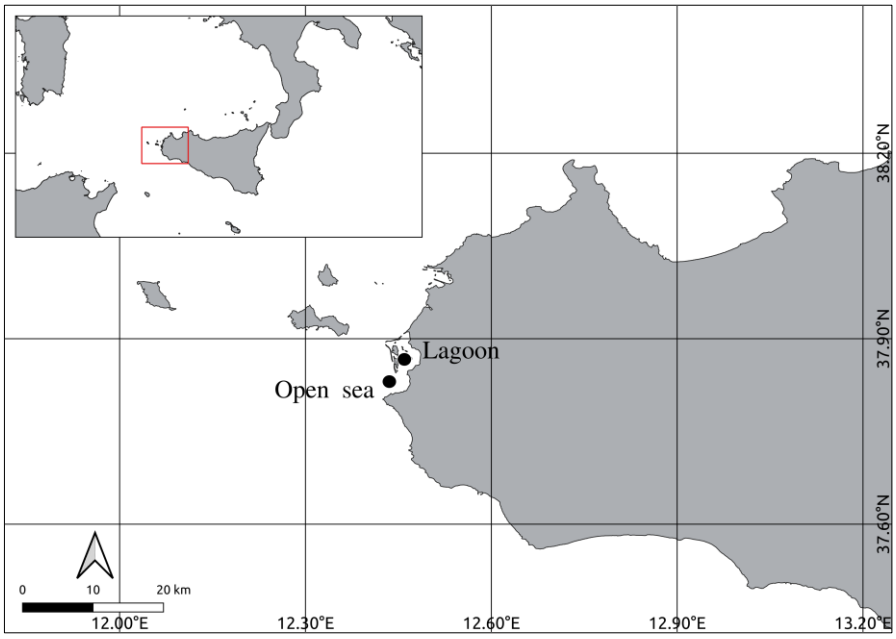

Figure 4.1.2.1 Map of Sicily showing the two sampling sites: inside of the Lagoon and in the Open sea.

All tanks were maintained for one month under stable acclimation conditions (~20 °C, 38 PSU). Temperature and salinity were measured daily with a Hanna Instruments probe. Artificial marine salt dissolved in tap water was used to recreate seawater conditions. After acclimation, a fully orthogonal experimental design was implemented with two temperature treatments (20 and 30 °C) and three salinity levels (38, 42, 48 PSU) (Figure 4.1.2.1). Temperature was increased stepwise by 2 °C per day using two thermostats per tank, while salinity was raised by 1–1.5 PSU per day, ensuring all tanks reached their final conditions simultaneously. Shoots were then maintained under treatment for 22 days.

Physiological and biochemical responses were measured at the start of the experiment (T_0) and after 15 and 22 days of exposure. Photosynthetic efficiency was assessed through maximum quantum yield of PSII (Fv/Fm) using a DIVING-PAM fluorometer (WALZ). Measurements were taken on the same four dark-adapted leaves and again after three hours of light exposure. Leaf selection followed established guidelines, preferentially using the second or third leaf of each shoot, or alternatively a young green leaf >5 cm (Ruocco et al., 2019; Nguyen et al., 2021). Measurements were taken 3–4 cm above the leaf meristem (Marín-Guirao et al., 2011; Mancuso et al., 2023). PAM fluorometry allowed non-destructive evaluation of photosystem II performance under differing thermal and osmotic conditions.

Leaf growth rates were determined following the Zieman (1974) punching technique. At the beginning of the experiment, eight shoots per treatment (four per site) were labelled and pierced. After 22 days, the distance between the punch mark and the leaf base was measured and divided by the elapsed time to calculate daily growth rates.

Biochemical stress markers - phenols, chlorophyll-a, and carotenoids - were quantified from four leaf samples for each basket collected at each time point. After PAM measurements, leaves were marked, stored at −80 °C, and subsequently lyophilized and ground for analysis. TPC was assessed using protocols modified from Harrison and Durance (1989) and Bolser et al. (1998). Chlorophyll-a and carotenoid concentrations were determined using a spectrophotometric procedure adapted from Lichtenthaler (1987). For Fv/Fm and biochemical markers, changes relative to baseline (i.e., time zero under standard conditions) were calculated as $\Delta X = X_t - X_{t0}$.

Statistical differences were evaluated by comparing values at 15 and 22 experimental days directly against their corresponding baseline (day 0) using multiple pairwise t-tests, with the significance threshold set at α

≤ 0.05. For growth rate, statistical differences were evaluated by comparing values among treatments within each experimental day by Dunn test, as growth could not be expressed as a variation relative to the baseline.

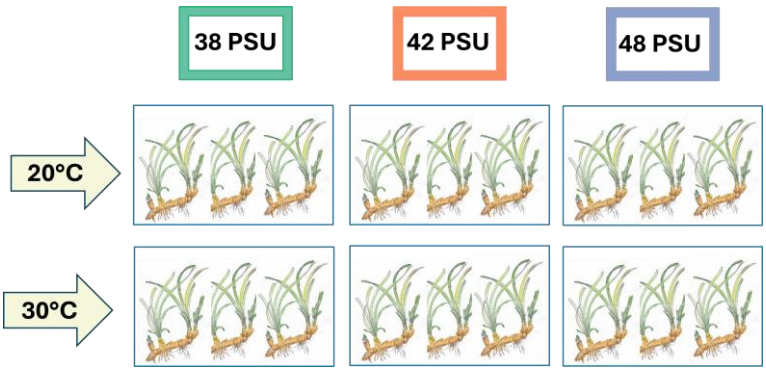

Figure 4.1.2.2 Experimental design with two temperature levels (20 and 30 °C) and three salinity levels (38, 42 and 48 PSU).

4.1.3 Results

The maximum quantum yield of PSII (Fv/Fm) showed contrasting responses between shoots collected at the two sites (**Errore. L'origine riferimento non è stata trovata.**1). Statistical differences were evaluated by comparing Fv/Fm values at 15 and 22 experimental days against their corresponding baseline (day 0) for each temperature–salinity combination, allowing the detection of treatment-induced deviations. In open-area shoots, high temperature (30 °C) caused significant reductions in Fv/Fm relative to baseline at both 15 and 22 days (**Errore. L'origine riferimento non è stata trovata.**1). During the 15 days, moderately elevated salinity appeared to compound thermal stress, suggesting an initial stress response. However, this pattern changed by day 22: Fv/Fm values showed their strongest decline at low salinity (38 PSU), while at higher salinities the response flattened, with no substantial deviation from baseline, suggesting a compensatory response.

Lagoon shoots displayed a different trend (**Errore. L'origine riferimento non è stata trovata.**1). Thermal stress induced significant declines in Fv/Fm only at 20 °C and 42 PSU, but their response to salinity varied over time. After 22 days, however, lagoon plants exhibited evident acclimation at intermediate-to-high salinity (38–42 PSU), consistent with a greater inherent tolerance to osmotic variability in populations originating from highly fluctuating environments.

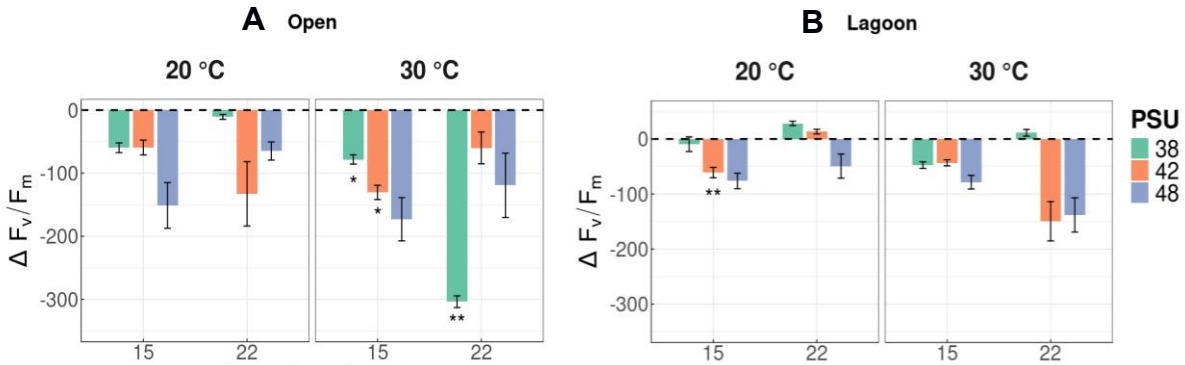

Figure 4.1.3.1 Delta variation of the maximum quantum yield of PSII (F_V/F_m) in shoots collected from the Open sea (A) and inside the Lagoon (B), under combined heat (20 and 30°C) and hypersalinity (38, 42, 48 PSU) treatments at 15 and 22 days, compared to 0 days. Dashed line indicates no change. Asterisks indicate significance levels of t-test pairwise comparisons: *p < 0.05, **p < 0.01, ***p < 0.001

Growth responses reflected also site-specific differences (**Errore. L'origine riferimento non è stata trovata.**2). Open sea shoots maintained stable growth across treatments, while lagoon shoots showed significant growth reductions under high salinity, when combined with elevated temperature.

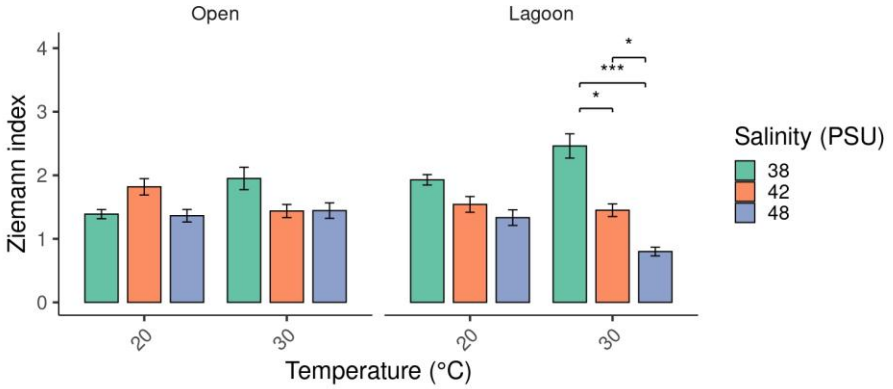

Figure 4.1.3.2 Leaf elongation (cm) measured by Ziemann punching method at 0 and 22 experimental days under combined heat (20 and 30°C) and hypersalinity (38, 42, 48 PSU) treatments. Asterisks indicate significance levels of multiple comparisons by Dunn test: *p < 0.05, **p < 0.01, ***p < 0.001.

Biochemical responses further highlighted differences in stress sensitivity (**Errore. L'origine riferimento non è stata trovata.**3). In open-area shoots, total phenolic content showed a significant decline only under the most extreme conditions (30 °C and 48 PSU), when values at 15 and 22 days were compared to the baseline at day 0. This reduction indicates a weakening of metabolic defences under dual thermal and hypersaline stress. In contrast, lagoon shoots exhibited no significant departures from baseline across treatments, suggesting a more stable antioxidant profile. Notably, unlike other measured variables, lagoon plants showed positive TPC variations in several cases, indicating that phenolic production may even be upregulated under certain stress combinations

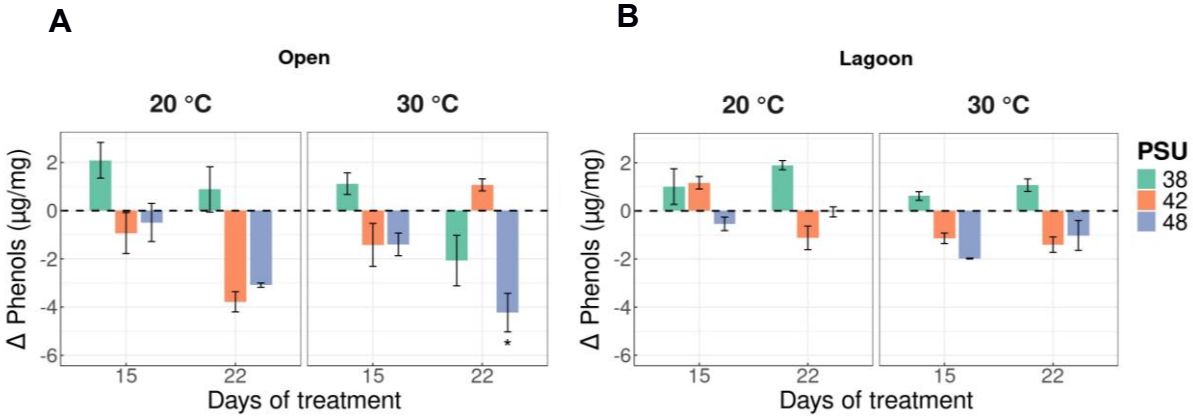

Figure 4.1.3.3 Delta variation of the total phenolic content of shoots collected from Open sea (A) and inside the Lagoon (B), under combined heat (20 and 30°C) and hypersalinity (38, 42, 48 PSU) treatments at 15 and 22 days, compared to 0 days. Dashed line indicates no change. Asterisks indicate significance levels of t-test pairwise comparisons: *p < 0.05, **p < 0.01, ***p < 0.001

As for carotenoid concentration in leaves, open-area shoots showed low and relatively stable variations at 20 °C, whereas pronounced negative variations emerged under the combined effects of high temperature and hypersalinity. In particular, at 30 °C and 48 PSU, carotenoid levels decreased markedly at both 15 and 22 days when compared to baseline (**Errore. L'origine riferimento non è stata trovata.**).

Lagoon shoots displayed a different pattern. At 30 °C, negative variations occurred primarily at higher salinities (42–48 PSU), whereas moderate salinity increases resulted in smaller changes. Overall, lagoon plants showed consistent declines relative to their baseline across all treatment combinations, including those conducted under standard experimental conditions (20 °C, 38 PSU), likely reflecting acclimation costs or carry-over stress.

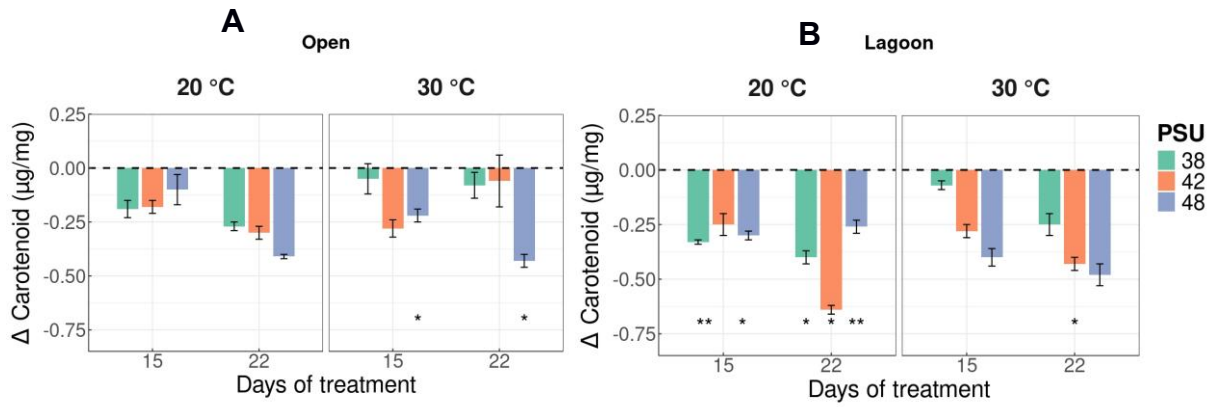

Figure 4.1.3.4 Delta variation of the total carotenoid content of shoots collected from Open sea (A) and inside the Lagoon (B), under combined heat (20 and 30°C) and hypersalinity (38, 42, 48 PSU) treatments at 15 and 22 days, compared to 0 days. Dashed line indicates no change. Asterisks indicate significance levels of t-test pairwise comparisons: *p < 0.05, **p < 0.01, ***p < 0.001

4.1.4 Discussion

This study confirmed that *Posidonia oceanica* is highly vulnerable to the combined effects of rising temperature and salinity, stressors that are becoming increasingly frequent in the Mediterranean Sea under climate change. The mesocosm experiment demonstrated clear impacts on photosynthetic performance, growth, and biochemical stress markers, highlighting the multifaceted nature of plant vulnerability. Elevated temperature consistently reduced photosynthetic efficiency, while hypersaline conditions amplified this decline. The combined stress led to significant impairments, with open-area shoots showing the steepest reductions.

Photosynthetic efficiency (F_v/F_m) showed contrasting responses between sites. Lagoon-origin plants partially recovered F_v/F_m at high salinity, indicating some acclimation to fluctuating conditions, whereas open sea shoots experienced sharp declines under combined heat and salinity stress, reflecting narrower plasticity (Marín-Guirao et al., 2016).

Growth was particularly sensitive in lagoon plants, where combined heat and hypersalinity suppressed leaf elongation, suggesting that maintaining photosynthetic performance may come at the expense of structural development, whereas open sea shoots maintained growth even under stress (Campbell & Fourqurean, 2014).

Total phenolic content, a proxy for antioxidant capacity, remained relatively stable in lagoon plants but declined in open-area shoots under the most extreme stress (30 °C and 48 PSU), indicating a loss of metabolic resilience (Dumay et al. 2004). Carotenoid concentrations declined consistently in lagoon plants,

even under control conditions, likely reflecting acclimation costs, whereas open sea shoots only showed pronounced decreases under combined heat and hypersalinity, highlighting their lower tolerance to simultaneous stressors (Marín-Guirao et al. 2013; Stipcich et al. 2025).

Overall, prior exposure to fluctuating lagoon conditions appears to confer partial stress resistance, maintaining photosynthesis and antioxidant capacity, but at a cost to carotenoids and growth. Open-area plants maintain growth under moderate stress but are less resilient under extreme conditions, with marked declines in photosynthesis, phenols, and carotenoids.

Taken together, these findings provide important insights into the *P. oceanica* vulnerability to high salinity and temperatures. While populations exposed to naturally variable environments may be better prepared to face future climate extremes, this resilience is accompanied by costs that may limit their long-term persistence. Conversely, plants from stable habitats may perform well under average conditions but collapse under compounding stressors. The dual picture underscores the urgency of protecting resistant populations while mitigating direct anthropogenic pressures, as the survival of *P. oceanica* meadows - and the ecosystem services they provide - will depend on both intrinsic resistance and effective management strategies in the face of accelerating climate change.

4.2 *Posidonia oceanica* barrier reef vulnerability to extreme storm events

4.2.1 Introduction

In the Mediterranean Sea, *Posidonia oceanica* forms biogenic barrier reefs, massive matte structures composed of rhizomes, roots, and trapped sediments, that can persist for millennia, shaping coastal geomorphology and storing blue carbon (Lo Iacono et al. 2008; Monnier et al. 2021). These barrier reefs are among the most complex and ecologically valuable coastal bioconstructions, functioning as long-term carbon sinks, sediment stabilizers, and natural breakwaters (Mateo et al. 2006; Boudouresque et al. 2016). Built over centuries through the vertical accretion of biogenic matte, these structures represent “natural monuments” of high conservation significance (Pergent et al. 2014; Tomasello et al. 2020). Yet, their persistence is increasingly jeopardized by the intensification of storm events driven by climate change (IPCC 2019; Oprandi et al. 2020), which may undermine the physical integrity of these shallow meadows. In this context, we report, in our recently published study, the first large-scale discovery of stranded *P. oceanica* matte blocks - forming a veritable seagrass “cemetery” - along the southern Sicilian coast at Scala dei Turchi, providing novel insights into the origin, vulnerability, and biological interactions of *P. oceanica* barrier reefs.

4.2.2 Materials and methods

The study combined field surveys, morphometric and density analyses, UAV-based photogrammetry, and hydrodynamic reconstructions to trace the provenance and detachment mechanisms of the stranded matte. The study was conducted along the Scala dei Turchi pocket beach, a Site of Community Importance (SIC ITA040015) on the southern coast of Sicily (Italy). The area is characterized by marl and limestone cliffs of the Trubi Formation and hosts an extensive *P. oceanica* barrier reef growing on rocky substrate near the shoreline (Figure 4.2.2.1).

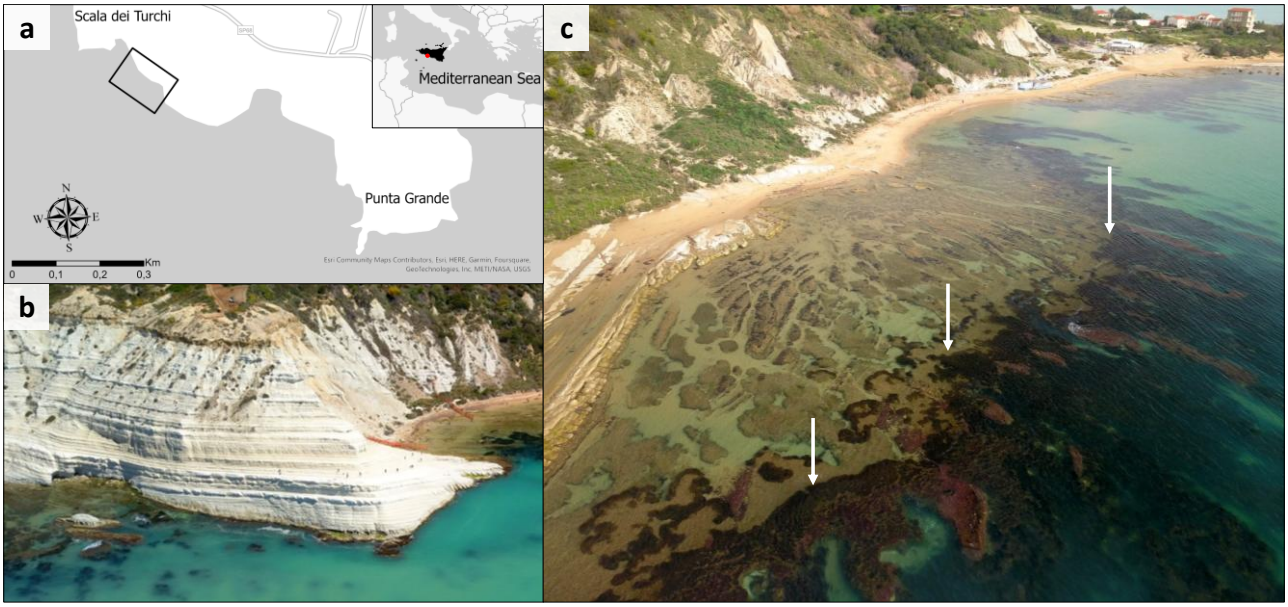

Figure 4.2.2.1 Study area on the southern coast of southern Sicily (Scala dei Turchi), showing the location of the *Posidonia oceanica* barrier reef and surrounding geomorphology b) Rocky ridge consisting of the Trubi Formation at Scala dei Turchi; c) *Posidonia oceanica* barrier reef marked by arrows. (ph A. Savona).

Stranded matte blocks were discovered in November 2018 (one upside-down block used for root morphology analysis) and again in November 2019 (five blocks, mostly stranded with leaf bundles facing upwards).

Shoot density was measured in triplicate or duplicate on four of the five 2019 blocks using 40 cm × 40 cm or 17 cm × 17 cm quadrats. The theoretical bathymetric origin (depth x in meters) was then inferred from the shoot density (y in shoots m−2) using the established model: x = exp ((y − 1045.8)/254). The five 2019 blocks were subjected to morphometry by assimilating their shapes to regular polyhedra (quadrangular rhomboid prism, quadrangular prism, or triangular prism) to calculate volume (V) using the formula V=(S×h), where S is the upper surface area and h is the height. Wet and dry mass were estimated by determining the density from 14 sampled subunits (slices) via Archimedes' principle and linear regression.

The extent of the barrier reef was mapped in July 2019 using an Unmanned Aerial Vehicle (UAV) at a flight height of 30 m, resulting in a ground sampling distance of 1 cm/pixel. Object-Based Image Analysis (OBIA), combined with machine learning (Kappa Nearest Neighbour algorithm), was used to classify the orthomosaic into: *Posidonia* beds, Ecomorphosis of "barrier-reef" *P. oceanica* meadows, Sand, and Rock.

Hydrodynamic conditions in the month preceding the November 2019 stranding event (October 21, 2019-November 21, 2019) were analyzed using hourly Significant Wave Height (Hs) data from the Copernicus Marine Service Programme. The maximum wave height (Hmax) hitting the coast was estimated using the formula: Hmax = Hs×2.

4.2.3 Results

The stranded blocks displayed intact rhizomes and roots, indicating complete detachment from the substrate rather than fragmentation. Their shapes were approximated to geometric solids, prisms and rhomboids, to estimate volume (0.03-0.27 m^3) and mass (17-156 kg wet weight) (Figure 4.2.3.1).

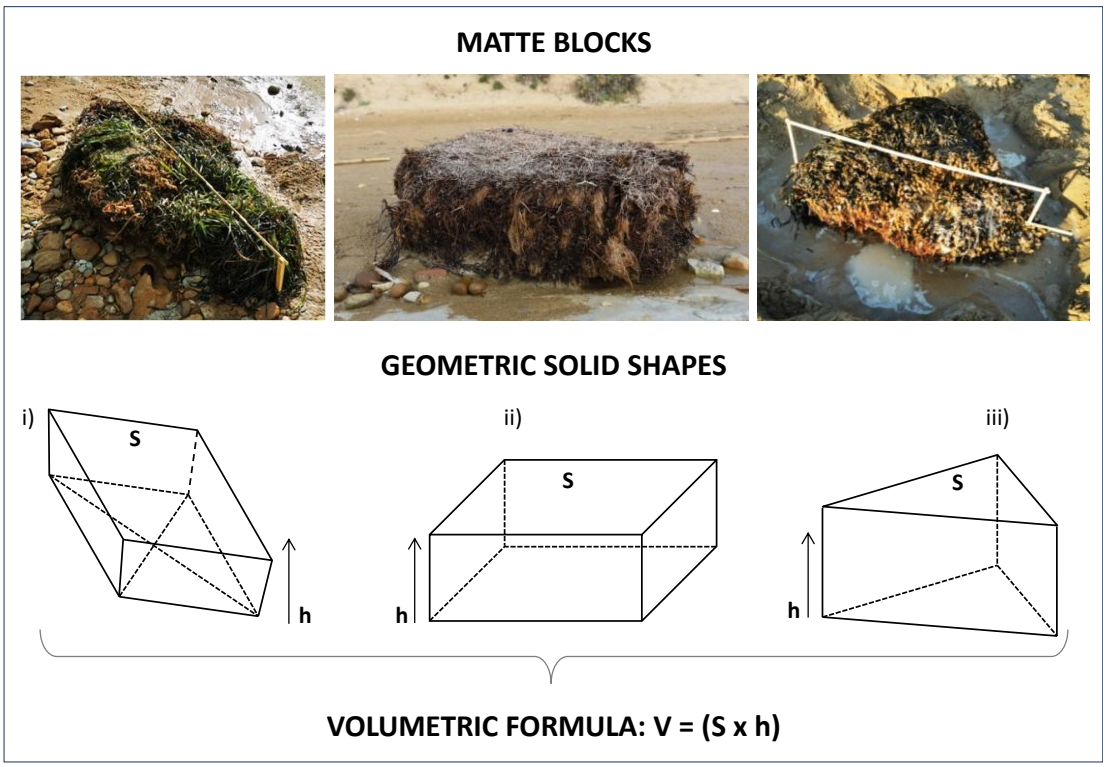

Figure 4.2.3.1 Examples of stranded *Posidonia oceanica* matte blocks and their geometric analogues used for volume estimation. (i) quadrangular rhomboid prism; (ii) quadrangular prism with rectangular base; (iii) regular triangular prism. The volumetric formula is also reported. V= volume, S = upper surface, h = height.

Morphological analyses of the upside-down blocks provided exceptional evidence of how *P. oceanica* roots adapt to rocky substrates. The roots formed flat, densely interwoven mats punctuated by subspherical and cylindrical aggregates, hypothesized to result from root growth into the burrows of boring bivalves such as *Pholas dactylus* and *Lithophaga lithophaga*. This plant-animal interaction, previously undocumented, suggests that bioerosion by endolithic molluscs may enhance substrate roughness, creating microhabitats that facilitate seagrass anchorage. Such symbiotic facilitation could represent a key mechanism for *P. oceanica* establishment on smooth carbonate rocks, expanding its ecological niche and contributing to reef formation. Shoot densities ranged from 911 to 2011 shoots m^{-2}, with theoretical bathymetric origins between 0.02 and 1.7 m depth, confirming that the detached blocks originated from the shallowest part of the reef (Figure 4.2.3.2). These findings indicate that the matte sections most vulnerable to detachment are those occupying the upper reef margin, directly exposed to high-energy wave action.

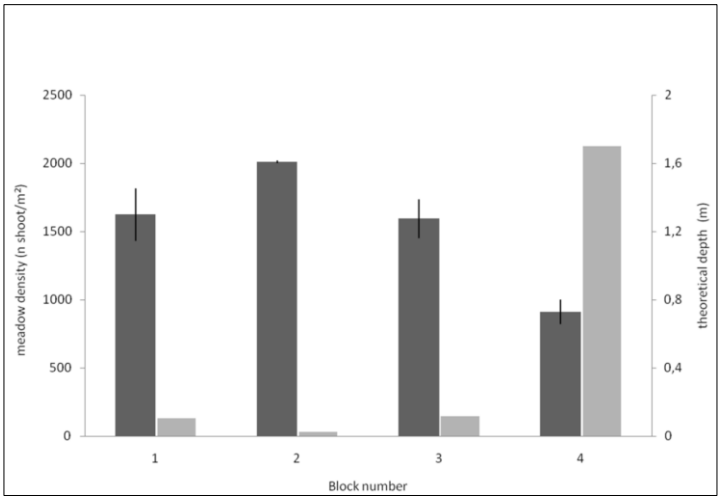

Figure 4.2.3.2 Mean shoot density (±SE) and corresponding theoretical depth of stranded *Posidonia oceanica* matte blocks.

High-resolution UAV imagery and Object-Based Image Analysis (OBIA) provided the first detailed spatial characterization of the Scala dei Turchi reef. The photomosaic revealed alternating ridges of *P. oceanica* , sand, and rock forming multi-arc "atoll" structures typical of biogenic barrier reefs. The classification achieved 83% overall accuracy (κ = 0.81) and delineated 2.8 ha of *P. oceanica* habitat (Figure 4.2.3.3).

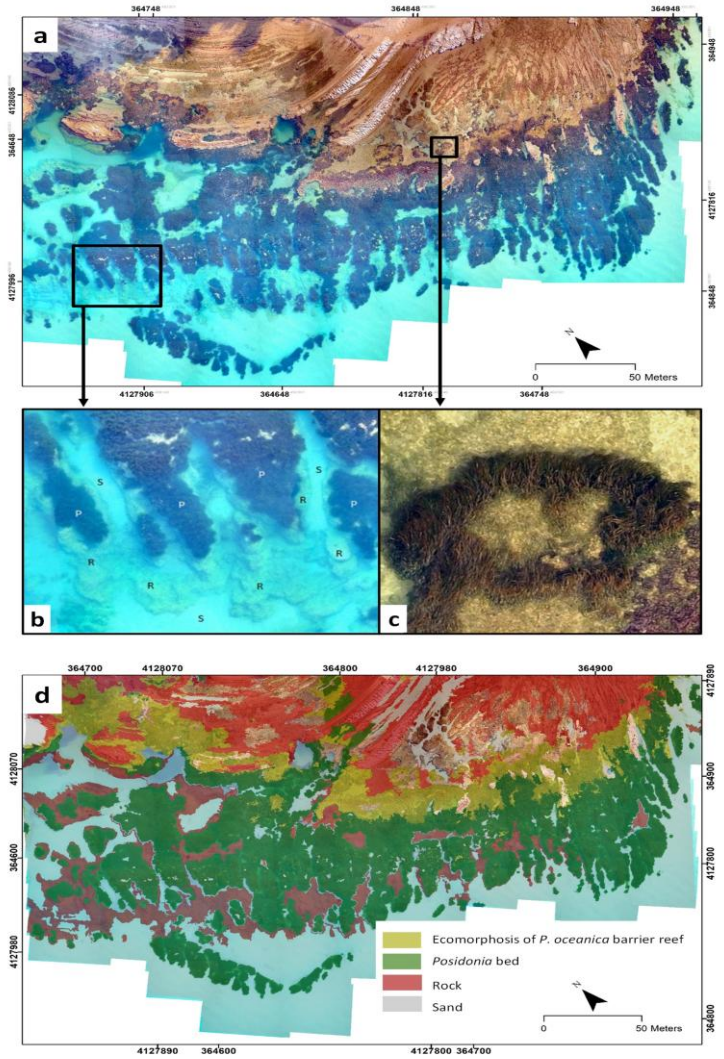

Figure 4.2.3.3 UAV orthomosaic and Object-Based Image Analysis classification of the *Posidonia oceanica* barrier reef showing spatial distribution of main habitat types. a) Photomosaic of the reef showing very clearly the distribution of *P. oceanica*, with focus on b) *P. oceanica* growing on rocks (P= *Posidonia*, S= sand, R= rock) and c) multi-arc atoll formed (sensu Tomasello et al., 2020). d) Object-based Image Analysis (OBIA) classification and thematic classes detected by means of Kappa Nearest Neighbour (KNN) algorithm classification.

Analysis of Copernicus Marine Service data for the month preceding the 2019 event revealed multiple storms, culminating in an extreme episode (significant wave height > 4 m; estimated Hmax > 8 m) just one week before the stranding (Figure 4.2.3.4). This wave energy was sufficient to uproot matte blocks anchored in less than one meter of water, transporting them over 80 m onto the shore. The findings confirm that *P. oceanica* barrier reefs, while effective in dissipating wave energy, are themselves highly susceptible to mechanical erosion during severe storms. The loss of entire matte sections, rather than individual shoots, implies structural weakening of the reef and positive feedback loops that exacerbate vulnerability to subsequent disturbances.

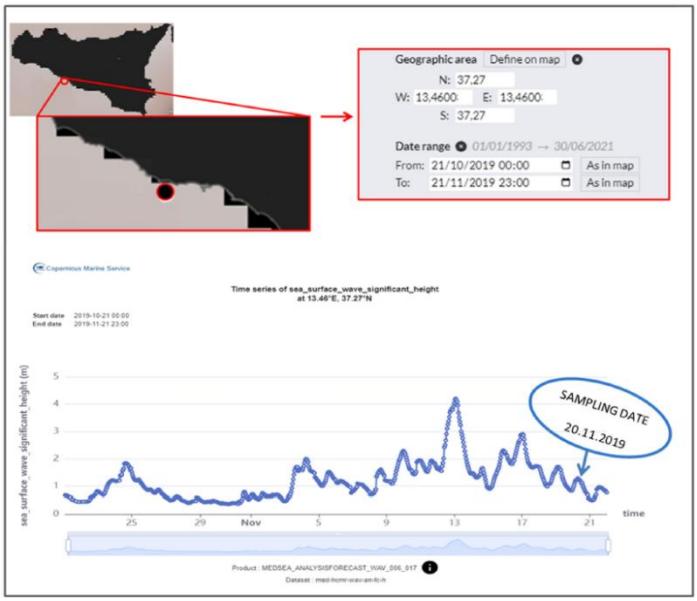

Figure 4.2.3.4 Time series of significant wave height preceding the discovery of stranded *Posidonia oceanica* matte blocks.

4.2.4 Discussion

The *matte* stranding phenomenon found in this study, unlike typical leaf or shoot wrack accumulation, represents large-scale biomechanical dislodgement of the reef's foundation. It underscores the urgent need to reassess the stability and resilience of *P. oceanica* barrier reefs in the face of climate-driven storm intensification (Menendez et al., 2008; Izaguirre et al., 2010; Duarte et al., 2013). Moreover, since such reefs form over centuries and support high biodiversity (Pergent et al., 2014; Tomasello et al., 2020)., their degradation would entail significant losses in coastal protection and carbon sequestration capacity (Pergent et al., 2014; Boudouresque et al., 2016).

The large-scale stranding of numerous *P. oceanica* matte blocks, forming a veritable "cemetery" along the southern Sicilian coast, constitutes the first documented evidence of erosion of a shallow *P. oceanica* reef resulting in the detachment and stranding of numerous and, in some cases, very large, matte blocks after a severe storm. This phenomenon represents large-scale biomechanical dislodgement of this reef foundation, distinguishing it from typical leaf or shoot wrack accumulation (Oprandi et al. 2020). It underscores the urgent need to reassess the stability and resilience of *P. oceanica* barrier reefs in the face of climate-driven storm intensification, as shallow seagrass meadows are known to be more vulnerable to mass loss than deeper meadows because the intensity of physical disturbance increases rapidly with decreasing depth (Gera et al. 2014).

The study provides the first quantitative and morphological evidence of storm-induced detachment , with shoot density models suggesting the blocks originated from very shallow depths (in most cases only a few centimeters below the water surface), highlighting that shallow reef zones, while effective at dissipating wave energy, are themselves highly vulnerable to destruction under intensifying storm regimes (Molinier and Picard, 1952; Hemminga and Duarte, 2000). The high-magnitude storm events, specifically the one that occurred 9 days prior to the survey with a significant wave height of about 4 m (suggesting waves of up to 8 m offshore), exceeded the anchoring strength of the root system and caused the collective uprooting.

Furthermore, the morphological analysis of the blocks (showing a flat root system interrupted by digitate protuberances) led to a hypothesis about a complex ecological mechanism: a facilitative interaction with boring bivalves, such as *Pholas dactylus* and *Litophaga litophaga*, common in the study area, which may enable *P. oceanica* to colonize flat rocky substrates by creating burrows for root penetration, expanding its ecological niche but potentially increasing exposure to mechanical stress and subsequent detachment.

Therefore, the Scala dei Turchi "seagrass cemetery" serves as a powerful indicator of the vulnerability of Mediterranean seagrass systems to extreme climate-driven events. Protecting these biogenic reefs will require sustained monitoring, identification of resilient populations, and mitigation of local anthropogenic pressures to preserve their crucial role as blue-carbon reservoirs and coastal buffers in a rapidly changing Mediterranean seascape.

4.3 Long-term growth dynamics and vulnerability of *Posidonia oceanica* barrier reefs to climate change

4.3.1 Introduction

Seagrass ecosystems are among the planet's most effective long-term carbon sinks, yet their capacity for sediment accretion and organic preservation varies greatly across space and time (Mateo et al. 2006; Apostolaki et al. 2022). Despite their ecological importance, little is known about how the long-term development of these reefs compares with their present-day growth performance. To address this gap, a multi-proxy study was conducted on three *Posidonia oceanica* barrier reefs along the Sicilian coast - Solanto, Maragani, and Marsala - integrating radiocarbon dating, stable isotope analysis ($\delta^{13}C$), and lepidochronology to reconstruct their millennial-scale evolution and contemporary dynamics.

4.3.2 Materials and methods

Sampling was conducted between 2018 and 2021 at three *P. oceanica* barrier reefs along the Sicilian coast - Solanto (North, semi-sheltered), Maragani (South, wave-exposed), and Marsala (West, moderately exposed, high sedimentation) (Figure 4.3.2.1). At each reef, three stations were selected. Divers collected two matte samples per station-one basal and one upper layer-resulting in 18 matte samples total (3 reefs × 3 stations × 2 depths). Matte was extracted by cutting ~70 cm horizontally into the matte wall after removing the outermost recent deposits to avoid contamination. Samples were sealed in plastic containers, kept cool and dark during transport, and stored at -20 °C until analysis. For short-term growth analysis, orthotropic shoots were collected from the living canopy at 50-100 cm depth. A total of 247 shoots were analyzed: 58 from Solanto, 72 from Maragani, and 117 from Marsala. Shoots were stored in seawater-filled insulated boxes and frozen at -20 °C before processing.

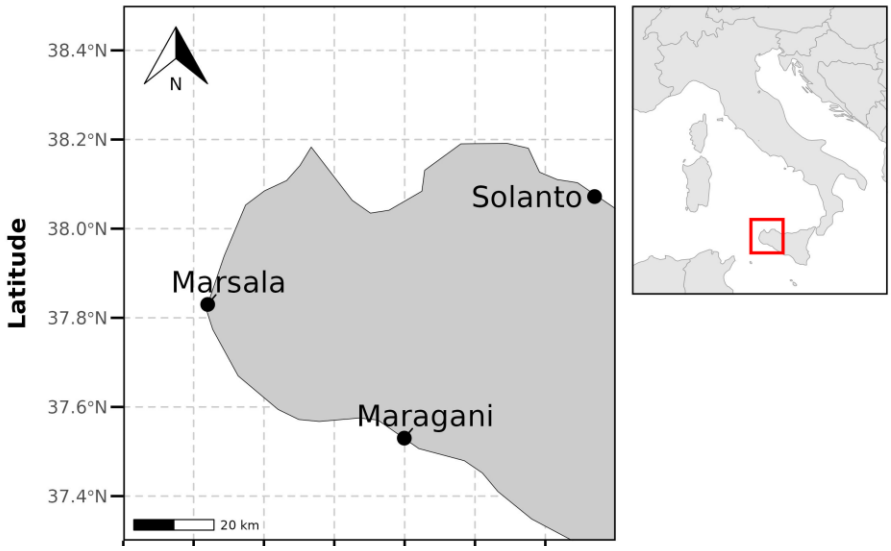

Figure 4.3.2.1 Map of Sicily showing the three *Posidonia oceanica* reef sites (Solanto, Maragani, Marsala).

Matte samples were pretreated (mechanical cleaning; acid-alkali-acid), combusted at 900 °C, and graphitized for Accelerator Mass Spectrometry (AMS). Radiocarbon ages were corrected for isotopic fractionation using AMS-measured $\delta^{13}C$ values. Post-1950 samples and stratigraphically inconsistent ages were excluded. Matte accretion rates were estimated from the age difference and vertical thickness between basal and upper layers.

Lepidochronological cycles were identified following Pergent et al. (1989). Annual rhizome segments were isolated, measured (length), dried (105 °C, 24 h), and weighed. Apical and <2-year-old segments were removed. Growth rate and annual production were calculated for each shoot. Rhizome length and weight were assigned to reference percentile classes (Tomasello et al. 2016) to evaluate growth performance independently of shoot age.

Spatial differences in matte accretion, $\delta^{13}C$, and lepidochronological metrics were assessed using Kruskal-Wallis and Dunn's post-hoc tests ($\alpha = 0.025$). Percentile distributions were compared with chi-square tests. Correspondence Analysis (CA) visualized relationships among sites and growth classes. All analyses were performed in R v4.3.1.

4.3.3 Results

Radiocarbon dating revealed millennial-scale formation across all sites, with basal layers ranging on average from ~600 to ~1300 years BP (Figure 4.3.3.11). Solanto and Maragani were the oldest reefs (>1000 years), while Marsala was younger (~600 years), reflecting different accretional histories.

Estimated mean vertical accretion rates of the *matte* varied widely: 3.5 mm yr^{-1} at Solanto, 2.0 mm yr^{-1} at Maragani, and up to 6.6 mm yr^{-1} at Marsala (Figure 4.3.3.22). Mean accretion rate in the upper layers was consistently slower across all reefs, suggesting a progressive decline in vertical growth as reefs matured and sea levels stabilized.

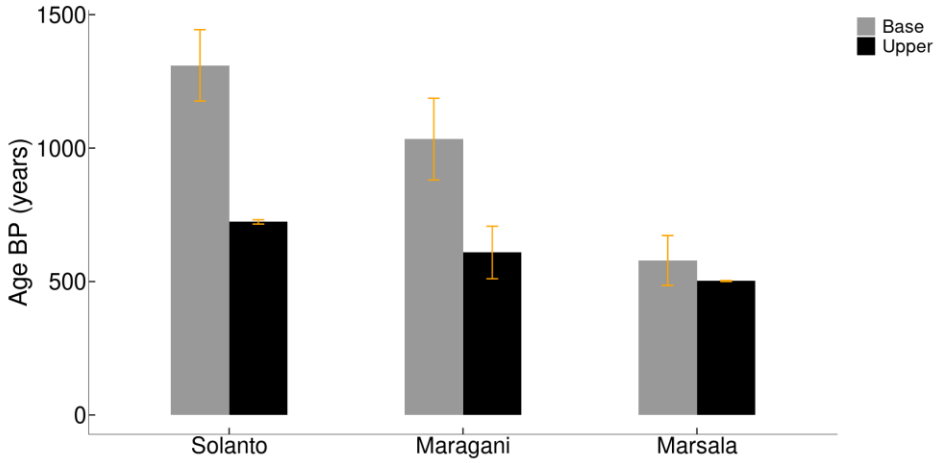

Figure 4.3.3.1 M*ean* (± SE) radiocarbon-based age (BP) of *matte* layers (basal, upper) across the three reef sites.

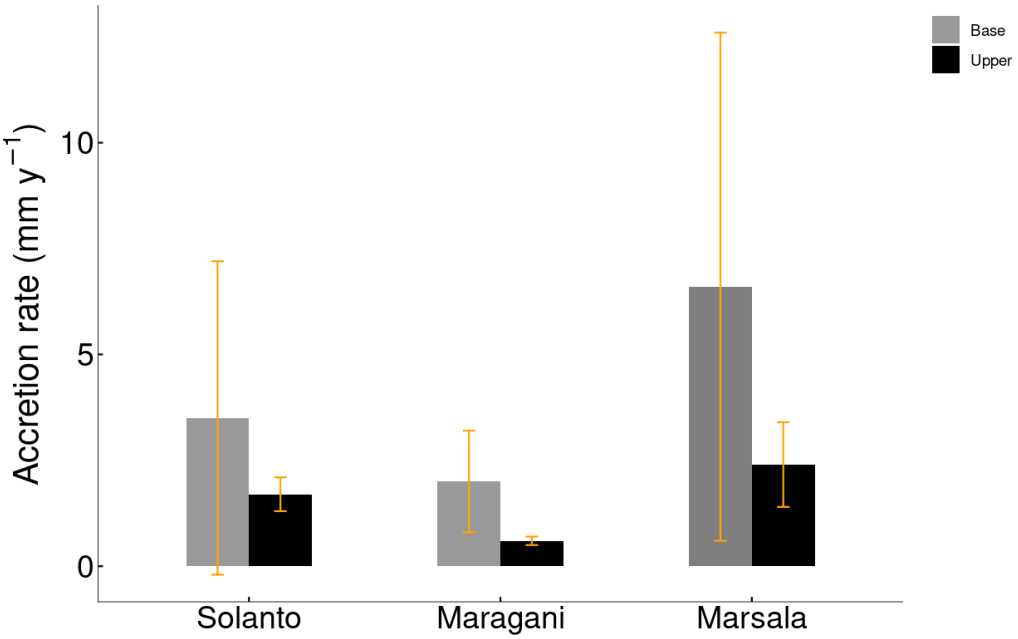

Figure 4.3.3.2 Mean (± SE) matte accretion rate of *matte* layers (basal, upper) across the three reef sites.

Lepidochronological analysis revealed strong contrasts in present-day shoot age, rhizome length, and productivity (3). Maragani displayed the longest and heaviest rhizomes, with mean elongation and primary production rates, approximately double those of Solanto. Marsala showed intermediate performance but greater variability, consistent with heterogeneous growth conditions. Solanto had the oldest but smallest rhizomes, reflecting reduced vigor and possible age-related stress in mature reefs.

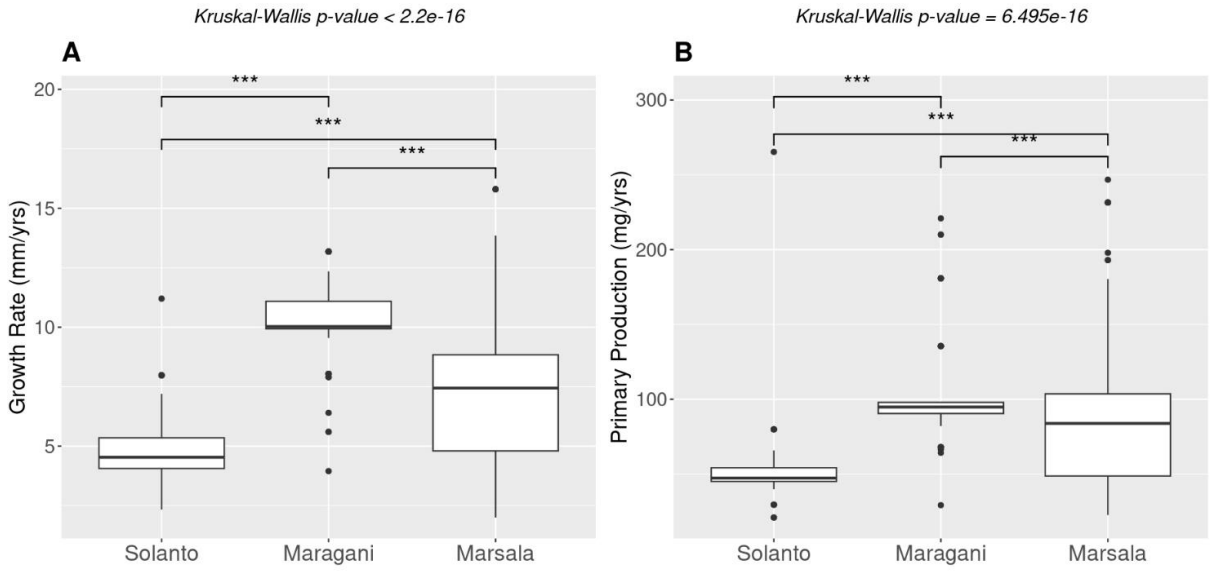

Figure 4.3.3.3 A) Rhizome elongation rate and (B) primary production across sites. Boxplots indicate median and interquartile ranges; differences are significant at $p < 0.001$.

Comparison with reference growth percentiles (Figure 4.3.3.4) revealed that Solanto rhizomes were concentrated in the lowest performance classes (< 5th percentile), Maragani exceeded the 50th percentile for most parameters, and Marsala showed intermediate, bimodal distributions. These spatial patterns were reinforced by correspondence analysis (Figure 4.3.3.5), which clearly separated Maragani along the high-growth axis, with Solanto at the opposite end and Marsala occupying an intermediate position.

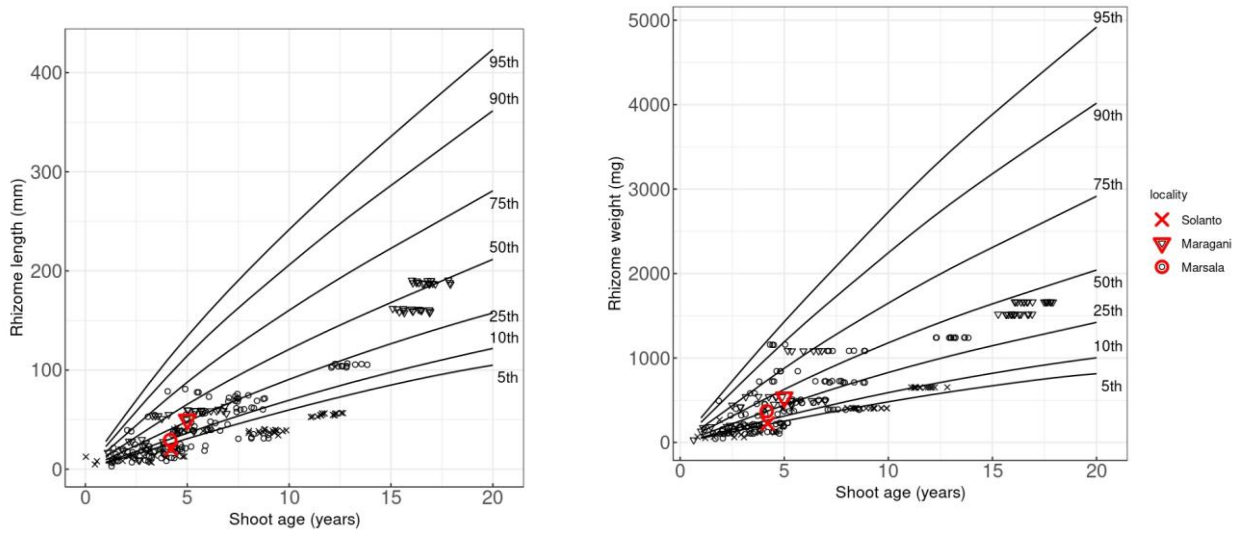

Figure 4.3.3.4 Reference growth charts showing mean rhizome length (A) and weight (B) percentiles. Site means (red points) indicate relative performance against standard growth distributions.

A) Rhizome length

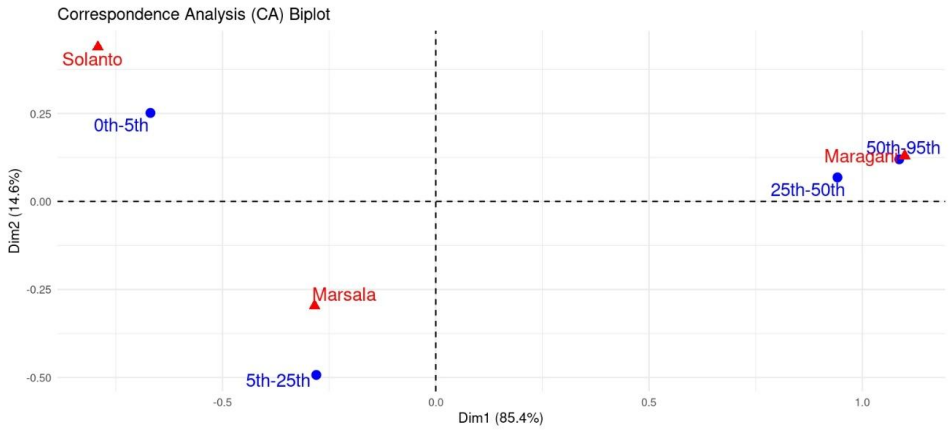

B) Rhizome weigth

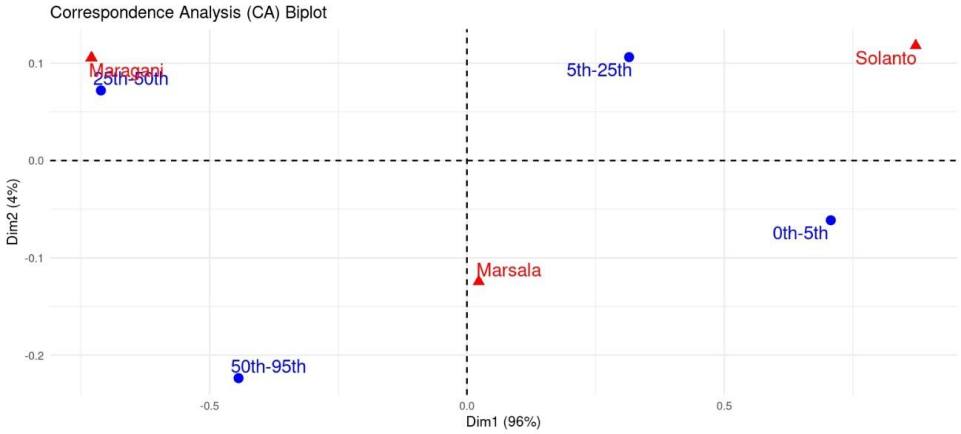

Figure 4.3.3.5 Correspondence analysis biplots of rhizome length (A) and weight (B). Sites in red, percentile classes in blue; Dim1 explains >85% of total variance.

4.3.4 Discussion

The contrasting patterns between millennial-scale matte accretion and modern rhizome growth show that *Posidonia oceanica* reef formation is driven by a complex interplay of biological production, sediment availability, and hydrodynamic forces. At Solanto, moderate long-term accretion coupled with the lowest contemporary productivity reflects a mature, sediment-limited system where shallow depth, hydrodynamic stress, and shoot aging constrain growth and carbon burial capacity (Tomasello et al. 2016; La Loggia et al. 2009). Maragani, despite similar age, exhibited the highest rhizome elongation and productivity, consistent with intermediate hydrodynamic exposure and periodic sediment resuspension that stimulate vertical growth while still enabling the preservation of matte over centuries (Manzanera et al. 2011; Bonamano et al. 2021). Marsala, the youngest formation, displayed the fastest accretion and substantial short-term growth variability, reflecting abundant sediment supply and hydrodynamic dampening associated with its position at the lagoon–open-sea interface and proximity to one of the Mediterranean's largest *P. oceanica* meadows (Gacia & Duarte 2001; Ruju et al. 2018).

Across all sites, the pronounced decrease in accretion rate toward the upper matte layers supports a basin-wide pattern of reduced vertical buildup in recent centuries, likely linked to sea-level stabilization, lower

sediment deposition, and self-limiting feedback in mature reefs (Monnier et al. 2021). The stark mismatch between modern rhizome elongation and the much slower recent matte accretion indicates significant losses of necromass, most plausibly through erosion, sediment remobilization, and storm-driven detachment-processes already documented as extensive "reef cemeteries" along nearby Sicilian coasts (Tomasello et al. 2025) and widely recognized as major drivers of seagrass sediment discontinuities (Marbà et al. 1996; Mateo et al. 1997; Gera et al. 2014).

These results emphasize that *P. oceanica* reefs are not static blue-carbon archives but highly dynamic systems whose millennial accumulation can be disrupted by contemporary climatic and mechanical stressors (Mazarrasa et al. 2017a and b). While older reefs such as Solanto show reduced vigour and lower carbon preservation potential, younger and sediment-rich systems like Marsala exhibit greater resilience yet remain vulnerable to episodic disturbances. By integrating radiocarbon dating and lepidochronologythis study provides the first combined reconstruction of historical deposition and present-day growth dynamics for *P. oceanica* barrier reefs in the central Mediterranean, demonstrating how long-term biogenic accretion can be compromised by modern processes. These findings underscore the need for management strategies that incorporate both geological and ecological timescales to safeguard the persistence and carbon-sink function of these vulnerable bioconstructions.

4.4 Conclusions

The studies presented in Section 4 collectively reveal the multidimensional vulnerability of the marine coastal ecosystems formed by the Mediterranean endemic seagrass species *Posidonia oceanica* to climate change, spanning physiological, structural, and temporal scales. Experimental evidence demonstrated that rising temperatures and increasing salinity - two key manifestations of a warming Mediterranean - profoundly impair the species' photosynthetic efficiency, biochemical defences, and growth, confirming its limited tolerance to compound stressors. At the ecosystem level, the discovery of storm-detached matte blocks exposed the fragility of *P. oceanica* barrier reefs, which, despite their function as natural coastal defences and carbon sinks, are themselves increasingly eroded by the intensification of extreme hydrodynamic events. Long-term analyses of reef accretion further emphasized how millennial-scale biogenic structures are being destabilized by modern disturbances, as the balance between growth, sedimentation, and erosion is disrupted. Together, these studies illustrate that *P. oceanica* vulnerability is not confined to immediate physiological stress but extends to the loss of structural integrity and historical resilience. Yet, they also contribute critical insights for mitigation and preservation: identifying populations with adaptive potential, understanding biomechanical thresholds of reef stability, and linking past accretion dynamics to present degradation. By integrating experimental, geomorphological, and paleoecological approaches, this research advances a comprehensive understanding of how climate-driven stressors threaten *P. oceanica* ecosystems, while providing an essential scientific basis for conservation strategies aimed at sustaining their ecological functions and blue-carbon value in an era of rapid environmental change.

5 Freshwater habitat vulnerability

5.1 Characterisation of the prdx4 gene in *Squalius cephalus* and its role in freshwater environments with varying impact of perfluoroalkyl substances (PFAS).

5.1.1 Introduction

The scientific community has increasingly focused on emerging pollutants in recent years due to their rising numbers, environmental persistence, and potential toxic effects on organisms. Despite their growing prevalence, there remains limited information about their transport, persistence, and overall impact on ecosystems. Per- and polyfluoroalkyl substances (PFAS) are chemical surfactant compounds produced since 1950 (Baran, 2001). They consist of a hydrophobic aliphatic tail composed of 4 to 16 carbon atoms; the hydrogen atoms are only partially or totally replaced by fluorine atoms, according to the structure - C_nF_{2n+1}- (Buck et al., 2011). They also have a functional group, generally carboxyl or sulfonic. PFAS are distinguished into short- and long-chain based on the number of fluorinated carbon atoms. The great variability of the shapes and structures of these compounds gives them multiple chemical-physical properties, leading to their increased use in different industrial sectors with a subsequent uncontrolled release of these substances into the environment.

Due to the strength of the fluoro-carbon bonds, PFAS exhibits remarkable chemical stability and high thermal inertia (Baran, 2001), which results in a high persistence in all environmental matrices, particularly in the water system, which serves as the main reservoir of these substances. PFAS have been detected in biological matrices, from apex predators to the lowest trophic levels (Teunen et al., 2021). In organisms, PFAS are rapidly absorbed by inhalation and ingestion and only partially metabolised. They mainly bioaccumulate in different body tissues, depending on the length of the alkyl chain, the molecule's functional group and the tissue's protein content. PFAS are frequently low-pKa acids charged at environmentally relevant pH levels, making it difficult to cross cell membranes by passive diffusion (Bangma et al., 2022). However, some PFAS can still cross cell membranes *via* passive diffusion, particularly those with shorter chain lengths and less ionisation (Zheng et al., 2023).

Research indicates that specific transport proteins use PFAS as substrates, facilitating their entry into cells and their movement within them (Dankers et al., 2013). In particular, these substances can bind the most abundant blood serum proteins, like globulins and albumin, the primary carriers of PFAS inside the body (Forsthuber et al., 2020). This bond can affect their toxicity, transport to active sites, and elimination of half-lives, hence their bioaccumulation within animals and humans (Fischer et al., 2024). Specifically, binding affinities for proteins have been reported for several PFAS, including perfluorooctane sulfonic acid (PFOS) and perfluorooctanoic acid (PFOA) (Jensen and Leffers, 2008). Indeed, PFAS can interact with proteins, interfering with their structure and function.

In addition, previous research showed how PFAS can interfere with the correct lipid metabolism of the cells. PFAS have a similar structure to fatty acids; as a result, they are transported by liver fatty acid-binding proteins (L-FABP) to hepatocytes, where they induce hepatotoxicity. Peroxisome proliferator-activated receptors (PPARs) are nuclear receptors which regulate lipid metabolism and adipogenesis (Behr et al., 2020). They are usually activated by fatty acids; due to their similarity, PFAS can bind these receptors, altering lipid homeostasis (Fragki et al., 2021). The structural differences between PFAS, particularly the carbon chain length, play a fundamental role in regulating lipid metabolism (Zhao et al., 2023). For instance, some C8 compounds (PFOS, chlorinated perfluorooctane sulfonate and 6:2Cl-PFESA) induce hepatic steatosis exclusively *via* lipid synthesis to induce adipogenesis, while 8:2Cl-PFESA, in addition, preferentially suppresses lipid excretion (Yi et al., 2019).

Moreover, PFAS are among the pollutants that can increase the production of reactive oxygen species (ROS), leading to an imbalance in the cellular redox equilibrium and raising the risk of oxidative stress (Bonato et al., 2020). An excess of ROS can cause damage to various macromolecules (proteins, lipids and DNA), interfering with their structure and function at the level of different cellular compartments and modulating

the gene expression (Juan et al., 2021). Organisms have evolved an antioxidant defence system able to respond to limit the risk of oxidative stress by activating multiple non-enzymatic and enzymatic antioxidants (Ferro et al., 2017; Ricci et al., 2017; Ferro et al., 2020; Bakiu et al., 2022; Schumann et al., 2023, 2024a).

Among the latter, peroxiredoxins (Prdx) play a fundamental role in detoxifying the cell from ROS, cooperating with glutathione peroxidase (GPx) and catalase as scavengers of organic and inorganic hydroperoxides. Prdxs are a multigenic family of ubiquitous peroxidase-active enzymes in living organisms (Al-Asadi et al., 2019; Tolomeo et al., 2019; Drago et al., 2022), widely distributed in various tissues and organs. Six isoforms are known in fish, each differing in their intracellular location (Ambruso, 2013). They are classified into three classes, according to the structure and mechanism of action: typical 2-Cys (Prdx1, 2, 3 and 4), atypical 2-Cys (Prdx5), and 1-Cys (Prdx6).

Prdx4 is a typical 2-Cys Prdx composed of two subunits: one contains a peroxidatic cysteine, while the other contains a resolving cysteine. The reaction with ROS involves two steps. In the first one, the peroxidatic cysteine attacks the peroxide substrate and is oxidised to S-hydroxycysteine Cys-SOH. In the second step, Cys-SOH reacts with the Cys-SH of the other subunit to form an inter-subunit disulphide bridge (Rhee, 2016). Oxidised Prdxs are then restored to a reduced state by a reducing agent, such as glutathione, NADPH and thioredoxins. Prdx4 is mainly present in the endoplasmic reticulum and in the extracellular environment (Lee, 2020), with a N-terminal signal peptide in its primary sequence, targeting it for secretion from the cell (Shi et al., 2014). Therefore, it protects the host from oxidative damage by removing ROS inside and outside the cell (Yamada and Guo, 2018).

To date, few works have investigated the structural and functional characterisation of Prdx4 in fish, and none have assessed its expression variation in environmental contexts impacted by anthropogenic contamination. Therefore, this study's primary objective was to characterise Prdx4 in the common chub (*Squalius cephalus*).

S. cephalus is a generalist species with extensive ecological plasticity (Balestrieri et al., 2006), allowing it to thrive in diverse and often polluted environments. Its resilience and adaptability make it a valuable bioindicator for assessing water contamination levels and understanding the vulnerability of aquatic ecosystems (Nyeste et al., 2019). Therefore, we evaluated how this freshwater fish species can face the stress caused by environmental concentrations of PFAS in rivers of the Veneto region (Italy). Veneto represents one of the most emblematic cases of PFAS water contamination, mainly originating from a fluorochemical plant, which has been active since 1964. The contamination involved the provinces of Vicenza, Padua and Verona, for a total estimated area of 190 km^2 (Pitter et al., 2020).

In the present study, we investigated the physiological responses from chronic exposure to PFAS in the kidney. Some previous studies identified the kidney as one of the main targets for PFAS accumulation (Cui et al., 2008; Yoo et al., 2009) and one of the responsible organs for perfluorocarbons (PFCs) excretion (Butenhoff et al., 2004). This physiological role could contribute to the increase in ROS production in the organ, with a consequent rise in oxidative stress risk.

We characterised the *prdx4* sequence, which was previously unknown, and performed phylogenetic analyses to verify if the molecular evolution of this protein led to the conservation of the principal functional domains of the protein or introduced differentiation in *S. cephalus* from orthologous genes of phylogenetically related species. Furthermore, we measured the mRNA accumulation of *prdx4* to assess whether this gene may undergo up-regulation or down-regulation following PFAS exposure. To evaluate the role of Prdx4 in counteracting oxidative stress, we also examined two indicators of lipid and protein oxidative damage.

5.1.2 Materials and methods

Sampling sites

Three sampling sites, characterised by different PFAS concentrations, were selected, all located around the province of Vicenza (Italy) within the Leogra-Bacchiglione basin. Leogra Torrent, in Torrebelvicino (VI) (45.71779193 N; 11.30627616 E) was referred to as the “very low polluted site” (used as control site); Roggia Moneghina River, in Grumolo delle Abbadesse (VI) (45.5116 N; 11.6560 E) as the “low polluted

site"; Retrone River, in Altavilla Vicentina (VI) (45.51350834 N, 11.5045197 E), as the "highly polluted site". Data on PFAS concentrations in surface waters were provided by the Regional Agency for Environmental Prevention of Veneto (ARPAV) (Table 5.1.1: Total PFAS average concentration in freshwater from the four sampling sites, measured by ARPAV in 2022 and 2023. The Gauss-Boaga coordinates, obtained with qGIS (version 3.22) software, are reported for the geo-localisation of the sites.). Contaminant levels, including pesticides, metals, and volatile organic compounds (VOCs), were below detection limits, suggesting PFAS as the primary pollutant.

Table 5.1.1: Total PFAS average concentration in freshwater from the four sampling sites, measured by ARPAV in 2022 and 2023. The Gauss-Boaga coordinates, obtained with qGIS (version 3.22) software, are reported for the geo-localisation of the sites.

SITE	Locality	Classification	Average concentration of total PFAS (ng/l)
Torrente Leogra	Grumolo delle Abbadesse	Very low polluted	<5
Roggia Moneghina	Torrebelvicino	Low-polluted	5.64
Retrone	Altavilla Vicentina	Highly-polluted	582.6

The fieldwork activity was carried out in a single day, ensuring minimal environmental variation between the three sites (temperature within a 0.5-degree range; pH approximately 8.0-8.1). Ten specimens of S. cephalus (Linnaeus, 1758) with comparable size (19.99 ± 5.14 cm) were sampled from each site with the electrofishing technique (authorised by decree of the director of the Agri-environment, Planning and Management of Fish and Wildlife Hunting of the Veneto Region, n. 336 of 14 December 2020). The individuals were immediately sacrificed using an overdose of clove oil (concentration of 0.070 mL/L). Afterwards, they were rapidly dissected to remove the kidneys, which were frozen in liquid nitrogen and stored at –80°C until analyses.

Studies were carried out following ARRIVE (Animal Research: Reporting of In Vivo Experiments) guidelines, in accordance with the Guidance on the operation of the Animals (Scientific Procedures) Act 1986 and associated guidelines, and with the EU Directive 2010/63 for the protection of animals used for scientific purposes.

RNA extraction, quantification, assessment of the RNA integrity and cDNA synthesis.

Kidney samples were processed using the guanidine thiocyanate-phenol-chloroform method to extract the total RNA content, according to the TripleXtractor protocol (Grisp, Porto, Portugal). NanoDrop™ 2000/2000c Spectrophotometer (Thermo Scientific, Wilmington, USA) was used to quantify the RNA concentration. The purity of the RNA was assessed by calculating the 260/280 and 260/230 absorbance ratios and the integrity by running an aliquot of 1000 ng/µL of RNA in a 1% agarose denaturing gel electrophoresis. RNA samples were reverse transcribed with a cDNA Synthesis Kit (biotechrabbit, Berlin, Germany) to obtain a 50 ng/µL concentrated cDNA.

Gene characterisation, primer design and assessment by PCR

The sequence of prdx4 of S. cephalus was unknown; therefore, we performed a preliminar gene characterisation. The primers for sequencing were designed on fathead minnow (Pimephales promelas), the most phylogenetically related species, in the NCBI GenBank® database. Primer3 v 4.1.0 program (primer3.ut.ee/) was used to design primers, which were subsequently analysed with the IDT OligoAnalyzer™ tool (eu.idtdna.com/calc/analyzer) and the Beacon DesignerTM program (premierbiosoft.com/qOligo/Oligo.jsp?PID=1). To identify conserved domains for primer design, a multiple sequence alignment was performed with the GenomeNet ClustalW program (genome.jp/tools-bin/clustalw), inserting sequences of other Cypriniformes. Only the primers located in regions with a > 90% degree of conservation were selected. They were amplified with PCR and tested by gel electrophoresis; the PCR products were purified with the GenUP™ PCR/Gel Cleanup Kit (biotechrabbit, Berlin, Germany) and sent to Eurofins Genomics Company (Ebersberg, Germany) for sequencing.

Phylogenetic analyses

The T-Coffee package was used (Notredame et al. 2000) to obtain multiple alignments of Prdx4 coding region and amino acid sequences. jModelTest2 (Darriba et al., 2012) was used to conduct a statistical selection of best-fit nucleotide substitution models to analyse the molecular evolution of organisms Prdx4. Analyses were performed using 88 candidate models and three types of criteria: Akaike information criterion (AIC), corrected AIC (cAIC) and Bayesian information criterion (BIC). The TrN+I+G resulted the best-fit model of all analysed coding region sequences evolution with a γ shape value (four rate categories) of 1.814 using all statistical criteria (–lnL = 9681.46).

Phylogenetic trees were built using the Bayesian inference (BI) method implemented in Mr. Bayes 3.2 (Ronquist et al. 2012). Four independent runs, each with four simultaneous Markov Chain Monte Carlo (MCMC) chains, were performed for 1,000,000 generations sampled every 1000 generations. Furthermore, we also used the maximum likelihood (ML) method implemented in PhyML 3.0 (Guindon et al. 2010), while the relative bootstrap analyses were performed on 100,000 trees. FigTree v1.4 software was used to display the annotated phylogenetic trees.

Quantification of gene expression

The *prdx4* mRNA concentration in the kidney was evaluated by qRT-PCR (*Applied Biosystems® 7500 Fast Real-Time PCR*). The qRT-PCR cycling parameters were the following: 95 °C for 2 min, 38 cycles at 95 °C for 20 s and 60 °C for 1 min, and finally 95 °C for 15 s, 60 °C for 1 min, 95 °C for 15 s, and 60 °C for 15 s for the melting profile analysis (detection of genomic contamination). Each sample was run three times (technical triplicate). On the sequence obtained by Eurofins, *ad-hoc* primers for gene expression analysis were designed (Table 5.1.2) and the amplification efficiency was verified at first (absolute quantification). To exclude individual-specific responses, the standard curve was set up with increasing concentrations of a pool of cDNA from various individuals. *Gapdh* was used as a housekeeping gene to normalise the transcription levels between different samples. Lastly, the formula $2^{-\Delta\Delta Ct}$ of the Pfaffl mathematical model (Pfaffl, 2001) was applied to calculate the gene expression by the comparative Ct method (Livak and Schmittgen, 2001). qRT-PCR provides, as a result, a relative quantification value, which relates the PCR signal of the target transcript in a treatment group to that of the untreated sample (control).

Table 5.1.2 List of primer pairs used for qRT-PCR, with amplicon size (bp). A annealing temperature was 60 °C for all primers.

GENE	PRIMER	SEQUENCES 5'→ 3'	Amplicon (bp)
prdx4	3_PRDX4_S.cephalus_F	GTTCGGTGGACTCGCAGTTTACTC	158
	3_PRDX4_S.cephalus_R	TCTGAGTGTGTGTCCCTGATCCTC	
gapdh	GAPDH_S.cephalus_F	ATCACAGCCACACAGAAGAC	126
	GAPDH_S.cephalus_R	AGGAATGACTTTGCCCACAG	

Advanced Oxidation Protein Products and Lipid Peroxidation

Advanced Oxidation Protein Products (AOPP) are uremic toxins created during oxidative stress by reacting plasma proteins with chlorinated oxidants such as chloramines or hypochlorous acid. AOPP were measured using the Witko-Sarsat (1996) spectrophotometric method on the microplate reader Infinite® 200 PRO (Tecan Trading AG, Switzerland) at a 340 nm wavelength. The concentration of AOPP was expressed as a micromoles/litre of chloramine-T equivalent.

The Lipid Peroxidation Assay kit (Sigma-Aldrich, Saint Louis, U.S.A.) was used to quantify lipid peroxidation, determined by the reaction of malondialdehyde (MDA) with thiobarbituric acid to form a colourimetric product, which is proportional to the present MDA. The sample optical density was read on the microplate spectrophotometer Multiskan™ SkyHigh (Thermo Fisher Scientific, Singapore) at 532 nm.

Both MDA and AOPP values were normalised on the total protein content of each sample. The protein amount of the cell extract was assessed *via* the Folin-Ciocalteau phenol reagent method (Lowry et al., 1951), using growing concentrations of bovine serum albumin as standard.

Statistical analysis

The results are shown as mean values of ten samples ± Standard Deviation. The Prism GraphPad software (Version 10.3.1, Boston, MA) was used for the statistical analysis of the data. A one-way variance analysis (ANOVA) was applied, followed by Tukey's test to determine the significance of the differences. A p-value < 0.05 was considered statistically significant.

5.1.3 Results

Phylogenetic analyses

The multiple alignment of the amino acid sequence of S. cephalus with Prdx4 of other species of teleosts (Figure 5.1.3.1 Multiple alignment of the amino acid sequence of *Squalius cephalus* with Prdx4 of other species of teleosts.Figure 5.1.3.1) showed the total conservation of the catalytic centre (FYPLDFTFVCPTEI); this sequence remains unaltered also considering the group of tetrapods. It contains two of the three residues of the catalytic triad (P and T) and the peroxidatic cysteine. The third residue of the catalytic triad (R) is fully conserved too. In addition, the amino acid sequence GEVCPA, containing the resolving cysteine, is present in all considered species. The structural motif GGLG and the threonine, which regulate the enzyme's peroxidase activity, remain unaltered in every species. The structural motif YF is conserved in teleosts and tetrapods. Unfortunately, the sequence of S. cephalus obtained from the sequencing is incomplete; this makes it impossible to verify that this motif is also conserved in this species. The initial part of the sequence appears less conserved between the species, with many amino acid substitutions, and contains the signal peptide that is cleaved in the translocation of Prdx4 in the endoplasmic reticulum or during its secretion.

```
S. cephalus       ----RYFQTS-REWLGVACTLLLI-----TESVVCDGANGRKEQECYNY
S. lalandi        MEFLCHTSLKQQQLLCSLCTALLLLL-TTTVTSADEGASARNSQ-CHNY
S. aurata         MESVVHTNQK-KELFCRPRAALLFFL-LTTLTFAEEGAQVKNSQ-CHNY
L. crocea         MDSVFQLHL--KEVSCALCAALLL---LFTVTSAEEAAHVKNSQ-CHNY
M. miiuy          MDSVLELHL--KEVFCTLCAALLL---LFTVTSAEEGAHVKNSQ-CHNY
M. piceus         MDVSRCIKTP-REWLGVLCTLLLL-----TESVVCDTANGRKEQECYNY
D. rerio          MDVSRCVKTP-REWLGVLWALLLL-----SESVVCDGANGKREQECYNY
E. Lucius         MDVILHMKMV-KELLSVFCTFCLV---TKLVTAVQDGSNGKKDQECYNY
T. fasciatus      MESLLHSNIK-KQLFCALCAALLL-----LTTSAEEGANVKS---CHNY
O. niloticus      MESVFHSDMK-KELFCVLCTALLL---LATVTSAEESAQVKNPQ-CQSY
O. latipes        MESGFSCTL--KEFLCALSASLLL---LGSIASAEE---GKNSQ-CHNY
P. nyererei       MESAFHTDM--KELFCALCTALLL---LATVTSAEESAQVKNPQ-CQSY
P. reticulata     MESGFSTGAK-KELLCAFCAALLL---VSAIASAEEGAHLKNSQ-CHNY
N. coriiceps      MEFLLHISLK-RDLFSILCTALLL----FLTTSAEE---VKDSQ-CHNY
S. salar          MDVMLHMKML-KDILSVFCTICFV---TNFSTAAQDGSNGKKDQECHNY
C. gobio          MGFLLHTNIK-KELFRALCIAVLL----FLTTSAEEDDKVKNSQ-CHNY
E. lanceolatus    MEFILHINVK-KKLFRALCTALLLF--LTTVTSAEEGANVKNSQ-CHNY
T. bernacchii     MEFLLHISLK-KDLFSILCTALLL----FLTTSAEE---VKDSQ-CHNY
G. acuticeps      MEFLLHIILK-KDLFSILCTALLL----FLTTSAEE---VKDSQ-CHNY
H. hippoglossus   MELVSHTGVKRQQLLSTSVLLLLFLDATTVTSAEEGANVRNSQ-CHNY
P. pungitius      MEFLSGTK---KDAFRALCGALLL----LCSASAEEGASGKNSQ-CHNY
C. tularosa       MESGLSPCA--KELLCAFCAALLL---FSAATSADESAHLKNSQ-CHNY
M. salmoides      MEFLSHNNLK-KELFCALCAALLL---LTRVTSAEEGDYVKNSQ-CHNY
P. promelas       MDVRRYVKTP-REWLGVACTLLLI-----TESVVCDGANGRKEQECYNY
C. idella         MDVSRCIKTP-REWLGVLCTLLLL-----TESVVCDTANGRKEQECYNY
O. eperlanus      MDVMSSVRM--SNIFSVFYTFCVF---TKFAYAVQESTNGKSDQECHNY
P. mariae         MESIFNTDMK-KELFCTLCTALLL---LATVTSAEESAQVKNPQ-CQSY
                             .         ..          . :    .    * .*
```

```
S. cephalus       AGGHVYPGEAFRAPVSDHSLHLSKAKISKPAPHWEGTAVINGEFKELKL
S. lalandi        AGGHVYPGEAFRVPVSDHSLHLSKAKISKPSPHWEGTAVINGEFKELKL
S. aurata         AGGHVYPGEAFRVPVSDHSLHLSKAKISKPAPHFEGTAVINGEFKELKL
L. crocea         AGGHVYPGEAFRVPVSDHSLHLSKAKISKPAPQWEGTAVINGEFKELKL
M. miiuy          AGGHVYPGEAFRVPVSDHSLHLSKAKISKPAPQWEGTAVINGEFKELKL
M. piceus         AGGHVYPGEAFRAPVTDHSLHLSKAKISKPAPHWEGTAVINGEFKELKL
D. rerio          AGGHVYPGEAFRVPVSDHSLHLSKAKISKPAPHWEGTAVINGEFKELKL
E. Lucius         AGGHVYPGEAFRVPVSDHSLHLSKAKISKPAPYFEGSAVINGEFKELKL
T. fasciatus      AGGHVYPGEAFRVPVSDHSLHLSKAKISKPAPHWEGTAVINGEFKEKSL
O. niloticus      AGGHVYPGEAFRVPVSDHSLHLSKAKISKPAPHWEGTAVINGEFKELKL
O. latipes        AGGHVYPGEAFRVPVSDHSLHLSKAKISKPAPHWEGTAVINGEFKELKL
P. nyererei       AGGHVYPGEAFRVPVSDHSLHLSKAKISKPAPHWEGTAVINGEFKELKL
P. reticulata     AGGHVYPGEAFRVPVSDHSLHLSKAKISKPAPNWEGTAVIDGEFKELKL
N. coriiceps      AGGHVYPGEAFRVPVSDHSLHLSKAKISKPAPHWEGTAVIDGEFKEAKL
S. salar          AGGHVYPGEAFRVPVSDHSLHLSKAKISKPAPYFEGSAVIDGEFKELKL
C. gobio          AGGHVYPGEAFRVPVSDHSLHLSKAKISKPAPHWEGTAVINGEFKELKL
E. lanceolatus    AGGHVYPGEAFRVPVSDHSLHLSKAKISKLAPNWEGTAVINGEFKELKL
T. bernacchii     AGGHVYPGEAFRVPVSDHSLHLSKAKISKPAPHWEGTAVIDGEFKEAKL
G. acuticeps      AGGHVYPGEAFRVPVSDHSLHLSKAKISKPAPHWEGTAVIDGEFKEAKL
H. hippoglossus   AGGHVYPGEAFRVPVSDHSLHLSKAKISKPAPHWEGTAVINGEFKEVKL
P. pungitius      AGGHVYPGEAFRVPVSDHSLHLSKAKISKPAPHWEGTAVINGEFKETKL
C. tularosa       AGGHVYPGEAFRVPVSDHSLHLSKAKISKPAPNWEGTAVINGEFKELKL
M. salmoides      AGGHVYPGEASRVPVSDHSLHLSKAKISKPAPHWEGTAVINGEFKEAKL
P. promelas       AGGHVYPGEAFRAPVSDHSLHLSKAKISKPAPHWEGTAVINGEFKELKL
C. idella         AGGHVYPGEAFRAPVTDHSLHLSKAKISKPAPHWEGTAVINGEFKELKL
O. eperlanus      AGGHVYPGEAFRVPVSDHSLHLSKAKISKPAPHWEGTAVIDGEFKELKL
P. mariae         AGGHVYPGEAFRVPVSDHSLHLSKAKISKPAPHWEGTAVINGEFKELKL
                  ********** *.**:************** :* :**:***:***** .*

S. cephalus       SDYKGKYLVFFFYPLDFTFVCPTEIIAFSDRVHEFQDINAEVVACSVDS
S. lalandi        SDYKGKYLVFFFYPLDFTFVCPTEIIAFSDRVHEFHAINTEVVACSVDS
S. aurata         SDYKGKYIVFFFYPLDFTFVCPTEIIAFSDRVHEFQAINTEVVACSVDS
L. crocea         SDYRGKYLVFFFYPLDFTFVCPTEIIAFSDRVHEFRAINTEVVACSVDS
M. miiuy          SDYRGKYLVFFFYPLDFTFVCPTEIIAFSDRVHEFRAINTEVVACSVDS
M. piceus         SDYKGKYLVFFFYPLDFTFVCPTEIIAFSDRVHEFQDINAEVVACSVDS
D. rerio          SDYKGKYLVFFFYPLDFTFVCPTEIIAFSDRVHEFQAINAEVVACSVDS
E. Lucius         SDYKGKYLVFFFYPLDFTFVCPTEIIAFSDHVHEFRAINAEVVACSVDS
T. fasciatus      SDYKGKYLVFFFYPLDFTFVCPTEIIAFSDRLHEFQAINTEVVACSVDS
O. niloticus      SDYKGKYLVFFFYPLDFTFVCPTEIIAFSDRLHEFQAINTEVVACSVDS
O. latipes        SDYKGKYLVFFFYPLDFTFVCPTEIIAFSDRVHEFRAINTEVVACSVDS
P. nyererei       SDYKGKYLVFFFYPLDFTFVCPTEIIAFSDRLHEFQAINTEVVACSVDS
P. reticulata     SDYKGKYLVFFFYPLDFTFVCPTEIIAFSDRVHEFQAINTEVVACSVDS
N. coriiceps      SDYKGKYLVFFFYPLDFTFVCPTEIIAFSDRVHEFKAINTEVVACSIDS
S. salar          SDYKGKYLVFFFYPLDFTFVCPTEIIAFSDRVHEFHAINAEVVACSVDS
C. gobio          SDYKGKYLVFFFYPLDFTFVCPTEIIAFSDRVHEFKDINTEVVACSIDS
E. lanceolatus    SDYKGKYLVFFFYPLDFTFVCPTEIIAFSDRVHEFQAINTEVVACSVDS
T. bernacchii     SDYKGKYLVFFFYPLDFTFVCPTEIIAFSDRVHEFKAINTEVVACSIDS
G. acuticeps      SDYKGKYLVFFFYPLDFTFVCPTEIIAFSDRVHEFKAINTEVVACSIDS
H. hippoglossus   SDYKGKYLVFFFYPLDFTFVCPTEIIAFSDRVHEFRAINTEVVACSIDS
P. pungitius      SDYKGKYLVFFFYPLDFTFVCPTEIIAFSDRMHEFQAINTEVVACSVDS
C. tularosa       SDYKGKYLVFFFYPLDFTFVCPTEIIAFSDRVHEFQAINTEVVACSVDS
M. salmoides      SDYRGKYLVFFFYPLDFTFVCPTEIIAFSDRVHEFRAINTEVVACSVDS
P. promelas       SDYRGKYLVFFFYPLDFTFVCPTEIIAFSDRVHEFRDINAEVVACSVDS
C. idella         SDYKGKYLVFFFYPLDFTFVCPTEIIAFSDRVHEFQDINAEVVACSVDS
O. eperlanus      SDYKGKYLIFFFYPLDFTFVCPTEIIAFSDRVHEFRAINADVVACSVDS
P. mariae         SDYKGKYLVFFFYPLDFTFVCPTEIIAFSDRLHEFQAINTEVVACSVDS
                  ***.***::**********************.:***. **::*****:**
```

```
S. cephalus          QFTHLAWINTPRKQGGLGPMKIPLLSDLSHQISKDYGVFLEDQGHTLRG
S. lalandi           QFTHLAWINTPRKQGGLGEMKIPLLSDLTHQISKDYGVYLEDQGHTLRG
S. aurata            QFTHLAWINTPRKQGGLGPMKIPLLSDLTHQISKDYGVYLEDQGHTLRG
L. crocea            QFTHLAWIITPRKQGGLGPMKIPLLSDLTHQISKDYGVYLEDQGHTLRG
M. miiuy             QFTHLAWINTPRKQGGLGPMKVPLLSDLTHQISKDYGVYLEDQGHTLRG
M. piceus            QFTHLAWINTPRRQGGLGPMKIPLLSDLTHQISKDYGVFLEDQGHTLRG
D. rerio             QFTHLAWINTPRKQGGLGPMKIPLLSDLTHQISKDYGVFLEDQGHTLRG
E. Lucius            QFTHLAWINTPRKQGGLGPMKIPLLSDLTHQISKDYGVFLEDAGHTLRG
T. fasciatus         QFTHLAWINTPRKQGGLGKMRIPLLSDLTHQISKDYGVYLEDQGHTLRG
O. niloticus         QFTHLAWINTPRKQGGLGKMKIPLLSDLTHQISKDYGVYLEDQGHTLRG
O. latipes           QFTHLAWINTPRKQGGLGEMKIPLLSDLTHQISKDYGVYLEDQGHTLRG
P. nyererei          QFTHLAWINTPRKQGGLGQMKIPLLSDLTHQISKDYGVYLEDQGHTLRG
P. reticulata        QFTHLAWINTPRKQGGLGPMKIPLLSDLTHQISKDYGVYLEDQGHTLRG
N. coriiceps         QFTHLAWINTARKEGGLGPMKIPLLSDLTHQISKNYGVYLEDQGHSLRG
S. salar             QFTHLAWINTPRKQGGLGPMKVPLLSDLTHQISKDYGVFLEDAGHALRG
C. gobio             QFTHLAWINTPRKQGGLGQMKIPLLSDLTHQISKNYGVYLEDQGHTLRG
E. lanceolatus       QFTHLAWINTPRKQGGLGPMKIPLLSDLTHQISKDYGVYLEDQGHTLRG
T. bernacchii        QFTHLAWINTARKEGGLGPMKIPLLSDLTHQISKNYGVYLEDQGHSLRG
G. acuticeps         QFTHLAWINTARKEGGLGPMKIPLLSDLTHQISKNYGVYLEDQGHSLRG
H. hippoglossus      QFTHLAWINTPRKQGGLGKMKIPLLSDLTHQISKDYGVYLEDQGHTLRG
P. pungitius         QFTHLAWINTPRKQGGLGPMRIPLLSDLTHQISKDYGVYLEDQGHTLRG
C. tularosa          QFTHLAWINTPRKQGGLGSMKIPLLSDLTHQISKDYGVYLEDQGHTLRG
M. salmoides         QFTHLAWINTPRKQGGLGPMKIPLLSDLTHQISKDYGVYLEDQGHTLRG
P. promelas          QFTHLAWINTPRKQGGLGPMKIPLLSDLNHQISKDYGVFLEDQGHTLRG
C. idella            QFTHLAWINTPRRQGGLGPMKIPLLSDLTHQISKDYGVFLEDQGHTLRG
O. eperlanus         QFTHLAWINTPRNQGGLGTMKIPLLSDLTHQIAKDYGVFLEDHGHTLRG
P. mariae            QFTHLAWINTPRKQGGLGQMKIPLLSDVTHQISKDYGVYLEDQGHTLRG
                     ******** *.*.:**** *.:*****:.***:*:***:*** **:***

S. cephalus          LFIIDDKGVLRQITMNDLPVGRSVDETLRLVQAFQYTDKHGEVCPAGWK
S. lalandi           LFIIDGKGILRQITMNDLPVGRSVDETLRLVQAFQYTDKHGEVCPAGWK
S. aurata            LFIIDGKGILRQITMNDLPVGRSVDETLRLVQAFQYTDKHGEVCPAGWK
L. crocea            LFIIDEKGVLRQITMNDLPVGRSVDETLRLVQAFQYTDKHGEVCPAGWK
M. miiuy             LFIIDEKGVLRQITMNDLPVGRSVDETLRLVQAFQYTDKHGEVCPAGWK
M. piceus            LFIIDDKGVLRQITMNDLPVGRSVDETLRLVQAFQYTDKHGEVCPAGWK
D. rerio             LFIIDGKGVLRQITMNDLPVGRSVDETLRLVQAFQYTDKHGEVCPAGWK
E. Lucius            LFIIDDKGVLRQITMNDLPVGRSVDETLRLVQAFQYTDKHGEVCPAGWK
T. fasciatus         LFIIDGKGILRQITMNDLPVGRSVDETLRLVQAFQYTDKHGEVCPAGWK
O. niloticus         LFIIDGKGILRQITMNDLPVGRSVDETLRLVQAFQYTDKHGEVCPAGWK
O. latipes           LFIIDNKGILRQITMNDLPVGRSVDETLRLVQAFQYTDKHGEVCPAGWK
P. nyererei          LFIIDGKGILRQITMNDLPVGRSVDETLRLVQAFQYTDKHGEVCPAGWK
P. reticulata        LFIIDGKGVLRQITMNDLPVGRSVDETLRLVQAFQYTDKHGEVCPAGWK
N. coriiceps         LFIIDDKGILRQITMNDLPVGRSVDETLRLVQAFQYTDKHGEVCPAGWK
S. salar             LFIIDDKGVLRQITMNDLPVGRSVDETLRLVQAFQYTDKHGEVCPAGWK
C. gobio             LFIIDDKGILRQITMNDLPVGRSVDETLRLVQAFQYTDKHGEVCPAGWK
E. lanceolatus       LFIIDGKGILRQITMNDLPVGRSVDETLRLVQAFQYTDKHGEVCPAGWK
T. bernacchii        LFIIDNKGILRQITMNDLPVGRSVDETLRLVQAFQYTDKHGEVCPAGWK
G. acuticeps         LFIIDDKGILRQITMNDLPVGRSVDETLRLVQAFQYTDKHGEVCPAGWK
H. hippoglossus      LFIIDDKGILRQITMNDLPVGRSVDETLRLVQAFQYTDKHGEVCPAGWK
P. pungitius         LFIIDDKGTLRQITMNDLPVGRSVDETLRLVQAFQYTDKHGEVCPAGWK
C. tularosa          LFIIDDKGILRQITMNDLPVGRSVDETLRLVQAFQYTDKHGEVCPAGWK
M. salmoides         LFIIDDKGILRQITMNDLPVGRSVDETLRLVQAFQYTDKHGEVCPAGWK
P. promelas          LFIIDDKGVLRQITMNDLPVGRSVDETLRLVQAFQYTDKHGEVCPAGWK
C. idella            LFIIDDKGVLRQITMNDLPVGRSVDETLRLVQAFQYTDKHGEVCPAGWK
O. eperlanus         LFIIDDKGVLRQITMNDLPVGRSVDETLRLVQAFQYTDKHGEVCPAGWK
P. mariae            LFIIDGKGILRQITMNDLPVGRSVDETLRLVQAFQYTDKHGEVCPAGWK
                     ***** ** ****************************************
```

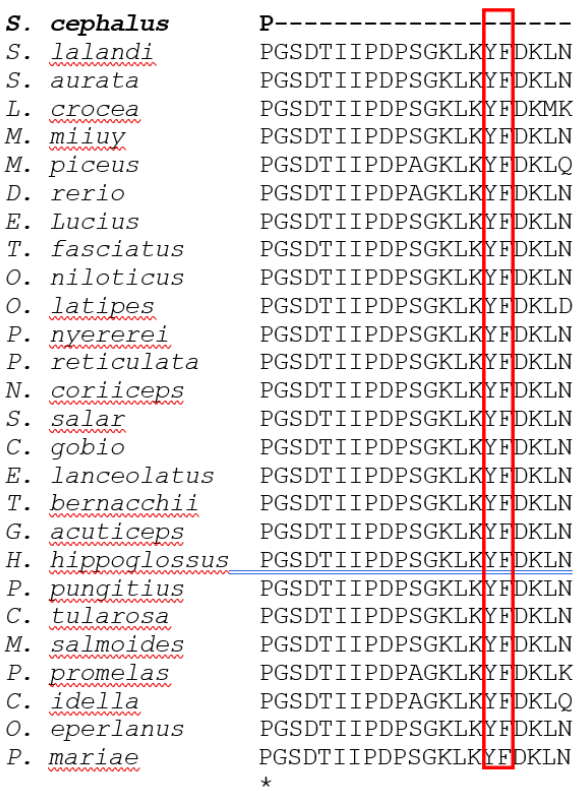

Figure 5.1.3.1 Multiple alignment of the amino acid sequence of *Squalius cephalus* with Prdx4 of other species of teleosts.

The cladogram obtained on the nucleotide sequences (Figure 5.1.3.2) is not entirely resolved, with an average posterior probability support of 87.5 % for all nodes in the BI analysis, and an average bootstrap support value of 56.3 % in the ML analysis. The sequences of the Cypriniformes (to which *S. cephalus* belongs) are closely related to each other and clearly separated from those of the other orders (posterior probability and bootstrap value of 100%).

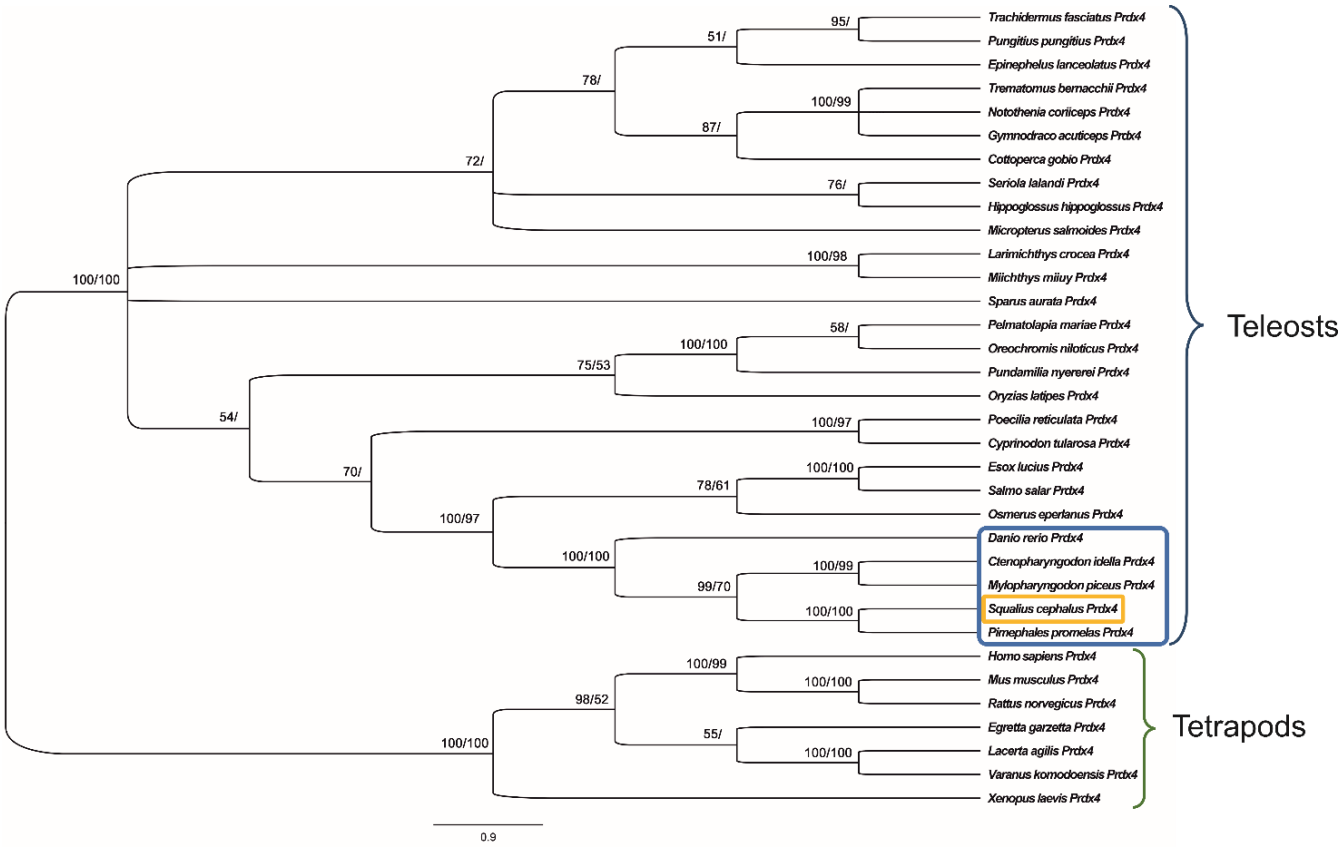

Figure 5.1.3.2 Phylogenetic relationships among Prdx4s of various organisms, reconstructed based on nucleotide sequences of the coding region and using both BI (arithmetic mean = - 9714.72; harmonic mean = - 9744.35) and ML (arithmetic mean = - 9683.35) methods. Posterior probability (first number) and bootstrap values (second number, if present) higher than 50 % are indicated on each node. The scale for branch length (0.9 substitution/site) is shown below the tree

Prdx4 gene expression in the kidney

From the results of prdx4 gene expression analysis (Figure 5.1.3.3), it is evident a statistically significant ($p < 0.001$) lower mRNA levels both at the "low polluted" site and at the "highly polluted" site compared to the "very low polluted" site. The decrease is 58% and 63.1%, respectively. No significant variation exists between the "low polluted" and "highly polluted" sites.

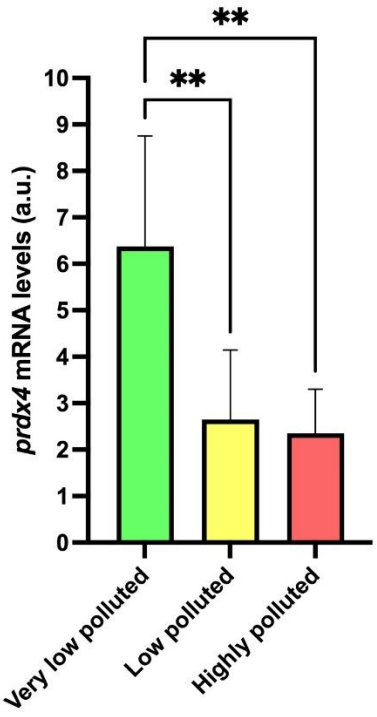

Figure 5.1.3.3 prdx4 mRNA expression levels in mean values (N=8) with relative standard deviations, illustrated by the error bars. Different colours represent the three sites: “very low polluted site” in green, “low polluted site” in yellow, and “highly polluted site” in red. Asterisks indicate a statistically significant difference from the “very low polluted” site (** $p < 0.001$).

Protein oxidation

The graph in Figure 5.1.3.4 shows a statistically significant increase ($p < 0.0001$) in AOPP levels of kidney tissue in both the “low polluted” and “highly polluted” sites compared to the “very low polluted” one (about 47% higher). There is no significant variation between the two polluted sites. Conversely, the graph of the skeletal muscle (Figure 5.1.3.4) shows a highly significant increase (about 137%; $p < 0.0001$) only in the “low polluted” site.

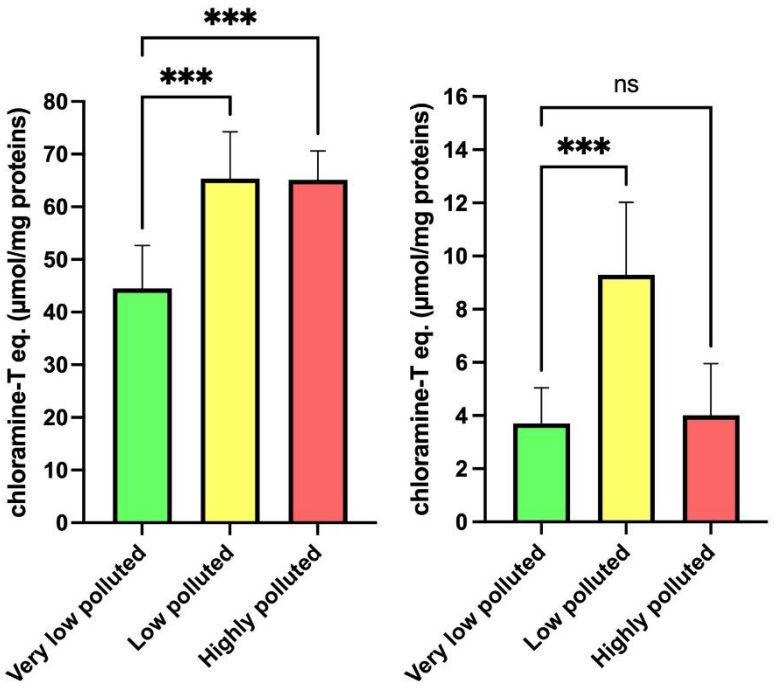

a) *b)*

Figure 5.1.3.4 . AOPP in kidney (a) and skeletal muscle (b) expressed in chloramine-T eq. (µmol/mg proteins), in mean values (N=8) with relative standard deviations. Different colours represent the three sites: "very low polluted site" in green, "low polluted site" in yellow, and "highly polluted site" in red. Asterisks indicate a statistically significant difference from the "very low polluted" site (*** $p < 0.0001$).

Lipid peroxidation

MDA levels measured in both "low polluted" and "highly polluted" sites did not statistically differ from the "very low polluted" site in kidney tissue (

Figure 5.1.3.5).The same pattern occurs in the skeletal muscle (

Figure 5.1.3.5), in fact the graph shows an absence of significant differences between all sites.

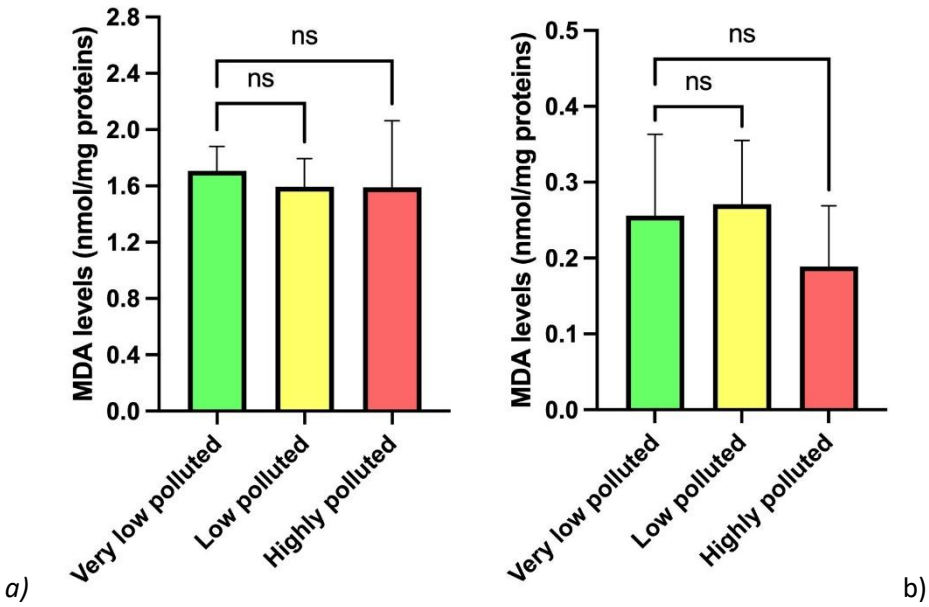

Figure 5.1.3.5 Lipid peroxidation in kidney (a) and skeletal muscle (b) expressed in MDA levels (nmol/mg proteins) and mean values (N=8) with relative standard deviations. Different colours represent the three sites: "very low polluted site" in green, "low polluted site" in yellow, and "highly polluted site" in red. ns indicates a not statistically different result from the "very low polluted" site

5.1.4 Discussion

The obtained sequence of the *prdx4* gene of *S. cephalus* consists of a partial coding sequence since both the C-terminal and N-terminal regions are incomplete. However, this part is predictable from the other teleosts' sequences due to its high homology degree, confirming the presence of all amino acids and structural motifs important for protein function. One of the structural motifs (YF) is contained in this C-terminal region. At the same time, the other one (GGLG) is located in the middle of the *prdx4* sequence, between the two catalytic cysteines and is part of the protein's loop region. Our results showed that these two motifs are conserved between all analysed species. From the literature, we know that they are conserved at a deeper phylogenetic level inside all the eukarya but differ in prokaryotic organisms (Wang et al., 2012). In eukaryotic organisms, these two structural motifs are responsible for the conformational change during the catalytic cycle and allow the formation of the disulphide bridge between the catalytic cysteines. They confer susceptibility at high levels of peroxides, guiding to inactivation and hyperoxidation (Bolduc et al., 2018).

Furthermore, our results showed the total conservation among all species of the three residuals of the catalytic triad (P, T and R). These are involved in the peroxidatic activity and the activation of the adjacent conserved cysteine (Hofmann et al., 2002). The sequence (FYPXDFTFVCPTEI), containing the catalytic centre, is conserved among all analysed species, including tetrapods. This result is explained by this region's fundamental role in the protein's functioning, containing the peroxidatic cysteine, which is responsible for the reduction of hydroperoxides (Bakiu and Santovito, 2015).

For the same reason, the sequence (GEVCPA) containing the resolving cysteine is fully conserved among all species, even tetrapods (Bakiu and Santovito, 2015). This residue is responsible for the recovery of the peroxidatic cysteine to a reduced state (Bolduc et al., 2018). Instead, the N-terminal region appears more variable and less conserved among species. This result is due to weaker selective pressures acting on this sequence. This region includes a signal peptide responsible for the transmembrane translocation of the enzyme to the ER lumen; it is rich in hydrophobic residues and before the end of the process it is removed from the enzyme through a peptidase (Zimmermann et al., 2011). This N-terminal region is the same that allows the secretion of the enzyme in the extracellular environment (Fujii et al., 2015). Also, the threonine

residual responsible for the phosphorylation of the enzyme is a common feature of all Prdx4s (Rhee and Woo, 2011).

The gene expression analysis results in the kidney show a down-regulation of *prdx4* transcriptional level with increased environmental PFAS concentration. A superficial assessment of this result might suggest that Prdx4 is less critical in antioxidant protection against oxidative stress risk in chronic PFAS exposure. This hypothesis is conceivable as we know the complexity of stress responses, which can involve the induction of several proteins alternatively and specifically activated at different extracellular and intracellular cellular sites (Piva et al., 2024; Schumann et al., 2024b). Therefore, in this case, we expect an intervention of other antioxidant defence components, such as other Prdxs isoforms, some GPx, or non-enzymatic components. Indeed, in the liver of the identical specimens, exposure to increased PFAS concentrations had led to increased transcription of the *sod2* gene, coding for mitochondrial superoxide dismutase (Piva et al., 2022). An alternative hypothesis to explain the down-regulation of *prdx4* would be related to steatosis, which is often found in organs where PFAS accumulate and which could represent a defence mechanism against the toxicity these substances exert on proteins.

Previous studies have demonstrated a positive correlation between lipid vacuolisation (steatosis) and PFAS accumulation in hepatocytes of various fish species, such as Padanian goby (*Padogobius bonelli*) (Piva et al., 2022). Similar correlations have been found in eels exposed to PFOA (Wolf and Wolfe, 2005), zebrafish exposed to PFOS (Du et al., 2017, Cheng et al., 2016), and rats exposed to PFOA and PFOS (Harper and Wolf, 2009). However, this correlation was not observed in common chub (Piva et al., 2022). The structural similarity between fatty acids and PFAS allows these substances to interact with PPAR receptors, found in the liver and kidney. PPARs regulate the transcription of genes involved in fatty acid metabolism, glucose homeostasis, and lipid uptake (Kiss-Toth and Roszer, 2008). This could explain the disruption of lipid homeostasis observed in tissues exposed to PFAS. The increasing lipid accumulation could appear as a forced consequence caused by the similar structure between PFAS and fatty acids. However, it could also be considered a defence mechanism to reduce the hydrophilicity of the intracellular environment, limiting PFAS bioaccumulation and reducing protein damage in highly polluted environments.

Prdx4 is specifically expressed in the endoplasmic reticulum (Valero et al., 2015), where it has two main functions: it acts as a scavenger against peroxides, and it inhibits the lipid accumulation in the cell (Yamada and Guo, 2018). By down-regulating the *prdx4* gene, the inhibition of cellular lipid accumulation would be blocked, initiating the vacuolisation process. However, it must be considered that only the liver was histologically analysed in this species to highlight steatosis, but we cannot exclude the possibility of lipid accumulation involving the kidney instead, as evidenced by studies in humans that have shown chronic kidney disease associated with PFAS exposure (Conway et al., 2018) and it is known that chronic kidney disease induces lipid dysmetabolism and lipid droplet accumulation in this organ (Mitrofanovaet al., 2023). There are certainly no data on fish, so it will be interesting to carry out studies in the future, perhaps using larger species than chub. Recent investigations have also demonstrated ectopic lipid deposition in the renal tubules concerning endoplasmic reticulum stress (Hosokawa et al., 2019).

The mechanism underlying lipid accumulation is known in mammals. Downregulation of prdx4 leads to the accumulation of misfolded proteins, activating the Unfolded Protein Response (UPR). This response regulates transcription factors such as ATF4 and XBP1, which directly influence lipid and glucose metabolism (Hetz et al., 2020). Furthermore, altered endoplasmic reticulum function can affect the secretion of lipoproteins, such as apoB, causing dyslipidaemia and steatosis (Conlon et al., 2016).

It is known that PFAS principally exert their toxicity against cytoplasmic proteins, which are purely hydrophilic molecules (Bangma et al., 2022). The absence of lipid peroxidation under conditions of PFAS exposure can be considered a common condition in many organs and tissues, as shown by data from the liver (Piva et al., 2022) and, in our work, the kidney and skeletal muscle (*Figure 4*).

Conversely, our results about AOPP levels show differences in oxidative stress responses between kidney and muscle tissues, which reveal complex and tissue-specific adaptive mechanisms. In the kidney, protein oxidation increases significantly at both “low” and “highly polluted” sites compared to the “very low polluted”, indicating heightened oxidative stress (*Figure 3a*). This suggests that even low PFAS concentrations are sufficient to promote the formation of ROS, which causes oxidative damage to proteins and that the damage remains even in chronic exposure conditions. It is plausible that the latter include enzymes involved in cellular oxidoreductive systems, resulting in altered ROS production. Given their short

half-life, it is conceivable that ROS oxidise primarily on the first molecules they encounter, i.e. the enzymes themselves. However, although significantly increased protein damage is present in the analysed kidneys from the most polluted sites, it is equally evident that the fish are healthy. The hypothesis is that they probably maintain high levels of antioxidant defences, avoiding even more significant molecular damage. This physiological response requires an extra investment of metabolic energy, which could affect these fish's life history (Souza et al., 2018).

An even higher level of PFAS (such as that present at the "highly polluted" site) did not determine a further increase in protein oxidation, probably because of the activation of the antioxidant system or other defence mechanisms. For example, by increasing the amount of fat inside the cell, the hydrophilicity of the intracellular environment is reduced, decreasing the potential of PFAS bioaccumulation in this tissue (Yoo et al., 2009). Therefore, the interaction between PFAS and the protein component becomes less probable. This hypothesis stems from the evidence that *in vitro* PFAS are able to bind to both of these types of molecules non-specifically and with very similar affinities (Qin et al., 2023).

This feature concerning the kidney cannot be extended to other tissues. In fact, AOPP levels in muscle tissue present a different pattern, increasing at the low-polluted site but decreasing at the "highly polluted" site compared to the "very low polluted" (*Figure 3b*). This trend suggests a negative feedback mechanism or adaptive response in muscle tissue at higher PFAS concentrations. The decrease in AOPP levels at the "highly polluted" site could indicate upregulated antioxidant defences or a shift in metabolic processes that mitigate oxidative damage, already shown in other freshwater fish exposed to environmental contaminants including PFAS (Houde et al., 2014; Michailidou et al., 2024), demonstrating tissue-specific responses to environmental pollutants. These findings highlight the differential sensitivity and adaptive capacity of various tissues, with the kidney experiencing direct oxidative stress, while muscle tissues may deploy alternative protective mechanisms.

Although we did not measure PFAS concentrations in the kidney, total PFAS concentrations in the skeletal muscle were found to be 1.4 µg/kg dry wt in the "very low polluted", 6.64 µg/kg dry wt at the "low polluted" site, and 41.16 µg/kg dry wt in the liver at the "highly polluted" site (Schumann et al., 2024b). As a reference, PFAS concentrations in the liver reached 303.64 µg/kg dry wt at the "highly polluted" site, 38.98 µg/kg dry wt at the "low polluted" site, and 12.45 µg/kg dry wt at the "very low polluted" site (Schumann et al., 2024b). These values confirm that the liver is the primary site of PFAS bioaccumulation, likely due to its role in lipid metabolism and detoxification. Given the structural and functional characteristics of the kidney and its immune function, it is plausible that PFAS accumulation in the kidney could mirror or even exceed that of muscle tissue, as happens in other freshwater fish (Goeritz et al., 2013; Surma et al., 2021) From these data, a correlation between PFAS concentration and the physiological parameters analysed is not evident. This finding was expected as cells may respond qualitatively differently depending on the presence of the inducing factor, in particular when it comes to antioxidant defences. Indeed, it is well known that certain antioxidant proteins (less performing but fast-activating, such as superoxide dismutases and metallothioneins) are considered the first line of defence against oxidative stress (Bakiu et al., 2022; Trentin et al., 2025), while others (with greater scavenger activity but delayed activation such as catalase and some isoforms of glutathione peroxidase) come into play later (Tolomeo eat al., 2022; Pacchini et al., 2023).

Additionally, our study did not show any significant correlation between the measured parameters (MDA or AOPP levels or gene expression) and the fish's sex. This suggests that PFAS-induced oxidative stress and physiological responses are independent of sex in *S. cephalus*, indicating that both males and females are equally affected by PFAS contamination.

5.2 Physiological responses of European chub (*Squalius cephalus*) to chronic PFAS pollution

5.2.1 Introduction

In 2013, a significant industrial PFAS contamination of surface water and groundwater was discovered in the Veneto region, Italy (Giglioli et al., 2023). According to annual monitoring data from the Regional Agency for Environmental Prevention and Protection of Veneto (ARPA Veneto, 2025), the presence of PFAS in

freshwater streams continues to be assiduous, making it necessary to investigate the ability of organisms to cope with the stress induced by prolonged exposure to PFAS (Vaccari et al., 2024).

Among the species currently subjected to this anthropogenic impact is *Squalius cephalus*, also known as European chub, a pelagic freshwater fish abundant throughout Europe, commonly used as a target species in ecotoxicological studies (Molbert et al., 2019; Sunjog et al., 2019; Staszny et al., 2021). *S. cephalus* specimens typically live 15 years, with males becoming fertile at 2–4 years and females at 4–6 years (Nyeste et al., 2024).

Our previous study showed that PFAS contamination in rivers of the Veneto region led to a significant increase in transcript levels of *gpx-4* and *sod-2*, two genes encoding mitochondrial antioxidant enzymes, in the liver of *S. cephalus* and another species, *Padogobius bonelli*. The results suggested that oxidative stress, which could lead to lipid peroxidation due to chronic PFAS exposure, was controlled in this organ by the antioxidant system at the mitochondrial level (Piva et al., 2022). The adequate protection of lipids from PFAS was also confirmed by analyses performed on the kidney of *S. cephalus*, in which, however, protein oxidation was detected also at low PFAS concentrations (Pacchini et al., 2025b). In this case, the gene encoding the isoform 4 of peroxiredoxins (*prdx4*) appeared not to be involved in the antioxidant defences, probably carried out by other components of the antioxidant system. Further analyses also revealed high stress levels in the muscle and blood of *S. cephalus* and *P. bonelli* (Schumann et al., 2024), underscoring the need to extend the investigation of responses against PFAS to other organs and genes.

Glutathione peroxidases (GPxs) and catalase (CAT) act mainly in H_2O_2 scavenging. GPxs reduce organic and inorganic peroxides to hydroxyl compounds, using glutathione (GSH) or other equivalents as reducing factors. Among the known eight GPx isoforms in humans, three are monomeric, i.e. GPx-4, -7 and -8, and the remaining five are homotetrameric. GPx-3, -6 and -7 are the only extracellular isoforms; the others are intracellular. Among the latter, isoform 4 is the only one present in mitochondria. The first four isoforms and GPx-6 are selenium (Se)-dependent, as they present a selenocysteine residue encoded by the stop codon TGA (Brigelius-Flohé and Maiorino, 2013; Ferro et al., 2020; Pacchini et al., 2025a). While GPx-4 can reduce complex fatty acid, phospholipid, and cholesterol hydroperoxides, including those inside membranes, GPx-1, -2, and -6 are supposed to react with less complex, soluble, but also small fatty acid hydroperoxides (Trenz et al., 2021). Unlike GPxs, CAT exists as a single isoform in animals that can be distinguished into three classes based on its sequence and structural differences. The monofunctional heme-containing enzyme is the most widespread CAT in all aerobic organisms. The bifunctional CAT-peroxidase belongs to the second class, which also contains the heme group but is relatively less abundant in nature and closely related to plant peroxidases. The third class belongs to the Mn-containing CAT group that lacks the heme group (López et al., 2024). CAT is a tetrameric protein that can cleave two H_2O_2 molecules into two water molecules and one oxygen molecule, acting mainly within peroxisomes. CAT has been reported to be implicated in mutagenesis, inflammatory conditions, and the suppression of apoptosis, all of which are known to be associated with oxidative stress conditions (Nandi et al., 2019).

The present work aims to gain a deeper understanding of how the components of the antioxidant system interact to counteract the adverse effects of PFAS in *S. cephalus* on the liver and caudal kidney. *S. cephalus* specimens were collected from four rivers characterised by different concentrations of total dissolved PFAS, from < 10 ng/l (control site) to over 1000 ng/l (highly-polluted site). The antioxidant molecular markers considered in this study were GPx isoforms 1 and 4 and CAT. Both gene expression and enzyme activity were assessed in the liver and caudal kidney, organs known for their roles in the bioaccumulation of pollutants in fish and detoxification processes, as they filter contaminants from the bloodstream and metabolise them for elimination, primarily via urine (Collard et al., 2018; Macorps et al., 2022).

Additionally, to better study the acclimatisation to the environment, the morphological characteristics of the fish were also examined, as well as the development of their organs, calculating the hepatosomatic index (HSI), Fulton's condition factor (FCF) and the spleen somatic index (SSI). Finally, liver and caudal kidney tissues were chemically analysed to verify if PFAS accumulation increased proportionally to the increase in PFAS concentration in the environment, and were examined by hematoxylin and eosin staining to highlight cellular damage and lipid content.

5.2.2 Materials and methods

Fifteen specimens of *S. cephalus*, 25 ± 6 cm in length, were sampled by electrofishing (authorised by decree of the director of the Agri-environment, Planning, and Management of Fish and Wildlife Hunting of the Veneto Region, n. 384 of May 17th 2024) in April 2024, from four selected freshwater streams. The sampling sites are drainage basins in agricultural areas of the Vicenza province (Veneto region, northeastern Italy) with different concentrations of total dissolved PFAS (i.e. PFBA, PFPeA, PFHxA, PFHpA, PFOA, PFNA, PFDA, PFUnDA, PFDoDA, PFBS, PFHxS, PFOS), and with other dissolved pollutants, such as metals and pesticides volatile organic compounds, at negligible concentration (< 10 ng/l), according to ARPAV periodic monitoring data measured over 2022–2023 (ARPA Veneto, 2025). Long-term industrial emissions of PFAS in the province of Vicenza were first identified in 2013 and attributed to the Rimar-Miteni plant, located in Trissino. Wastewater from the facility was discharged into the Agno-Fratta-Gorzone river system, leading to widespread downstream dispersion of PFAS through a complex hydrological network (Castiglioni et al., 2015). The Rimar-Miteni plant ceased operations and was declared bankrupt in November 2018. Following this, the Veneto Region launched extensive environmental monitoring programs to assess PFAS levels in surface and groundwater (World Health Organization Regional Office for Europe, 2017).

Considering the limit of quantification (LOQ) of 500 ng/l for total PFAS established by the Directive (EU) 2020/2184 of the European Parliament and of the Council of December 16th 2020, on the quality of water intended for human consumption, we named the four sampling sites as follows: control site (total PFAS < 10 ng/l), low-polluted site (total PFAS at 10-500 ng/l), medium-polluted site (total PFAS at 500-1000 ng/l), and highly-polluted site (total PFAS > 1000 ng/l) (Table 5.2.1Table 5.2.1 Total PFAS average concentration in freshwater from the four sampling sites, measured by ARPAV in 2022 and 2023. The Gauss-Boaga coordinates, obtained with qGIS (version 3.22) software, are reported for the geo-localisation of the sites.).

Table 5.2.1 Total PFAS average concentration in freshwater from the four sampling sites, measured by ARPAV in 2022 and 2023. The Gauss-Boaga coordinates, obtained with qGIS (version 3.22) software, are reported for the geo-localisation of the sites.

Sampling sites	Gauss-Boaga coordinates	Total PFAS average concentration (ng/l)
Control site (Roggia Moneghina)	X: 1707494.771; Y: 5043242.570	< 10
Low-polluted site (Fosso Brenta)	X: 1688840.326; Y: 5047241.734	185.263
Medium-polluted site (Scolo Togna)	X: 1685003,474; Y: 5029108,091	855.704
Highly-polluted site (Torrente Poscola)	X: 1686344.594; Y: 5046652.211	1116.14

The study area, represented in Figure 5.2.2.1 , was georeferenced in QGIS (v. 3.22) using the Gauss–Boaga coordinate system (EPSG: 3003/3004) (Table 5.2.1), in accordance with ARPAV data standards: the control site, located in Grumolo delle Abbadesse (VI), corresponds to the Roggia Moneghina (Bacchiglione river basin); the low-polluted site, located in Sovizzo (VI), corresponds to the Fosso Brenta (Bacchiglione river basin); the medium-polluted site, located in Lonigo (VI), corresponds to the Scolo Togna (Fratta-Gorzone river basin); the high-polluted site, located in Trissino (VI), corresponds to the Torrente Poscola (Fratta-Gorzone river basin). The medium-polluted site is historically known to receive industrial discharges from the former Rimar–Miteni plant, the highly-polluted one is where the Rimar–Miteni plant was located.

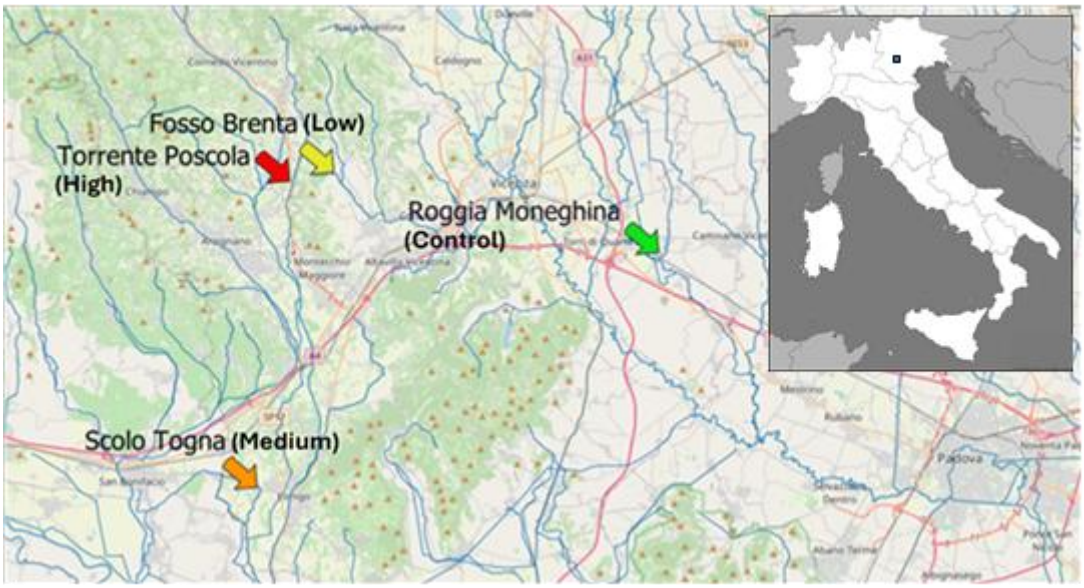

Figure 5.2.2.1 Map of the study area in the Veneto region (Vicenza province), showing Roggia Moneghina as control site, Fosso Brenta as low-polluted site, Scolo Togna as medium-polluted site, and Torrente Poscola as highly-polluted site, indicated by green, yellow, orange, and red arrows, respectively. Gauss-Boaga coordinates of the sites are reported in Table 5.2.1

The sampled fish, after being euthanised with an overdose of essential clove oil prepared in water-soluble form by dilution with ethyl alcohol (concentration 7 µL/L), were stored on ice and immediately transferred to the Department of Biology of the University of Padua to proceed with the dissection and the removal of organs.

Before dissection, all specimens were weighed and measured for total body length. The liver, caudal kidney, intestine, gills, gonads, spleen, heart, brain, white muscle, and tail were removed from the fish. The sex of the individuals, all of fertile age, was assigned through macroscopic observation of the gonads. The liver and spleen were weighed to calculate the HSI and SSI indices, respectively. All the dissected organs were frozen in liquid nitrogen and stored at –80°C for future molecular, biochemical and chemical analyses. In addition, for histological analyses, part of the dissected organs was fixed in Karnovsky's solution (4% paraformaldehyde, 0.1% glutaraldehyde in 0.2 M cacodylate buffer containing 1.7% NaCl, pH 7.4), dehydrated in 80% ethanol and stored at -20°C. In the present study, the molecular and fat accumulation responses to PFAS-induced stress were analysed in the liver and caudal kidney of S. cephalus.

Primers for selection (100-200 nt) and quantification of cat and gpx-1 expressions by quantitative real-time PCR (qRT-PCR) (Table 4) were designed on the coding sequences (CDSs) of the respective genes of Pimephales promelas, collected from NCBI database (accession number for cat: XM_039669564.1; accession number for gpx-1: XM_039688995). P. promelas is a fish of the Cyprinidae family, phylogenetically close to S. cephalus. After checking primer parameters by IDT Oligo Analyser tool (https://www.idtdna.com/calc/analyzer), primers for cat and gpx-1 were synthesised by Merck Life Science S.r.l. (Milan, Italy). Primers for gpx-4 and gapdh (housekeeping gene), reported in Table 5.1.1, were the same as those used in our previous study (Piva et al., 2022).

Table 5.2.2 Primer sequences used for qRT-PCR. For all the primers, 60°C was used as the annealing temperature.

Primers	Sequences 5'-3'
CAT_RT_forward	GCGTCCTGAATCGTTGCACCA
CAT_RT_reverse	TGACCCTCAGCGTTGACCAGT
GPx1_RT_forward	TCCATTCCCATTCGATGACCCAAT

GPx1_RT_reverse	GGCACTCCATCAGAACCGATAAGA
1_FW_GPx4_CAV_RT	AGCGGACATAAAGGAGTTTGCT
1_RV_GPx4_CAV_RT	CCTCTTCACGACCCGACCTT
sq_GAPDH_b_fw	ATCACAGCCACACAGAAGAC
sq_GAPDH_b_rv	AGGAATGACTTTGCCCACAG

Total RNA was extracted from the liver and caudal kidney tissues of eight specimens from each sampling site, using PRImeZOL (Canvax) as a lysis buffer according to the manufacturer's protocol. Total RNA extracted from liver tissues was purified with 8 M lithium chloride to remove carbohydrate contaminants (Bakiu et al., 2022a); further purification of all RNA samples was performed with the RQ1 RNase-Free DNase (Promega) kit to remove any possible genomic contamination. Total RNA concentration and purity were assessed with the Nanodrop ND-1000 spectrophotometer (Thermo Fisher Scientific), and its integrity and the absence of genomic DNA contamination were verified through electrophoresis on a 1% agarose gel.

Reverse transcription from 1 µg of each extracted total RNA was performed with the BiotechRabbit cDNA Synthesis Kit, which includes Oligo (dT) primer for selecting poly(A) tailed mRNA.

The obtained cDNAs were checked by qualitative PCR performed with 2X YourTaq PCR Master Mix (BiotechRabbit) kit, and the primers reported in Table 4, on a SimpliAmp Thermal Cycler (Applied Biosystems). Amplicons corresponding to *cat*, *gpx-1*, *gpx-4*, and *gadph* were visualised on a 1.5% agarose gel, and amplicons obtained for *cat* and *gpx-1* were gel-purified with Wizard SV Gel and PCR Clean-Up System (Promega) kit and validated by sequencing, performed by Eurofins genomics (Europe Shared Services GmbH, Ebersberg, Germany). The obtained *cat* and *gpx-1* sequences were checked with the BLAST tool (https://blast.ncbi.nlm.nih.gov/Blast.cgi).

Eight cDNAs (biological samples) from the liver and caudal kidney of *S. cephalus*, for each sampling site, were amplified with primers reported in Table 4, according to qPCRBIO SyGreen Mix Separate-ROX (PCR Biosystems) kit instructions. ROX concentration in the reaction mix, used as a quencher, was adjusted to 100 nM. qRT-PCR analysis of *cat*, *gpx-1*, *gpx-4*, and *gapdh* (housekeeping gene) was performed on a 7500 Real-Time PCR Systems (Applied Biosystems) thermal cycler according to the following amplification thermal profile: 95 °C for 2 min, 38 cycles at 95 °C for 20 s and 60 °C for 1 min (amplification plot), and, finally, 95 °C for 15 s, 60 °C for 1 min, 95 °C for 15 s, and 60 °C for 15 s (melting curve). First, primer amplification efficiency was verified by absolute quantification using scalar-diluted cDNAs. Each cDNA (< 100 ng) was run three times (technical triplicate), and the melting profile was analysed to verify the absence of genomic contamination.

Relative values obtained by qRT-PCR were used in the $2^{-\Delta\Delta CT}$ Pfaffl mathematical model (Pfaffl, 2001). Transcription levels were normalised to those of the housekeeping gene to compensate for variations in the amounts of cDNA.

Liver and caudal kidney tissues were homogenised in a buffer containing 10 mM Tris-HCl (pH 7.6), 1 mM EDTA, 1 mM dithiothreitol, 0.5 M sucrose, and 0.15 M KCl, with the Kinematica Polytron PT-MR 3000 Homogeniser. After centrifugation at 13000 ×*g* for 1 h at 4°C, cell-free extracts were analysed for total soluble proteins (mg/mL) by the Folin phenol reagent method (Lowry et al., 1951). To do this, a calibration curve was first built using scalar concentrations of bovine serum albumin as standards. Total protein concentrations were used to normalise the data of CAT and Se-GPx activities.

CAT activity was determined using Aebi's method (Aebi, 1984). The decrease in absorbance in 1 mL reaction mix, containing 50 mM potassium phosphate buffer (pH 7.0), 10 mM H_2O_2, and 30 µl of the cell-free extract, was measured at 240 nm for 1 min and expressed as units of CAT/mg proteins. One unit of CAT was defined as the amount of enzyme catalysing the scavenging of 1 µmol of H_2O_2/min.

Livingstone's method was applied to measure the Se-GPx activity in cell-free extracts (Livingstone et al., 1992). 900 µl of the mixture were prepared, containing 100 µl of cell-free extract in 50 mM potassium phosphate buffer (pH 7.0), 1 mM EDTA, 1 mM sodium azide, 0.2 mM NADPH, 1 U/mL of glutathione reductase, and 1 mM GSH; 100 µl of 20 mM H_2O_2 were added to initiate the reaction. The decrease in NADPH concentration was recorded at 340 nm in 5 min. Data were expressed as units of Se-GPx/mg

proteins, where one unit of Se-GPx was defined as the amount of enzyme catalysing the oxidation of 1 µmol GSH/min.

Dehydration of liver and caudal kidney of fish (biological duplicate) from control and highly-polluted sites was completed in ethanol 100% and, before proceeding with embedding in Paraplast X-TRA (Tyco Kendall), organs were treated with xylene for 1 h. 5 µm of histological sections were obtained with a Leica Reichert-Jung 2040 Autocut microtome and left to adhere to microscope glass slides (Menzel-Glaser, ThermoFisher Scientific). Tissue sections were deparaffinised in xylene and gradually rehydrated through a descending ethanol series. Sections were stained in hematoxylin solution (Sigma-Aldrich) for 1 min and subsequently rinsed under running tap water for 15 min. Staining was continued with 1% eosin Y (Sigma-Aldrich) in 80% ethanol for 30 s. Dehydration of the sections was rapidly completed in 100% ethanol, followed by a brief treatment with xylene. Finally, the sections were mounted with Eukitt (Electron Microscopy Sciences) and examined under the Olympus CX31 light microscope to assess morphological changes and lipid content.

PFAS effects on the physiology of *S. cephalus* were also evaluated by calculation of the following somatic indices (Singh and Reddy, 1990; Nilsson et al., 1996; Martínez et al., 2004):

HSI (g/g) = (liver weight / total body weight) ×100

SSI (g/g) = (spleen weight / total body weight) ×100

FCF (g/cm) = [total body weight / (total length of the individual)^3] ×100

Pure PFAS analytical standards, including the ^{13}C-labeled standards $^{13}C_2$-PFOA and $^{13}C_4$-PFOS, were obtained from Wellington Laboratories (Guelph, Ontario, Canada). Ultrapure water was freshly produced on each day of analysis using a Sartorius system (Milan, Italy). PFAS quantification was performed by ultra-high-performance (UHP) liquid chromatography (LC) coupled with tandem mass spectrometry (MS/MS).

Fish tissues were pre-treated following the approach described by Gasparini et al. (2024), with slight modifications. Briefly, 50 µL of an internal standard mixture, comprising 100 ng/mL of $^{13}C_2$-PFOA and $^{13}C_4$-PFOS in water, was added to 5 g of fish tissue (biological duplicate/triplicate when possible) to assess bioaccumulation. Then, 2.5 mL of 200 mM sodium hydroxide and 10 mL of methanol were added to each sample, which was then homogenised using an Ultraturrax (IKA, Staufen, Germany). After homogenisation, 150 µL of 4 M hydrochloric acid was added and samples were agitated on a vortex mixer, then centrifuged at 10,000 ×*g* for 10 min. A solid-phase extraction using Oasis GCB/WAX cartridges (6 mL, 150 mg, 30 µm; Waters, Milford, MA, USA) was performed to extract target analytes from tissue cell-free extracts. Cartridges were conditioned with 4 mL of methanol and 4 mL of water. Then, 8 mL of tissue supernatant or 50 mL of water sample was loaded, and cartridges were washed with 4 mL of 2% formic acid in water, followed by 4 mL of methanol. Target analytes were eluted with 3 mL of 1% ammonium hydroxide in methanol. The eluates were evaporated under a gentle nitrogen stream at 45 °C, reconstituted in 200 µL of an 80:20 (v/v) water:methanol solution, and transferred into polypropylene vials for UHPLC-MS/MS analysis.

The system consisted of an Acquity UPLC binary pump (Waters, Milford, MA, USA), equipped with the perfluorinated compounds isolation kit to avoid background contamination. Chromatographic separation was performed using a Waters Acquity UPLC BEH C18 column (50 × 2.1 mm, 1.7 µm), maintained at 40 °C. The mobile phase consisted of 5 mM ammonium acetate in water and methanol at a flow rate of 0.3 mL/min under programmed conditions. The UPLC was interfaced to an XEVO TQ-S Micro triple quadrupole mass spectrometer (Waters, Milford, MA, USA), set in negative electrospray ionisation mode with a capillary voltage of -0.50 kV. The source and desolvation temperatures were 150°C and 500 °C, respectively; the cone gas was set at 50 L/h, and the desolvation gas at 900 L/h, while argon was used as the collision gas. The specific transitions monitored for each analyte, along with the corresponding cone voltage (CV) and collision energy (CE) values, are reported in Table 5.2.3. Data were acquired and processed using MassLynx 4.2 software (Waters, Milford, MA, USA).

Table 5.2.3 Optimized mass transitions for PFAS and their internal standards, with corresponding cone voltage and collision energy. The first transition was used for quantification and the second for confirmation

Analyte	MRM transitions (*m/z*)	Cone voltage (V)	Collision energy (eV)
PFBA	212.0 > 169.0 212.0 > 64.7	8 8	7 22
PFBS	299.0 > 79.9 299.0 > 98.9	22 22	28 28
PFPeA	263.0 > 219.0 263.0 > 69.0	6 6	7 32
PFHxA	313.0 > 269.0 313.0 > 118.9	10 10	7 18
PFHxS	399.0 > 79.9 399.0 > 98.9	20 20	36 34
PFHpA	363.0 > 319.0 363.0 > 169.0	15 15	8 16
PFOA	412.9 > 369.0 412.9 > 169.0	15 15	9 18
PFOS	498.0 > 98.9 498.0 > 79.9	30 30	40 45
PFNA	463.0 > 418.9 463.0 > 218.9	20 20	9 15
PFDA	512.8 > 469.0 512.8 > 218.9	20 20	10 17
GenX	285.0 > 169.0 285.0 > 118.9	12 12	7 28
$^{13}C_2$-PFOA	415.0 > 370.0	20	9
$^{13}C_4$-PFOS	503.0 > 80.0	20	9
$^{13}C_3$-GenX	286.0 > 169.0	12	9

During each day of analysis, method validation was carried out directly in the sample matrix (a pooled homogenate of various tissues) using the matrix standard addition approach. Calibrators (range: 0.005–5.0 µg/kg) and quality control (QC) samples at four concentration levels (0.005, 0.2, 1.0, and 5.0 µg/kg), containing all target analytes, were freshly prepared to assess the method's performance in terms of specificity, linearity, precision, and accuracy. Peak area ratios between analytes and internal standards were plotted against the corresponding concentrations, and a linear least squares regression model was applied. All calibrators had to be within ±15% of their nominal values, and the resulting correlation coefficient (r^2) had to be ≥ 0.99. All QC samples had to confirm the good accuracy (within ±15%) and precision (coefficient of variation < 15%) of the method for all analytes. The limit of quantification (LOQ) for all PFAS was set at 5 µg/kg, and the limit of detection (LOD) was defined as 2 µg/kg. The recovery was within 93–107 % for all compounds. The use of isotopically labelled internal standards minimised matrix effects and further improved the reliability of quantification, confirming the robustness and validity of the method.

Finally, specificity was proved by the absence of chromatographic signals at the retention times of the target analytes in blank samples, even after the injection of the highest-concentration calibrators.

For all analyses, data were expressed as means ± standard deviations for each sampling site, with eight biological samples (n = 8), and statistically compared using the JASP program (Version 0.19). Although the number of specimens analysed is limited, it remains consistent with sample sizes commonly employed in stress physiology research and is sufficient to generate meaningful results (Weber et al., 2020; Solé et al., 2021; Atli et al., 2024)

After checking the variance's uniformity with Levene's test ($p > 0.05$), a one-way variance analysis (ANOVA) was applied, followed by Tukey's test to analyse statistically significant ($p < 0.05$) differences among the means.

5.2.3 Results

Due to the limited availability of tissue samples, PFAS concentrations could not be measured in the organs of the single specimens, but it was necessary to pool tissues from 8 fish per site. This approach, although reducing replication and preventing formal statistical analysis, is a common and accepted practice in bioaccumulation studies when sample sizes or tissue amounts are limited (Smith et al., 2018; Jones and Lee, 2020). Therefore, the results presented here should be considered as indicative rather than statistically conclusive.

As shown in Table 5.2.4, PFOS was the predominant PFAS accumulated in both liver and caudal kidney of S. cephalus, followed by perfluorodecanoic acid (PFDA). In the liver and caudal kidney, the accumulation of these two PFAS progressively increased from the control site to the highly polluted site. In particular, PFOS concentrations in the liver increased nearly tenfold, while PFDA levels rose more than fivefold.

In the caudal kidney, PFOS concentrations at the highly polluted site were approximately five times higher than those at the control site, whereas PFDA showed a sixfold increase.

Table 5.2.4 Concentrations of different PFAS compounds were detected in the organs of S. cephalus from the four sampling sites (the total environmental PFAS average concentration, as referenced in Table 3, has been reported). Due to insufficient tissue availability, samples from 8 specimens were pooled. Dashes (-) indicate PFAS not detected.

SITES AND TOTAL PFAS	ORGANS	PFOS (µg/l)	PFOA (µg/l)	PFDA (µg/l)	PFNA (µg/l)	PFHxS (µg/l)	PFBS (µg/l)
CONTROL (< 10 ng/l)	Liver	7.58	-	4.00	-	-	-
	Caudal kidney	14.29	-	5.38	-	-	-
LOW-POLLUTED (185 ng/l)	Liver	-	0.43	2.24	-	-	-
	Caudal kidney	-	1.33	4.11	-	-	-
MEDIUM-POLLUTED (856 ng/l)	Liver	55.40	0.36	3.31	0.062	0.95	0.067
	Caudal kidney	41.87	1.84	10.12	0.25	0.52	0.030
HIGHLY-POLLUTED (1116 ng/l)	Liver	72.78	0.64	21.67	-	0.55	0.15
	Caudal kidney	70.54	0.96	32.90	-	-	-

Statistically significant decreases (53% and 37%, respectively) in cat transcription levels were observed in the liver of S. cephalus only for the low- and medium-polluted sites compared to levels measured for the control site (Figure 5.2.3.1). No statistically significant variation in cat mRNA expression levels was observed in the caudal kidney of fish from the polluted sites with respect to fish from the control site.

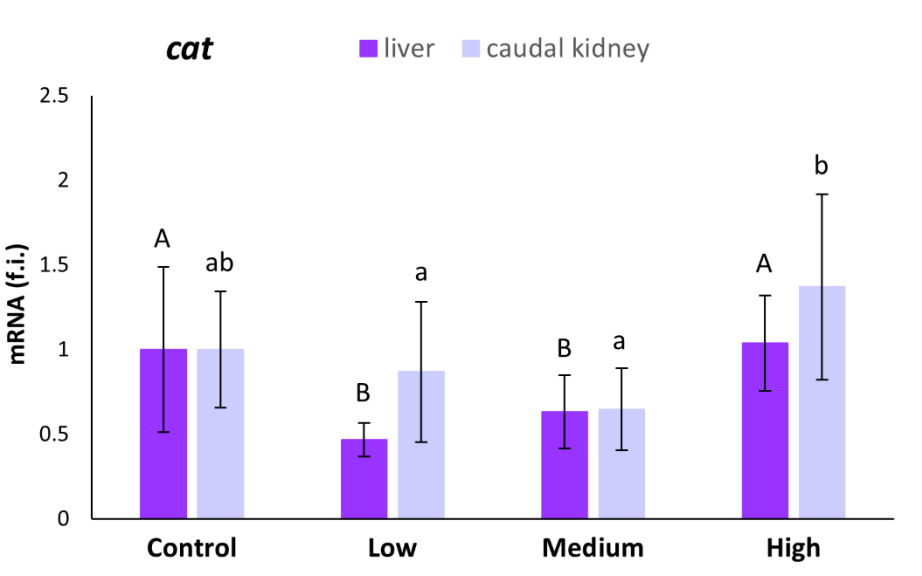

Figure 5.2.3.1 Relative expression levels (fold induction, f.i.) of the cat mRNA in the liver and caudal kidney of S. cephalus specimens from the four sampling sites (control, low-polluted, medium-polluted, highly-polluted). Transcription levels for the polluted sites were normalised with respect to those for the control site (mean = 1). Different letters refer to statistically significant differences among the means ($p < 0.05$).

The *gpx-1* transcription levels were statistically higher in the liver of specimens from the highly-polluted site than in the liver of fish from the control site (140%) and the other two polluted sites (Figure 5.2.3.2). The same was observed for the medium-polluted site in the caudal kidney. For this site, *gpx-1* transcription levels increased by 124% with respect to levels in the kidney of fish from the control site (Figure 5.2.3.2).

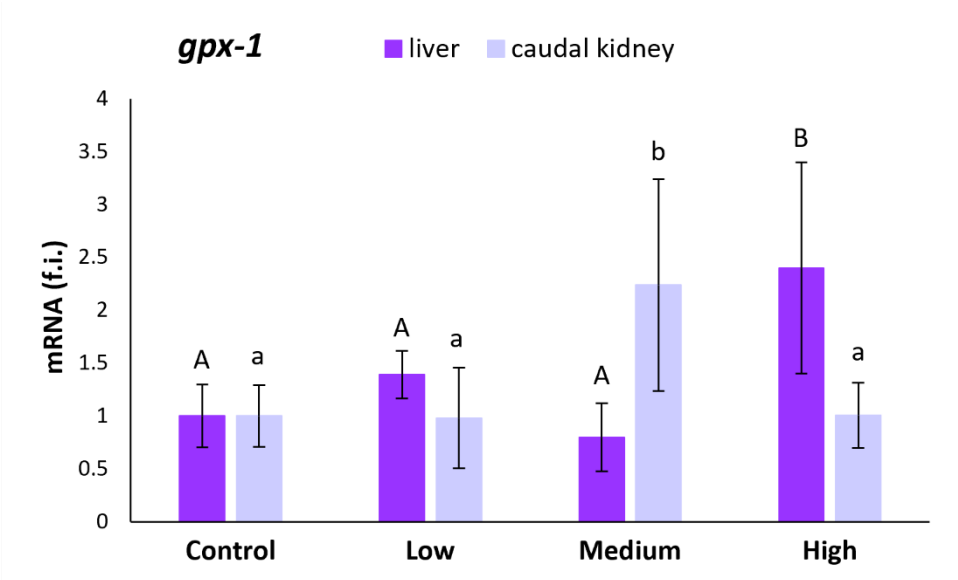

Figure 5.2.3.2 : Relative expression levels (fold induction, f.i.) of gpx-1 mRNA in the liver and caudal kidney of S. cephalus specimens from the four sampling sites (control, low-polluted, medium-polluted, highly-polluted). Transcription levels for the polluted sites were normalised with respect to those for the control site (mean = 1). Different letters refer to statistically significant differences among the means ($p < 0.05$).

The *gpx-4* mRNA expression levels in the liver statistically decreased (47%; $p < 0.05$) in specimens from medium-polluted ones with respect to fish from the control site. On the contrary, the liver samples from the highly-polluted site showed an increase of 204% (Figure 9). In the case of the caudal kidney, statistically significant increases ($p < 0.05$) in *gpx-4* expression levels, with respect to levels referred to the control site, were observed only for the low- (82%) and highly-polluted (112%) sites (Figure 5.2.3.3).

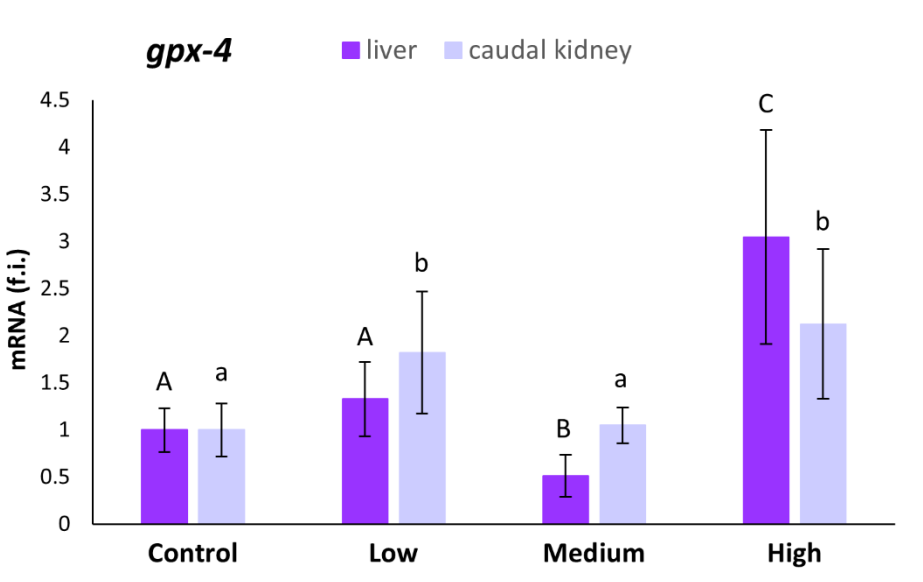

Figure 5.2.3.3 Relative expression levels (fold induction, f.i.) of gpx-4 mRNA in the liver and caudal kidney of S. cephalus specimens from the four sampling sites (control, low-polluted, medium-polluted, highly-polluted). Transcription levels for the polluted sites were normalised with respect to those for the control site (mean = 1). Different letters refer to statistically significant differences among the means ($p < 0.001$).

CAT activity in the liver of *S. cephalus* remained relatively constant in the specimens from the control and polluted sites (Figure 5.2.3.4). Inside the caudal kidney, the CAT activity statistically increased in specimens from the medium- (32%) and highly-polluted (39%) sites compared to fish from the control site (Figure 5.2.3.4).

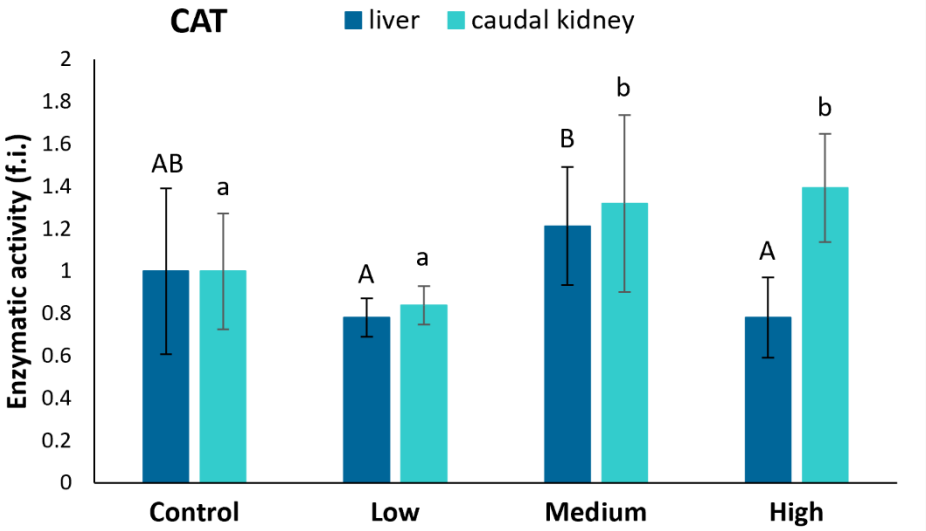

Figure 5.2.3.4 CAT activity (fold induction, f.i.) in the liver and caudal kidney of S. cephalus specimens from the four sampling sites (control, low-polluted, medium-polluted, highly-polluted). Active protein levels for the polluted sites were normalised with respect to those for the control site (mean = 1). Different letters refer to statistically significant differences among the means ($p < 0.05$).

No statistically significant differences were found among the four sampling sites regarding the Se-GPx levels in the liver (Figure 5.2.3.5). In the caudal kidney, the activity of Se-GPx showed statistically significant increases in fish from the low- (42%) and highly-polluted (35%) sites compared to fish from the control one (Figure 5.2.3.5).

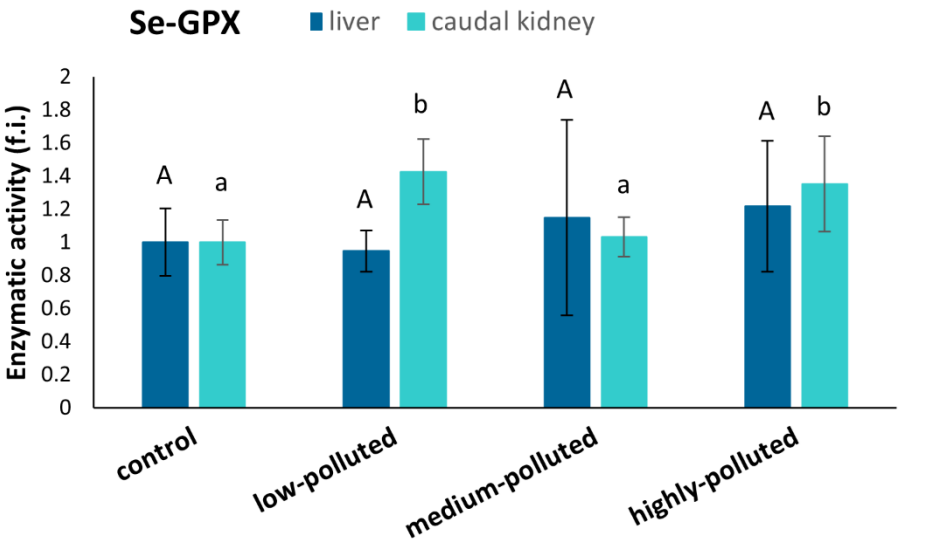

Figure 5.2.3.5 Se-GPx activity (fold induction, f.i.) in the liver and caudal kidney of specimens from the four sampling sites (control, low-polluted, medium-polluted, highly-polluted). Active protein levels for the polluted sites were normalised with respect to those for the control site (mean = 1). Different letters refer to statistically significant differences among the means ($p < 0.05$).

Hematoxylin and eosin staining revealed structural alterations in the renal glomeruli of fish from the highly-polluted site, which appeared contracted compared to those from control fish (Figure 5.2.3.6E vs. Figure 5.2.3.6D). In specimens from the polluted site, both the glomeruli and infiltrating erythrocytes in the kidney exhibited lipid vacuolisation, not only in the cytoplasm (Figure 5.2.3.6E and Figure 5.2.3.6F), but also within the nuclei (Figure 5.2.3.6F). Additionally, a marked release of lipid content outside the cells was observed in the liver tissue of fish from the highly polluted site (Figure 5.2.3.6B and Figure 5.2.3.6C), in contrast to the liver of control fish (Figure 5.2.3.6A).

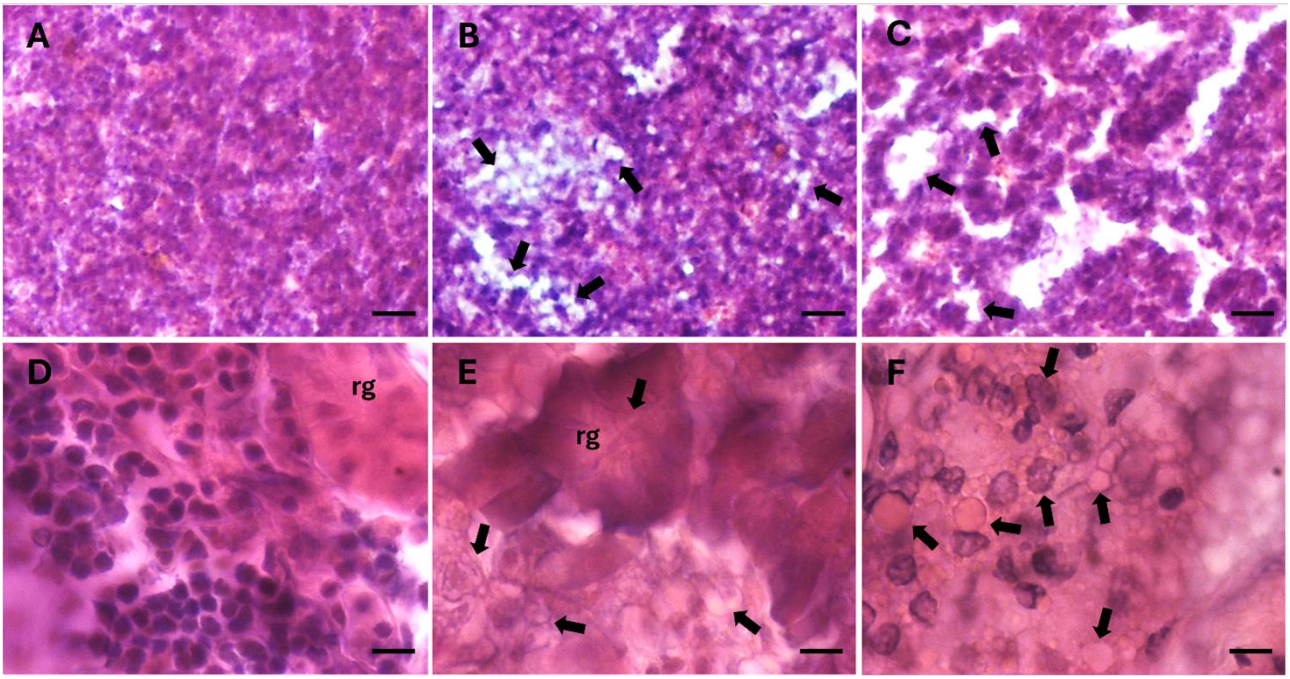

Figure 5.2.3.6 : Histological sections of liver (A-C) and caudal kidney (D-F) of S. cephalus from the control site (A, D) and the highly PFAS-contaminated site (B-C, E-F). Arrows indicate lipid accumulation within tissues. Nuclei are stained in dark purple, cytoplasm in fuchsia. rg: renal glomerulus. Scale bar: 100 µm (A-C), 10 µm (D-F).

Figure 5.2.3.7 shows the SSI, HSI, and FCF indices calculated for *S. cephalus* from the four sampling sites. The SSI index showed a statistically significant increase (95%; $p < 0.05$) in the specimens from the low-polluted site with respect to those from the control one. Conversely, fish from the highly-polluted site showed a statistically significant decrease (43%; $p < 0.05$) in the SSI index when compared to fish from the control site (Figure 5.2.3.7A). The HSI index showed statistically significant increases ($p < 0.05$) for fish from the medium- (47%) and highly-polluted (149%) sites, compared to fish from the control one (Figure 5.2.3.7B). Similar to HSI, the FCF index showed statistically significant increases ($p < 0.05$) for fish from the medium- (30%) and highly-polluted (27%) sites compared to fish from the control one (Figure 5.2.3.7C).

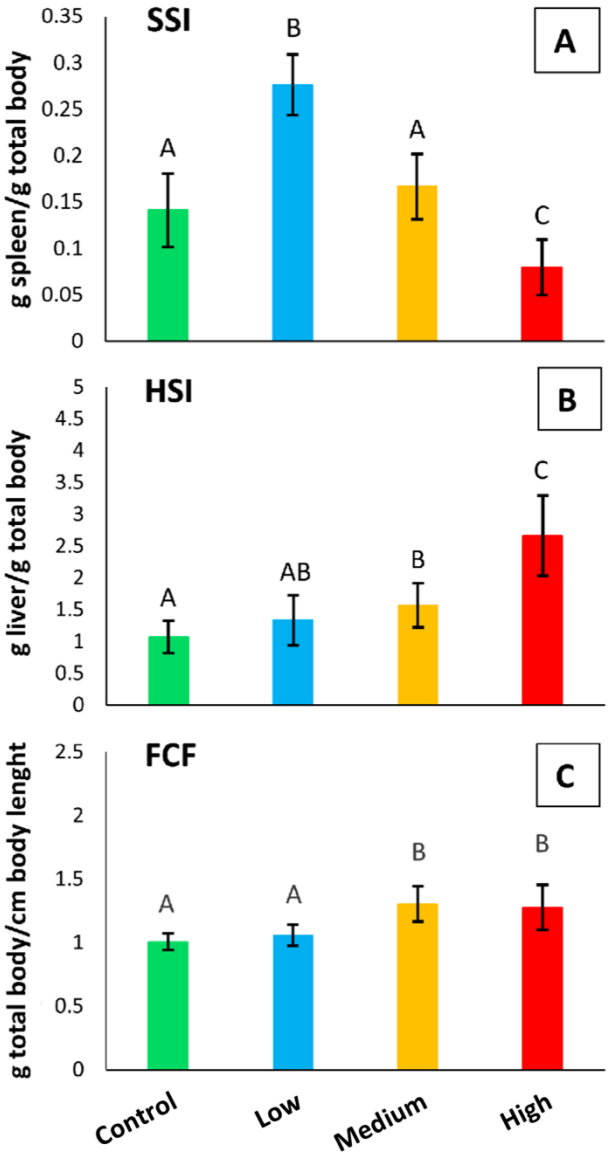

Figure 5.2.3.7 A) SSI, (B) HSI, and (C) FCF somatic indices referred to S. cephalus specimens from the four sampling sites (control, low-polluted, medium-polluted, highly-polluted). Different letters refer to statistically significant differences among the means ($p < 0.05$).

5.2.4 Discussion

Most research on PFAS focuses on human health (Biggeri et al., 2024), while little is known about their effects on freshwater fauna. Given that water is the primary polluted matrix in Veneto (Vaccari et al., 2024), investigating the role of chronic exposure to PFAS on the physiology of *S. cephalus*, an endemic and cosmopolitan fish species in the region, may be fundamental to better understanding their impact on river ecosystems.

Previous studies have shown that *S. cephalus* can activate a range of physiological responses at both cellular and systemic levels in response to PFAS exposure (Piva et al., 2022; Schumann et al., 2024; Pacchini et al.,

2025b). In the present study, in addition to evaluating three somatic indices to obtain a general overview of the well-being of the sampled *S. cephalus* specimens, we investigated the antioxidant responses of this freshwater fish that counteract oxidative stress induced by H2O2 overproduction. To this aim, we examined the induction of CAT and Se-GPx, both at transcriptional and enzymatic activity levels, in the liver and caudal kidney, two organs involved in the accumulation and detoxification of xenobiotics.

Regarding the HSI, we observed a clear increase in liver size in fish from medium- and highly-polluted sites. This finding is consistent with previous evidence linking liver enlargement in *S. cephalus* to total PFAS concentrations (Piva et al., 2022) and, in our case, specifically to PFOS and PFDA, the predominant compounds detected in our analyses. Hepatic PFOS levels reached 55.40 µg/L and 72.78 µg/L at the medium- and highly-polluted sites, respectively, while PFDA concentrations were 3.31 µg/L and 21.67 µg/L. These concentrations are in line with the liver being a primary PFOS target organ (Wang et al., 2022) and fall within ranges associated with hepatic steatosis in fish and rodents chronically exposed to PFAS (Attema et al., 2022; Cheng et al., 2016). Such steatosis, driven by stress-induced lipid accumulation in hepatocytes, may reduce PFAS interactions with cellular proteins by modifying the hydrophilicity of the intracellular environment and promoting non-specific binding to lipids (Yoo et al., 2009; Qin et al., 2023). Moreover, PFAS can disrupt lipid metabolism through activation of PPARα and PPARγ, further enhancing lipid deposition (Li et al., 2024; Wang et al., 2023; Johnson et al., 2024), while lipid droplets may confer a protective effect by sequestering reactive lipid peroxidation products and limiting oxidative damage (Martinez et al., 2023). The liver is not the only organ affected by weight increases following PFAS exposure, as indicated by the FCF index, which in our study also revealed higher total body weight in S. cephalus from medium- and highly-polluted sites.

Our histological analyses revealed lipid accumulation not only in the liver but also in the caudal kidney. While there is limited evidence in fish regarding renal lipid deposition linked to PFAS, human studies have associated chronic kidney disease with PFAS exposure (Conway et al., 2018), and this condition is known to cause lipid dysmetabolism and lipid droplet accumulation in the kidney (Mitrofanova et al., 2023). Supporting this hypothesis, we observed downregulation of prdx-4 mRNA expression in the caudal kidney of S. cephalus chronically exposed to PFAS (Pacchini et al., 2025b). Since this antioxidant enzyme inhibits lipid accumulation in cells (Yamada and Guo, 2018), its reduced expression may reflect a cellular response facilitating lipid deposition in the kidney. Similarly, Kim et al. (2023) demonstrated that reduced antioxidant enzyme activity promotes lipid droplet formation under chemical stress.

The SSI index results showed the highest values in fish from the low-polluted site and the lowest in those from the highly-polluted site. The spleen is particularly interesting because it plays a crucial role in regulating the immune system. Previous studies on mice exposed to PFOS have evidenced a decrease in spleen weight, which was associated with an increase in liver weight (Wang et al., 2011), suggesting an adverse effect of this PFAS on the immune system. Spleen immunosuppression was also highlighted in zebrafish exposed to PFOA (Zhong et al., 2020). The spleen plays a crucial role in erythropoiesis, the process of producing red blood cells. However, in fish from medium- and highly-polluted sites, this function may be predominantly carried out by the head kidney (Chen et al., 2013; Witeska, 2013). The increase in spleen weight observed at the low-polluted site is likely due to enhanced erythrocyte production or activation of the immune response. This response may be necessary when evaluating prolonged exposure to PFAS, even at low concentrations. Based on these considerations, it is plausible that the spleen enlarges at the low-polluted site as a primary defence mechanism against the effects of PFAS. When these effects become too excessive for the organism (medium- and highly-polluted sites), the spleen goes under stress, decreasing its mass. Therefore, the spleen appears to play a secondary role in defending against PFAS when their concentrations are high, leaving the liver and the body's general lipid accumulation to deal with the harmful effects of PFAS.

We observed a limited activation of the studied antioxidant enzymes in the liver. No change in CAT activity is consistent with previous findings in rainbow trout liver (Tilton et al., 2008) and in primary cultured hepatocytes of freshwater tilapia (Liu et al., 2007) exposed to PFOA, as well as in salmon hepatocytes exposed to perfluorooctane sulfonamide (PFOSA) (Olufsen and Arukwe, 2015). Similarly, a non-activation of GPx activity was known in Atlantic salmon hepatocytes exposed to PFOSA (Wågbø et al., 2012) and in hepatocytes of freshwater tilapia exposed to PFOA (Liu et al., 2007). This result can be explained by the fact that other components of the antioxidant system may have been activated. It is known, for example,

that in the cell, in addition to CAT and GPx, the Prdxs, as mentioned above, also operate as H2O2 scavengers (Al-Asadi et al., 2019).

In contrast, the caudal kidney showed induction of both CAT and Se-GPx. This finding is expected, given that the kidney is the second most important organ for PFAS accumulation (Savoca and Pace, 2021), as also confirmed by our chemical analyses, which demonstrated increasing levels of PFOS and PFDA in fish moving from the control site to the highly-polluted one. Specifically, PFOS levels reached 70.54 µg/L and PFDA 32.90 µg/L in the caudal kidney of fish from the highly-polluted site. Similar trends of PFAS bioaccumulation, with PFOS predominance in various organs, have been reported in freshwater fish (Pivonkova et al., 2020; Smith et al., 2021). PFDA has been shown to induce oxidative stress and mitochondrial dysfunction in cellular and zebrafish embryo models, impairing fatty acid β-oxidation and increasing reactive oxygen species production (Widhalm et al., 2024; Piva et al., 2022). These effects support the mechanistic plausibility of the observed activation of antioxidant enzymes such as CAT and Se-GPx in the caudal kidney, as a defensive response to PFAS-induced oxidative stress. The complementary induction of these enzymes, varying across pollution levels, suggests a dynamic adjustment of the antioxidant system to the intensity of oxidative challenge.

In specimens sampled from the low-polluted site, there is a renal increase in Se-GPx activity but not in CAT. The opposite occurs in the medium-polluted site. Notably, antioxidant defences work in a complementary manner: Godin and Ganrett (1992) previously correlated a low GPx activity with a high CAT activity; the opposite condition was pointed out in the liver of two Antarctic fish species, where high Se-GPx activity corresponded to lower CAT activity (Santovito et al., 2012). CAT typically plays a minor role at low H2O2 concentrations but becomes useful when this reactive oxygen species (ROS) increases (Regoli et al., 2005). Therefore, we can assume that Se-GPx has a first-line defence role against PFAS-induced oxidative stress, while CAT activity is enhanced when the risk of oxidative stress increases. In the highly-polluted site, both enzymes' high activities were expected as ROS production could be so high that all antioxidant defences are required to counteract oxidative stress. The cooperation of different antioxidant system components is crucial, especially if the studied fish come from an environment subjected to viability in PFAS concentrations over time, so they must be ready to counteract future PFAS damages effectively.

The expressions of cat, gpx-1, and gpx-4 mRNAs were measured in the liver and caudal kidney and compared among the four sampling sites, whether polluted or not by PFAS, and with the amount of the relative active proteins for each site.

Another interesting feature of the activation of the antioxidant system in S. cephalus exposed to PFAS is the mismatch between the expression profiles at the gene (mRNA) and protein (enzyme activities) levels, which is not directly attributable to the different half-lives of the respective molecules. The absence of correlation between gene transcription and messenger translation referring to anti-stress proteins, such as those of the antioxidant system, was documented in our previous works in aquatic organisms (Ferro et al., 2013; Drago et al., 2022), including fish (Sattin et al., 2015; Tolomeo et al., 2019; Bakiu et al., 2022b; Pacchini et al., 2023). Many authors attribute this phenomenon to a post-transcriptional control on protein synthesis operated by stress granules (SGs) (Takahashi et al., 2013; Harvey et al., 2017; Curdy et al., 2021; Drago et al., 2021; Bakiu et al., 2024). These non-membranous cytoplasmic foci operate in the recruitment of silenced mRNAs due to the presence of specific mRNA-binding proteins (Drago et al., 2021, 2023; Piva et al., 2024). The mechanism by which these proteins operate in mRNA selection within SGs remains a subject of study (Khong et al., 2017). However, SG-based regulation could explain why increased CAT and Se-GPx activity in the caudal kidney did not match increased mRNA expression for the cat and gpx-1 genes. Indeed, the presence of PFAS-induced oxidative stress could induce the disassembly of SGs, leading to the release of specific mRNAs contained therein, which unlocks their translation and facilitates the biosynthesis of antioxidant enzymes.

The potential interaction between SGs and the antioxidant system requires future confirmation, and investigations into this effect are already underway. What is already evident is that not all components of the antioxidant system are subject to such regulation. Indeed, in the caudal kidney, our data indicate that the gpx-4 expression profile perfectly correlates with Se-GPx activity, thus suggesting that this isoform makes the main contribution to enzyme formation. Like other GPx isoforms, GPx-1 is predominantly expressed inside the cytoplasm, whereas GPx-4 is the only one present inside mitochondria (Pei et al., 2023), which are considered one of the PFAS intracellular toxicity targets (Hagenaars et al., 2013).

Therefore, GPx-1 is probably not the most essential isoform in response to the stress caused by these pollutants.

5.3 Gen-X induced oxidative stress in *Procambarus clarkii* hepatopancreas and gills

5.3.1 Introduction

Among the long-chain perfluoroalkyl acids, perfluorooctanoic acid (PFOA) and perfluorooctane sulfonate (PFOS) have the most extensive production history and are the most widely detected in the environment (American Academy of Pediatrics Council on Environmental Health, 2018). Their toxicological profiles and persistence have led to stringent regulatory measures worldwide. In 2009, PFOS and related compounds were the first PFAS to be restricted for use under the Stockholm Convention, listed in Annex B, which allows limited and specific uses under strict conditions. In contrast, PFOA and related compounds were added to Annex A in 2019, requiring the complete elimination of their production and use (Secretariat of the Stockholm Convention., 2019). Moreover, within the European Union, both PFOS and PFOA are regulated under the EU POPs Regulation, with PFOS restricted in Annex I and PFOA banned under the 2020/784 amendment (European Union, 2020). Since 2023, PFOA has also been classified as a Group 1 carcinogen by the International Agency for Research on Cancer (IARC Working Group on the Identification of Carcinogenic Hazards to Humans, 2025).

In light of these restrictions, the chemical industry has developed alternative fluorinated compounds that retain beneficial chemical properties while reducing their toxicity potential (Wang et al., 2013). Among the perfluoroalkyl ether carboxylic acids (PFECAs), hexafluoropropylene oxide dimer acid (HFPO-DA) and its ammonium salt are commercially known as Gen-X (Conley et al., 2021). It was first synthesised in 2009 by DuPont (now Chemours) as a replacement for PFOA as a polymerisation aid in the manufacturing of high-performance fluoropolymers (Beekman et al., 2016).

It was initially considered a safer alternative due to its shorter chain length (C6HF11O3) and reduced potential for bioaccumulation (Feng et al., 2021). The introduction of one or more oxygen atoms that form alkyl ether linkages (C–O–C) in the fluoroalkyl chain (Xiao, 2017), and the decrease in the number of carbon atoms (Rayne and Forest, 2009), make PFECAs more hydrophilic and degradable in water (Guo et al., 2024). Furthermore, highly hydrophilic compounds, particularly when ionised, are eliminated more rapidly via renal pathways due to enhanced active tubular secretion and reduced passive reabsorption, thereby lowering their bioaccumulation potential (Varma et al., 2009). Consistently, Gen-X shows faster clearance than PFOA, with studies reporting ~95% elimination in zebrafish larvae within 48 h (Satbhai et al., 2022), undetectable levels in mouse offspring by weaning (Cope et al., 2021), and reduced adsorption (40% vs. 99%) compared to PFOA (Wen et al., 2023).

However, emerging research suggests that Gen-X shares several critical legacy PFAS properties (Gomis et al., 2015) and can also exhibit toxic effects, particularly in the liver, kidney, immune, reproductive and endocrine systems of mammals (Guo et al., 2024).

Furthermore, both in vivo and in vitro experiments focusing on Gen-X and other PFAS provide evidence of oxidative stress induction in various organisms, such as *Chlorella pyrenoidosa* (Liu et al., 2021), *Dendrobaena veneta* (Pietropoli et al., 2025), mussels (Cunha et al., 2025), zebrafish larvae (Ivantsova et al., 2023) and HepG2 human liver cancer cell lines (Yoo et al., 2021). In response to this stress, antioxidant defence mechanisms have been observed, including increased activity of antioxidant enzymes (SODs and GPxs), activation of the glutathione-ascorbate cycle, and reduced ROS levels, suggesting a mitigating capacity. Despite these defences, Gen-X exposure also induces cellular damage, manifested by decreased cell viability and apoptosis in HepG2 cells, DNA damage in *D. veneta*, damage to the photosynthetic system in *C. pyrenoidosa,* and altered neurotoxicity-related genes and reduced locomotor activity in zebrafish larvae. Moreover, proteomic analyses reveal that pollutant exposure induces oxidative stress and metabolic shifts in Procambarus clarkii, with protein and lipid oxidation patterns reflecting the levels of contamination (Fernández-Cisnal et al., 2017).

Reports on the presence of Gen-X are concentrated primarily in Europe (Germany and the Netherlands), the United States and China, where the industrial replacement of PFOA is most widespread (Feng et al., 2024).

With a predicted pKa < 1, Gen-X exists almost entirely in its anionic form at neutral pH, explaining its high water solubility, hydrophilicity, and nonvolatility, which makes it persistent and mobile in aquatic environments (Xiao, 2017). Its resistance to hydrolysis and biodegradation, as reported in standardised OECD (Organisation for Economic Co-operation and Development) tests (ECHA, 2013), highlights its potential for long-term accumulation. In fact, it has been detected worldwide in both surface and groundwater at varying concentrations, raising concern about human exposure through drinking water (Feng et al., 2021; Vierke et al., 2014).

Regarding surface waters, in Germany, the Altes River, located near a fluoropolymer production facility, showed an average Gen-X concentration of 0.980 µg/L, accounting for 50% of the total PFASs (Joerss et al., 2020). In the Netherlands, typically, levels in surface water range from 1.7 to 812 ng/L (Gebbink et al., 2017). However, a well-documented incident caused the Dordrecht River to reach the highest Gen-X concentration ever recorded, up to 27.4 µg/L (de Kort et al., 2019). In the United States, rivers in North Carolina near a manufacturing plant that has been producing Gen-X since 2009 have reached an average concentration of 272.7 ng/L (Pétré et al., 2021). In contrast, the substitution is not yet as widespread in China, where concentrations in most rivers remain significantly lower (n.d.–3.10 ng/L) than in Europe (Yao et al., 2022). Nevertheless, extreme concentrations have been observed near one of the most extensive fluorochemical facilities in Shandong, China, with values increasing from 0.012 µg/L to 14.107 µg/L after passing the plant, underscoring the impact of direct industrial discharge (Feng et al., 2023).

Given the importance of aquatic invertebrates as bioindicators of riverine ecosystems, the red swamp crayfish P. clarkii (Girard, 1852) was selected as an experimental model to investigate the potential ecotoxicological effects of Gen-X exposure. It is a benthic freshwater crustacean, originally native to Mexico and Central and South America, that has become one of the most widely distributed crayfish species worldwide following its intentional introduction for aquaculture in the 1950s (Gherardi, 2006). It has been listed among the 100 most harmful invasive species by the European Union (Regulation (EU) 1143/2014) (Souty-Grosset et al., 2016). Although non-native and thus not fully representative of local faunal vulnerability, P. clarkii has been extensively used as a bioindicator of environmental pollution [36], as its tolerance and resilience enable it to survive in highly contaminated habitats while still exhibiting measurable physiological responses (Fernández-Cisnal et al., 2018). In fact, studies have demonstrated its capacity to bioaccumulate heavy metals (Savoca et al., 2025) and microplastics (Pastorino et al., 2023) in its tissues, reflecting contamination levels in water and sediment. Practically, the species' wide geographic distribution makes it easily accessible for sampling, and its robustness under controlled laboratory conditions facilitates maintenance, handling, and reproducible experimental studies (Ramalho et al., 2008).

Given the growing concern over Gen-X as an emerging contaminant, this study aimed to investigate its potential to induce oxidative stress in the hepatopancreas and gills of P. clarkii following a 28-day subchronic exposure, by evaluating macromolecular damage to proteins and lipids and the activity of key antioxidant enzymes, such as superoxide dismutases (SODs), selenium-dependent glutathione peroxidases (Se-GPxs), and catalase (CAT).

5.3.2 Materials and methods

Specimens of *P. clarkii* were collected by nets in May 2024 from rivers in the Friuli Venezia Giulia region, near Trieste (northeastern Italy). Specifically, an isolated population inhabiting an artificial canal within the "Bonifica del Brancolo" ("Brancolo Reclamation Area", Goriza province, Italy; 45°46'N, 13°30'E) was sampled.

Animals were transported to the laboratory, where all individuals were weighed, and carapace length and width were measured. Sex was determined through macroscopic observation of the last two pairs of abdominal appendages, which, in the case of a male, are united and sclerotised to form the copulatory organ (gonopodium). A total of 80 healthy individuals (with no visible injuries) were selected and evenly distributed across four experimental tanks (20 individuals per tank), maintaining a balanced sex and size ratio (26.7 g ± 7.5). Before starting the experiment, crayfish were maintained for 30 days in 100-L glass tanks to allow physiological stabilisation before any experimental treatment. This acclimation period aimed

to minimise baseline variability in stress biomarkers and ensure that any observed physiological responses were attributable to the exposure treatment rather than to capture-related stress.

At time zero (T0), three tanks were exposed to Gen-X by adding a stock solution (1 mg/L) to achieve the following water concentrations: 0.5, 1, and 10 µg/L. Measured concentrations in the three treatment tanks closely matched the nominal doses at T0. They remained stable over the 28 days, with only minimal decreases observed at day 14 (T14) and at day 28 (T28) (Table 5.3.1Chemical analysis of Gen-X concentration in the water from all four tanks at three different times of exposure (0, 14, 28 days). Every Gen-X value is the mean of two experimental replicates of water samples). One tank was left uncontaminated and served as a control.

Table 5.3.1Chemical analysis of Gen-X concentration in the water from all four tanks at three different times of exposure (0, 14, 28 days). Every Gen-X value is the mean of two experimental replicates of water samples

Tank/Treatment	Exposure time	Gen-X (µg/L)
CONTROL	T0	0.000
	T14	0.000
	T28	0.000
LOW DOSE (0.5 µg/L)	T0	0.510
	T14	0.505
	T28	0.479
MEDIUM DOSE (1 µg/L)	T0	0.965
	T14	0.991
	T28	0.989
HIGH DOSE (10 µg/L)	T0	8.955
	T14	8.479
	T28	8.415

After 28 days of Gen-X exposure (T28), surviving individuals were extracted from the tanks one by one, anaesthetised on ice for 5 minutes to reduce metabolic activity and then weighed, measured for length and width, and sexed. Each specimen was processed individually, with the duration of the pre-sacrifice procedures recorded to ensure a holding time of less than 15 minutes, thereby avoiding any alteration of stress-related gene and protein expression resulting from sampling. Then, they were rapidly dissected to collect the following tissues: hepatopancreas, gills, muscle, and ovaries (in females). All biological samples were immediately frozen in liquid nitrogen and stored at −80 °C until further analysis.

The number of surviving individuals per treatment group was as follows:

- Control: 17 individuals
- 0.5 µg/L: 18 individuals
- 1 µg/L: 20 individuals
- 10 µg/L: 18 individuals

Minimal mortality was observed during the experiment, likely due to both natural causes and the known aggressive and cannibalistic behaviour of *P. clarkii* when kept in groups (He et al., 2021), particularly during the vulnerable post-moult phase (Figler et al., 2005). Although they were provided with food, the experimental tanks were stocked at a population density consistent with previous studies (Nie et al., 2024) and equipped with shelters to minimise intraspecific competition, minimal mortality was expected.

All tanks were housed in a thermostatic room at 22.7 ± 1.5 °C under a 12-hour light (12L): 12-hour darkness (12D) photoperiod, simulating the species' natural circadian rhythm. Throughout the entire experiment (acclimatation and exposure), water was filtered and oxygenated (pH: 7.5 ± 0.3), and the volume in each tank was maintained constant at 100 L by compensating for evaporation losses. A temperature logger was

placed in the control tank and recorded data every 30 minutes during the experiment. An adequate number of polyvinyl chloride pipes was provided as shelters to minimise stress and promote natural behaviour. Crayfish were regularly fed twice a week, with Dr. Bassleer Biofish Food Shrimp Sticks (crude protein 16 %, crude fibre 15 %, crude ash 9 %, crude oils and fats 4 %) and food amounts adjusted to the total tank biomass (approximately 28 g). Dead individuals were promptly removed to prevent contamination from decomposition products (e.g., ammonia and other nitrogenous wastes) and microbial proliferation.

From each tank, at 0, 14, and 28 days of exposure, 100 mL of water samples were collected and chemically analysed. This allowed us to obtain the analytical confirmation of nominal Gen-X doses at time 0 and also to determine the residual concentration of the substance after 28 days of treatment.

In addition, hepatopancreas, gills, and muscle were collected from 5 to 7 individuals per treatment group to estimate bioaccumulation in different tissues.

Pure Gen-X analytical standard ($^{13}C_3$-Gen-X) was obtained from Wellington Laboratories (Guelph, Ontario, Canada). For the analytical procedure, LC-MS grade methanol and ammonium acetate were obtained from Sigma-Aldrich (Milan, Italy). Ultrapure water was freshly produced on each day of analysis using a Sartorius system (Milan, Italy). Oasis PFAS (GCB 50 mg/WAX 200 mg 60 µm) cartridges were purchased from Waters (Milford, MA, USA).

Gen-X quantification was performed by ultra-high performance liquid chromatography coupled with tandem mass spectrometry (UHPLC-MS/MS). Hepatopancreas and gills were pre-treated as described for fish tissues by Pacchini et al. (Pacchini et al., 2025a), with slight modifications. Briefly, 50 µL of an internal standard mixture ($^{13}C_3$-Gen-X at 500 ng/mL in water) was added to 5 g of crayfish tissue to assess bioaccumulation. Then, 2.5 mL of sodium hydroxide (200 mM) and 10 mL of methanol were added to each sample, which was then homogenised using an Ultraturrax (IKA, Staufen, Germany). After homogenization, 150 µL of 4 M hydrochloric acid was added, and the samples were vortexed. Subsequently, they were centrifuged at 10,000 × *g* for 10 min. A solid-phase extraction (SPE) using Oasis PFAS cartridges was performed to extract target analytes from the tissue supernatants. Cartridges were conditioned with 4 mL of methanol and 4 mL of water. Then, 8 mL of tissue supernatant was loaded, and cartridges were washed with 4 mL of 2% formic acid in water, followed by 4 mL of methanol. Target analytes were eluted with 3 mL of 1% ammonium hydroxide in methanol. The eluates were evaporated under a gentle nitrogen stream at 45 °C, reconstituted in 200 µL of an 80:20 (*v/v*) water: methanol solution, and transferred to polypropylene vials for UHPLC-MS/MS analysis. For water samples, 200 µL aliquots were transferred to polypropylene vials, spiked with 50 µL of $^{13}C_3$-Gen-X (25 µg/L in methanol), vortex-mixed, and directly injected into the analytical system. The system consisted of an Acquity UPLC binary pump (Waters, Milford, MA, USA), equipped with the PFC isolation kit to avoid background contamination. Chromatographic separation was performed using a Waters Acquity UPLC BEH C18 column (50 × 2.1 mm, 1.7 µm), maintained at 40 °C. The mobile phase consisted of 5 mM ammonium acetate in water (A) and methanol (B), with a flow rate of 0.3 mL/min, under programmed conditions. The UPLC was interfaced to an XEVO TQ-S Micro triple quadrupole mass spectrometer (Waters, Milford, MA, USA), operated in negative electrospray ionisation (ESI-) mode with a capillary voltage of -0.50 kV. The source and desolvation temperatures were 150 and 500 °C, respectively; the cone gas was set at 50 L/h and the desolvation gas at 900 L/h, while argon was used as the collision gas. The specific transitions monitored for each analyte, along with the corresponding cone voltage (CV) and collision energy (CE) values, were: 285.0>169.0 m/z (CV 12 V; CE 8 eV) and 285.0>185.0 m/z (CV 12 V; CE 88 eV) for Gen-X; and 287.0>168.9 m/z (CV 12 V; CE 6 eV) for ^{13}C3-Gen-X. Data were acquired and processed using MassLynx 4.2 software (Waters, Milford, MA, USA).

Each day of analysis, method validation was performed directly in the sample matrix (a pooled homogenate of various tissues) using the matrix-standard addition approach. Calibrators (range: 0.1–20.0 µg/kg) and quality control (QC) samples at four concentration levels (0.1, 0.5, 1, and 10.0 µg/kg), containing all target analytes, were freshly prepared to assess the method's performance in terms of specificity, linearity, precision, and accuracy. Fresh calibration curves were prepared in water over the range of 0.25-25 µg/L for the quantification of Gen-X in water samples, and QC samples were prepared at 0.25, 0.75, 2.5, and 10 µg/L.

Peak area ratios for analytes and internal standards were plotted against their corresponding concentrations, and a linear least-squares regression model was applied. All calibrators had to be within ±15% of their

nominal values, and the resulting correlation coefficient (r^2) had to be ≥ 0.99. All QC samples had to confirm the method's accuracy (within ±15%) and precision (coefficient of variation < 15%) for all analytes.

The limit of quantification (LOQ) was set at 0.1 ng/g for tissue samples and at 0.25 µg/L for water samples. The limit of detection (LOD) was set at 0.03 µg/kg for tissues and 0.08 µg/L for water samples. The recovery was within 94–105%. The use of isotopically labelled internal standards minimised matrix effects and further improved the reliability of quantification, confirming the robustness and validity of the method. Finally, specificity was proved by the absence of chromatographic signals at the retention times of the target analytes in blank samples, even after the injection of the highest-concentration calibrators.

Tissue samples of hepatopancreas and gills were homogenised on ice in a buffer containing 20 mM Tris-HCl (pH 7.6), 1 mM ethylenediaminetetraacetic acid (EDTA), 1 mM dithiothreitol (DTT), 0.5 mM sucrose, and 0.15 mM KCl, using a high-speed mixer-homogeniser (Polytron PT 3000, Kinematica AG, Luzern, Switzerland). The homogenates were centrifuged at 13,000 × g for 1 h at 4 °C, and the resulting supernatants were rapidly frozen in liquid nitrogen and stored at −80 °C until biochemical analyses. These cell-free extracts were used to assess the enzymatic activity of SODs, Se-GPxs and CAT, as well as to measure markers of cellular damage, including advanced oxidation protein products (AOPP) and lipid peroxidation (LPO).

AOPP were measured using the spectrophotometric method of Witko-Sarsat et al. (Witko-Sarsat et al., 1998), adapted for a 96-well microplate format. Briefly, a calibration curve was constructed with chloramine-T (N-chloro-p-toluenesulfonamide sodium salt) diluted in phosphate-buffered saline (PBS) over a concentration range of 0–100 µmol/L. For each assay, 40 µL of tissue homogenate (diluted 1:5 in PBS) was mixed with 160 µL PBS, 10 µL of 1.16 M potassium iodide (KI), and 20 µL of acetic acid. Standards and blanks were prepared under the same conditions, substituting the sample volume with either chloramine-T solution or PBS. Absorbance was immediately read at 340 nm using a microplate reader (Synergy HT, BioTek Instruments, Winooski, VT, USA). AOPP concentrations were expressed as µmol/L chloramine-T equivalents, corrected for the sample dilution factor, and finally normalised to the total protein content of each extract (µmol AOPP per mg protein).

LPO was assessed by quantifying malondialdehyde (MDA) using the RayBio® Lipid Peroxidation (MDA) Assay Kit (RayBiotech Life Inc., Peachtree Corners, GA, USA), following the manufacturer's instructions. Briefly, aliquots of tissue homogenates were incubated with thiobarbituric acid (TBA) at 95 °C for 60 min to form the MDA–TBA adduct. After cooling on ice, samples were centrifuged at 1,600 × g for 10 min at room temperature to remove precipitated material, and the supernatants were transferred to a 96-well microplate. Absorbance was measured at 532 nm using a microplate reader (Thermo Fisher Scientific Varioskan LUX Multimode, Life Technologies Holdings Pte Ltd, Singapore). MDA levels were expressed as nmol MDA per mg protein, calculated from a standard curve prepared with known MDA concentrations.

SODs activity was determined using the SOD Assay Kit (Merck KGaA, Darmstadt, Germany), following the manufacturer's instructions. Briefly, tissue samples were homogenised in the provided buffer and homogenates were centrifuged at 10,000 × g for 10 min at 4 °C to remove cellular debris. SODs activity was measured based on the enzyme's ability to inhibit the reduction of the WST-1 tetrazolium salt by superoxide anions generated in the reaction. Absorbance was measured at 450 nm using a microplate reader (Infinite 200 PRO, Tecan Group Ltd., Switzerland). Enzyme activity was expressed as units of SOD per milligram of protein (U SOD/mg protein), with one unit defined as the amount of enzyme required to inhibit 50% of the WST-1 reduction.

Se-GPx activity was measured by the spectrophotometric method described by Livingstone et al., using H_2O_2 as the substrate. In this assay, Se-GPxs catalyse the reduction of H_2O_2 by reduced glutathione (GSH), producing oxidised glutathione (GSSG). GSH is then regenerated by glutathione reductase at the expense of nicotinamide adenine dinucleotide phosphate (NADPH), which is oxidised to $NADP^+$. The decrease in NADPH absorbance at 340 nm was monitored using a UV-1800 spectrophotometer (Shimadzu Corporation, Kyoto, Japan). Enzyme activity was expressed as units of Se-GPxs per milligram of protein (U Se-GPx/mg protein), with one unit defined as the amount of enzyme required to oxidise 1 µmol of NADPH per minute.

CAT activity was determined following the method of Aebi (Aebi, 1984). The assay relies on the enzymatic decomposition of H_2O_2 to H_2O, which is monitored by the decline in absorbance at 240 nm using a UV-

1800 UV-Vis spectrophotometer (Shimadzu Corporation, Kyoto, Japan). Enzyme activity was expressed as units of CAT per milligram of protein (U CAT/mg protein), where one unit corresponds to the amount of enzyme required to decompose 1 µmol of H_2O_2 per minute.

The quantity of proteins in the cell-free extract was quantified using the Folin–Ciocalteu phenol reagent method described by Lowry et al. (Lowry et al., 1951), with a calibration curve constructed from increasing concentrations of bovine serum albumin (BSA). Enzyme activities of SODs, Se-GPxs and CAT and indicators of cellular damage (AOPP, LPO) were all normalised to the total protein content of each sample.

All experimental procedures were conducted in accordance with the current European and Italian legislation on the use of animals for scientific research (Directive 2010/63/EU and Italian Legislative Decree 26/2014). Although *P. clarkii* is considered an invasive alien species and is included in the Union list under Regulation (EU) No 1143/2014, the use for research purposes in controlled laboratory settings is permitted under strict conditions. Specimens used in this study were collected under authorisation from the competent regional authorities (Friuli Venezia Giulia Region), and their maintenance in captivity was carried out in compliance with national and regional guidelines. All efforts were made to minimise animal suffering and reduce the number of individuals used, in accordance with the principles of the 3Rs (Replacement, Reduction, and Refinement). At the end of the experiment, all individuals were disposed of in accordance with regional regulations and the authorised experimental protocol.

Statistical analysis was provided using OriginPro 2025 (Academic Version 10.2.0.188; Northampton, MA, USA), and results are expressed as mean values (N = 10) ± standard deviation (SD). The Shapiro–Wilk test was used to assess normality within each group, and the Levene's test was used to determine homogeneity of variance. As all datasets met these assumptions, one-way ANOVA was applied to evaluate differences among treatment groups, followed by Tukey's HSD post hoc test to identify significant pairwise differences. Statistical significance was set at $p < 0.05$. All results are available from the data repository.

5.3.3 Results

Due to limited tissue availability, Gen-X concentrations could not be measured in the organs of the single specimens; therefore, tissues from 5 to 7 individuals per group were pooled. This approach, although it reduces replication and precludes formal statistical analysis, is a common and accepted practice in bioaccumulation studies when sample sizes or tissue amounts are limited (Pillet et al., 2023). Therefore, the results presented here should be considered indicative rather than statistically conclusive.

Bioaccumulation analyses of crayfish tissues after 28 days revealed a dose-dependent uptake of Gen-X (Table 5.3.2). The hepatopancreas showed the highest accumulation levels across all treatments, reaching values above 25 µg/L in the high-dose group. In contrast, the gills accumulated intermediate concentrations, while the muscle tissues consistently exhibited the lowest levels.

Table 5.3.2 Chemical analysis of Gen-X bioaccumulation in *P. clarkii* tissues (gills, hepatopancreas, muscle) after 28 days of exposure. Every Gen-X value is the mean of the indicated replicates resulting from homogenisation pools of 5-7 individuals. Data are expressed in µg/g of fresh weight (FW).

Tank/Treatment	Exposure time	Gen-X (µg/L)
CONTROL	T0	0.000
	T14	0.000
	T28	0.000
LOW DOSE (0.5 µg/L)	T0	0.510
	T14	0.505
	T28	0.479
MEDIUM DOSE (1 µg/L)	T0	0.965
	T14	0.991
	T28	0.989

HIGH DOSE (10 µg/L)	T0	8.955
	T14	8.479
	T28	8.415

As shown in Figure 5.3.3.1A, AOPP levels in the hepatopancreas increased significantly after the 10 µg/L Gen-X treatment, with values approximately 185% higher than the control (*p = 1.34E-5*).

In the gills (Figure 5.3.3.1B), a comparable trend was observed, with a marked increase in protein oxidation detected exclusively at the highest concentration (approximately 100% above the control; *p = 9.69E-6*).

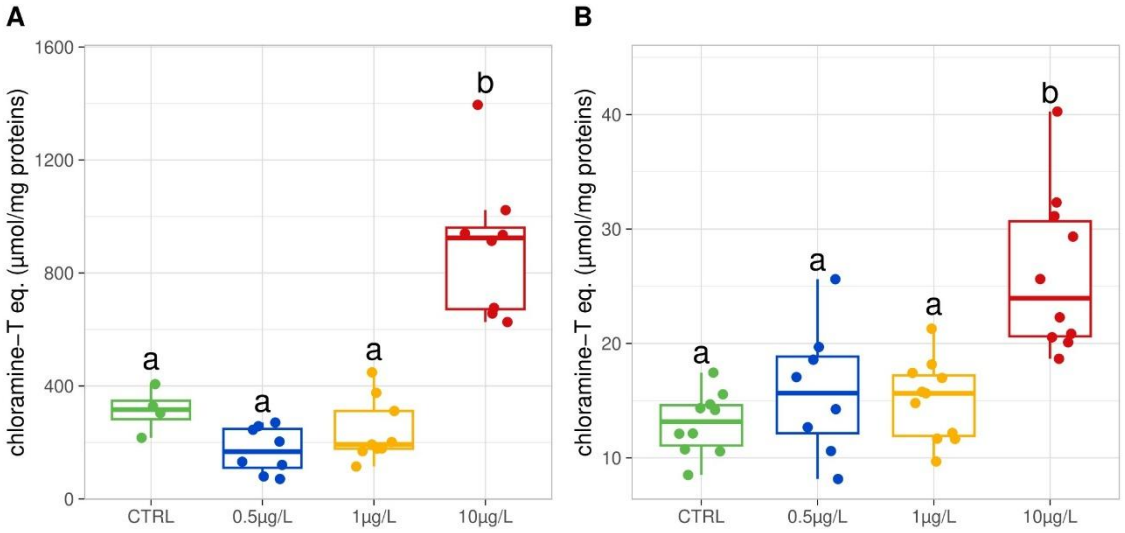

Figure 5.3.3.1. Advanced oxidation protein products (AOPP) levels in (A) hepatopancreas and (B) gills, expressed as chloramine-T equivalents (µmol/mg proteins), in mean values (N=10) with relative standard deviations. Different colours represent the four treatments: CTRL, 0.5 µg/L, 1 µg/L and 10 µg/L. Different letters above the bars indicate significant differences among treatments ($p < 0.05$).

LPO in hepatopancreas (Figure 5.3.3.2A) showed a significant increase compared to the control at both 1 µg/L and 10 µg/L of Gen-X, with rises of 275% (*p = 1E-15*) and 234% (*p = 1E-15*), respectively. In contrast, the gills (Figure 5.3.3.2B) exhibited a significant elevation in MDA levels only at the highest concentration (10 µg/L), corresponding to a 117% increase (*p = 2.4E-3*).

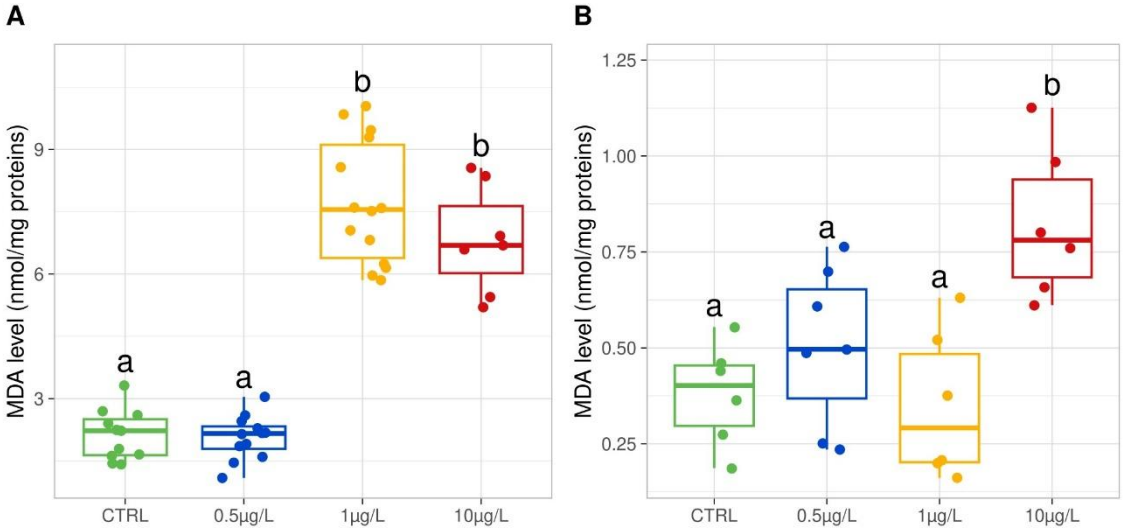

Figure 5.3.3.2. Lipid peroxidation (LPO) levels in (A) hepatopancreas and (B) gills, expressed as MDA levels (nmol/mg proteins), in mean values (N=10) with relative standard deviations. Different colours represent the four treatments: CTRL, 0.5 µg/L, 1 µg/L and 10 µg/L. Different letters above the bars indicate significant differences among treatments ($p < 0.05$).

SODs mean activity showed tissue-specific responses. In the hepatopancreas (Figure 5.3.3.3A), SODs mean activities in the 1 µg/L and 10 µg/L groups decreased by approximately 44% (*p = 3.55E-4*) and 65% (*p = 1E-15*), respectively, compared to the control. In contrast, SODs mean activity in gills (Figure 5.3.3.3B) rises progressively from the control, starting at 1 µg/L with a 20% increase (*p = 1.3E-1*) and at 10 µg/L with a 33% increase (*p = 2.66E-3*).

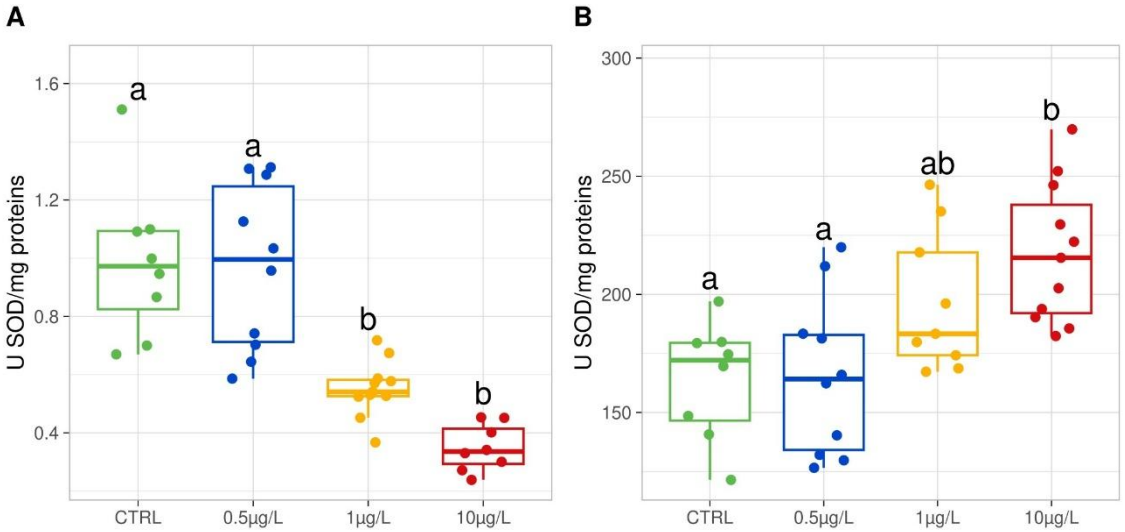

Figure 5.3.3.3. Enzymatic tissue activity of superoxide dismutases (SODs) in (A) hepatopancreas and (B) gills, expressed as units (U) of enzyme/mg proteins. Different colours represent the four treatments: CTRL, 0.5 µg/L, 1 µg/L and 10 µg/L. Different letters above the bars indicate significant differences among treatments ($p < 0.05$).

Se-GPxs mean activity showed concentration-dependent modulation in both the hepatopancreas and gills. In the hepatopancreas (Figure 17A), Se-GPxs activity increased by approximately 73% at 0.5 µg/L compared to the control (*p = 1.41E-4*). However, at 1 µg/L, it declines by approximately 64% compared to the 0.5

µg/L dose (*p = 1E-15*), returning to control values. At 10 µg/L, activity further decreases relative to the control (approximately 78%, *p = 8.47E-4*) and relative to 0.5 µg/L (approximately 87%, *p = 1E-15*), but without a statistically significant difference from 1 µg/L.

In the gills (Figure 5.3.3.4B), Se-GPxs activity showed a marked induction at 0.5 µg/L (approximately 51% vs. control, *p = 9.82E-3*). In contrast, at 1 µg/L, the activity is reduced by approximately 55% compared with the 0.5 µg/L dose (*p = 9.09E-6*), returning to control values. Lastly, at 10 µg/L, the reduction in activity is approximately 95% relative to the control (*p = 1.35E-6*) and 97% relative to 0.5 µg/L (*p = 1E-15*).

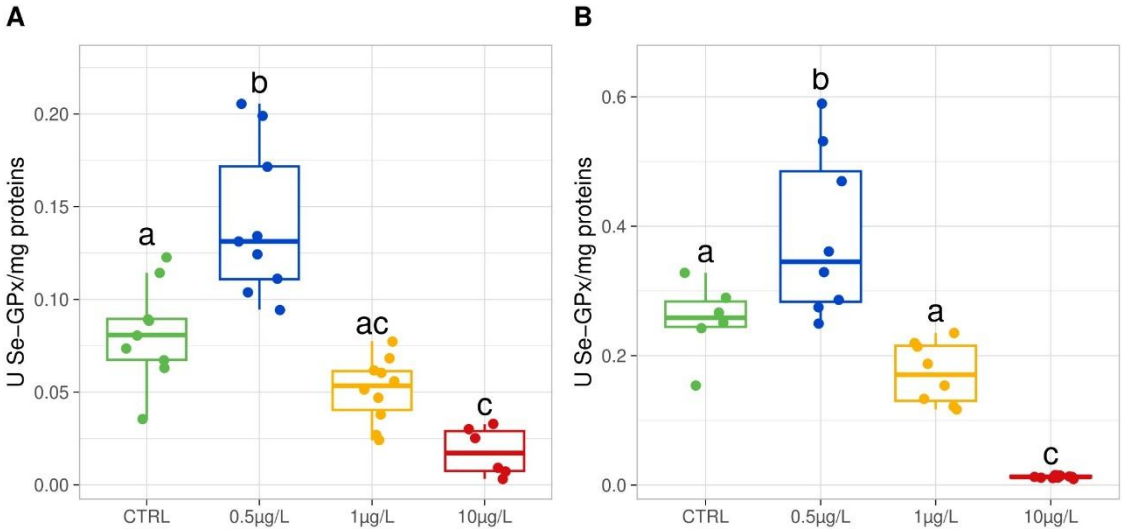

Figure 5.3.3.4. Enzymatic tissue activity of selenium-dependent glutathione peroxidases (Se-GPxs) in (A) hepatopancreas and (B) gills, expressed as units (U) of enzyme/mg proteins. Different colours represent the four treatments: CTRL, 0.5 µg/L, 1 µg/L and 10 µg/L. Different letters above the bars indicate significant differences among treatments ($p < 0.05$).

CAT mean activity exhibited distinct patterns between hepatopancreas and gills. In the hepatopancreas (Figure 5.3.3.5A), CAT activity was significantly reduced by exposure to the lowest dose of Gen-X (0.5 µg/L) by approximately 73% (*p = 1.48E-3*). In contrast, at the two higher concentrations, the activity remained similar to that of the control values. In contrast, the gills (Figure 5.3.35B) showed a different trend, with CAT enzymatic activity increasing by approximately 78% at 1 µg/L of Gen-X compared to the control (*p = 1.75E-3*).

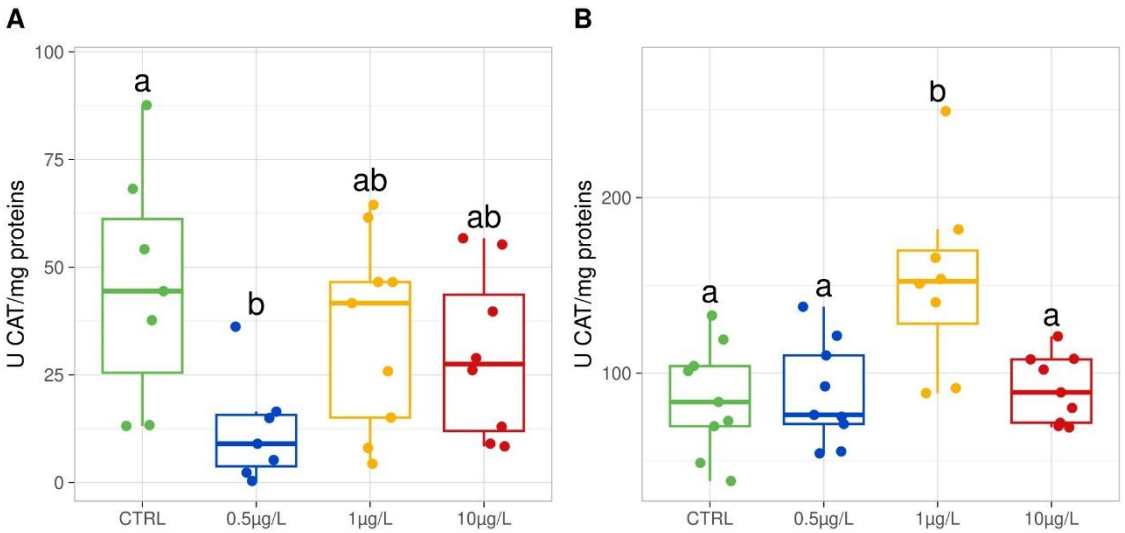

Figure 5.3.3.5. Enzymatic tissue activity of catalase (CAT) in (A) hepatopancreas and (B) gills, expressed as units (U) of enzyme/mg proteins. Different colours represent the four treatments: CTRL, 0.5 µg/L, 1 µg/L and 10 µg/L. Different letters above the bars indicate significant differences among treatments ($p < 0.05$).

5.3.4 Discussion

Tissue analyses revealed a differential distribution of Gen-X, with the hepatopancreas as the primary site of accumulation, followed by gills, and muscle as the least affected. Previous studies reported a similar organ-specific bioaccumulation pattern of pollutants, such as metals in *P. clarkii*: hepatopancreas > gills/exoskeleton > muscle (Alcorlo et al., 2006; Ariano et al., 2021; Zhang et al., 2023), consistent with the hepatopancreas's central role in metabolism and detoxification. These findings emphasise the importance of organ-specific accumulation when evaluating contaminant effects and provide the basis for investigating whether Gen-X exposure was associated with oxidative stress, assessed through biochemical markers of macromolecular damage and the activity of key antioxidant enzymes.

The analysis of oxidative damage indicators suggests that Gen-X exposure can compromise cellular integrity in *P. clarkii* in a dose-dependent and organ-specific manner. At the highest pollutant dose, both the hepatopancreas and gills underwent oxidative damage to proteins and lipids, indicating that antioxidant defences were no longer sufficient to counteract excessive ROS production and prevent cellular injury.

Proteins are highly vulnerable to oxidative modification, as ROS readily react with amino acid residues, causing structural alterations, enzymatic inactivation, and the accumulation of AOPP (Martínez-Sánchez et al., 2005). In addition, PFAS (including Gen-X) can threaten proteins both indirectly, by increasing ROS production, and directly, by binding to plasma and intracellular proteins. For example, Gen-X has a well-known high affinity for liver fatty acid-binding protein (Sheng et al., 2018). Compared with LPO, which represents an early, often reversible event, protein oxidation reflects a more chronic, irreversible form of damage. ROS immediately attack lipids but are also rapidly replenished for membrane turnover in the cell. In contrast, damaged proteins tend to accumulate over time, especially if the degradation systems (proteasome, autophagy) are unable to dispose of them (Pajares et al., 2015).

In terms of LPO (Figure 15), the hepatopancreas proved to be the most sensitive organ, showing marked oxidative damage already at the medium dose (1 µg/L). This trend is consistent with the physiological features of this organ. First, as the primary site of energy metabolism, the hepatopancreas contains a high density of mitochondria, where oxidative phosphorylation naturally generates superoxide radicals as primary by-products (Wei and Yan, 2015). Under normal conditions, these ROS are efficiently neutralised by antioxidant defences; however, any interference with the electron transport chain, such as that potentially induced by Gen-X, can increase electron leakage and further amplify ROS production, enhancing the risk

of oxidative stress (Kang and Hamasaki, 2003). Second, the hepatopancreas is also the tissue in which xenobiotics preferentially bioaccumulate, leading to higher intracellular concentrations of Gen-X compared to other organs (Ariano et al., 2021; Bian et al., 2024) and thus intensifying local exposure, as confirmed by our chemical analyses. Additionally, it serves as the primary site of xenobiotic biotransformation. During this process, pollutants are metabolised by enzymatic systems, but this detoxification pathway often produces reactive intermediates that exacerbate oxidative stress (Deng et al., 2018). Finally, the hepatopancreas is rich in membrane lipids, particularly polyunsaturated fatty acids (PUFAs), which are highly susceptible to peroxidation (Zhang et al., 2022). Excess ROS, whether of mitochondrial origin or derived from Gen-X biotransformation, readily attack the double bonds of unsaturated fatty acids, triggering LPO-mediated chain reactions that compromise membrane integrity and cellular function (Bortot et al., 2025). Additionally, lipid-derived reactive products can react with proteins, promoting their subsequent oxidation and damage (Hematyar et al., 2019). Another possible explanation for the higher lipid levels in the hepatopancreas is lipid accumulation following Gen-X bioaccumulation in tissues. This steatotic response has been frequently reported after PFAS exposure and bioaccumulation in hepatocytes of various fish species, including Padanian goby (Piva et al., 2022), eels (Wolf and Wolfe, 2005), zebrafish (Cheng et al., 2016; Du et al., 2017), and also rats (Harper and Wolf, 2009). Such lipid deposition may represent a cellular adaptive mechanism that creates a more hydrophobic microenvironment, thereby reducing PFAS–protein interactions and limiting subsequent protein oxidation and structural damage. To confirm this hypothesis, the gene expression of peroxiredoxin 4 (*prdx4*), coding for an enzyme involved in the inhibition of lipid accumulation within the endoplasmic reticulum, should be measured. Downregulation of prdx4 expression with increasing Gen-X concentration would signal the cell to promote vacuolization, as reported in fish kidney (Pacchini et al., 2025c). In contrast, the gills displayed an increase in LPO at the lipid level only at the highest exposure dose, suggesting that basal defences are generally sufficient to buffer stress until pollutant accumulation reaches critical levels and becomes overwhelming.

The increase in oxidative damage to proteins and lipids appears to be closely linked to the weakening of antioxidant defences, as indicated by our data on the enzyme activities of SODs, GPxs, and CAT.

Regarding enzymatic defences, in the hepatopancreas, SODs activity (Figure 16) began to decrease even in animals exposed to the lowest Gen-X dose, becoming statistically lower at the 1 µg/L concentration. This reduction in SODs activity at the two higher doses of Gen-X aligns with the strong oxidative damage detected in the hepatopancreas, suggesting that impairment of the first enzymatic line of defence against superoxide radicals enhances macromolecular oxidation. Similar inhibitory effects on SODs have been reported in aquatic invertebrates exposed to PFAS and other contaminants, where enzyme inactivation has been attributed to oxidative modifications of the Cu/Zn or Mn catalytic centres (Lewandowski et al., 2018), or to the oxidation of critical cysteine residues (St. Dimitrova et al., 1994). Chronic oxidative stress may lead to cumulative enzyme dysfunction or degradation, reflecting a collapse of antioxidant defences at high pollutant loads (Lushchak, 2016). Another possibility views the SODs downregulation as an adaptive strategy for energy allocation, allowing for the maintenance or enhancement of other antioxidant defences that are more effective against the predominant ROS (Kim et al., 2015). Consistently, reduced SODs activity has also been reported in copepods (Ali et al., 2014) and fish (Shao et al., 2012; Waheed et al., 2020) at the highest exposure to various pollutants. At the lowest concentration, the absence of enzyme induction can be explained by the high basal production of superoxide radicals in the hepatopancreas, due to its intense mitochondrial metabolism, which already requires sustained SODs activity under normal conditions and may mask further induction at low pollutant doses (Zenteno-Savín et al., 2006). Alternatively, minor increases in superoxide may be counterbalanced by other antioxidant components, such as metallothioneins or non-enzymatic scavengers, preventing detectable changes in SODs activity at this dose (Bakiu et al., 2022b, 2022a; Priante et al., 2022).

In contrast, SODs activity in the gills remained stable at the lowest dose, starting to increase slightly at the medium dose, and significantly surpassing the control at the highest dose. This pattern of progressive increase in SODs activity suggests a gradual increase in superoxide radical formation rate and a concomitant activation of the specific scavengers represented by SODs. This different behaviour of the gills is probably related to lower Gen-X uptake compared to the hepatopancreas. In addition, the reduced basal metabolism of the gills may also play an important role. In fact, despite the gills being directly in contact with contaminated water, often gill antioxidant responses following environmental stress are anyway less sensitive than those of metabolically active organs, as reported for other crustaceans (Schvezov et al., 2017;

Woo et al., 2013). Lower gill metabolism may therefore reduce the likelihood of ROS formation, even in the presence of a disturbing factor such as Gen-X.

Se-GPxs activity also did not appear to be directly proportional to Gen-X exposure. In both organs, it exhibits a biphasic response, characterised by an initial upregulation at low doses, followed by strong inhibition at higher concentrations. This suggests that the enzyme is recruited as part of a rapid early defence against minor peroxide accumulation in cells, as already evidenced in other aquatic animals (Pacchini et al., 2025a). This physiological response probably primarily involves mitochondria and GPx4, which is specifically expressed in them, confirming that PFAS act primarily at the level of these organelles (Pacchini et al., 2025b, 2023; Piva et al., 2022). However, this enzyme loses functionality when pollutant pressure exceeds the organism's defensive capacity. This could be caused by selenocysteine oxidation (Asahi et al., 1997; Orian et al., 2015), active-site damage (Staimer et al., 2012), or saturation of enzymatic capacity (Jomova et al., 2023). The collapse of GPxs activity at elevated doses coincides with the accumulation of protein and lipid oxidation products, indicating that the failure of this enzyme is a critical turning point in the breakdown of cellular homeostasis (Waheed et al., 2020). This observed trend has been described in other aquatic models exposed to environmental stressors (Figueroa et al., 2023; Frank et al., 2023, p. 202; Mamdouh et al., 2021).

CAT (Figure 5.3.3.5) also exhibits organ-specific and Gen-X dose-dependent modulation. In the hepatopancreas, CAT activity showed a non-linear pattern, being significantly reduced at the low dose (0.5 µg/L) and then partially recovering at higher exposure levels. The marked CAT inhibition observed at the lowest Gen-X concentration may reflect a compartment-specific overproduction of hydrogen peroxide within peroxisomes, where CAT is primarily located (Fransen et al., 2012). In this case, local H_2O_2 accumulation could temporarily exceed the enzymatic detoxification capacity, leading to substrate-induced inactivation or oxidative damage to CAT. Conversely, at higher Gen-X concentrations (1 and 10 µg/L), ROS generation may shift towards mitochondrial or cytosolic sources, where other antioxidant systems such as GPxs and peroxiredoxins (Prdxs) are more active (Al-Asadi et al., 2019; Ferro et al., 2018). This redistribution of oxidative processes and antioxidant defences would reduce the direct burden on peroxisomal CAT, resulting in activity levels comparable to those of control. No change in CAT activity at high Gen-X concentrations is consistent with previous findings in rainbow trout liver (Tilton et al., 2008) and in primary cultured hepatocytes of freshwater tilapia (Liu et al., 2007) exposed to PFOA, as well as in salmon hepatocytes exposed to perfluorooctane sulfonamide (PFOSA) (Olufsen and Arukwe, 2015). This stability could also indicate that other antioxidant mechanisms are sufficient to detoxify hydrogen peroxide, making CAT activation unnecessary (Rhee et al., 2005). Additionally, since CAT acts in peroxisomes, the absence of modulation suggests that ROS production in response to Gen-X may not predominantly occur in this compartment (Fransen et al., 2012).

In contrast, the gills showed upregulation of CAT activity at moderate Gen-X exposure (1 µg/L), consistent with a need to detoxify the cell from hydrogen peroxide produced within peroxisomes. This also suggests that CAT plays a preventive action against oxidative stress, representing a first line of defence against increased H_2O_2 (Nitta et al., 2020), and is involved in the primary stress response in gills. Therefore, at this PFAS concentration, ROS generation, particularly H_2O_2, is moderate enough to stimulate CAT activity without overwhelming its capacity, enabling efficient detoxification. However, this response was not sustained at the highest concentration (10 µg/L), suggesting that the gills' antioxidant capacity was probably overwhelmed under severe stress, leading to enzyme inhibition or exhaustion (Livingstone, 2001).

Taken together, these results suggest a differential recruitment of peroxide-detoxifying enzymes in the gills, with Se-GPxs primarily responding in the cytoplasm and mitochondria at lower exposures, and CAT becoming activated at moderate stress, confirming the compartment- and tissue-specific strategy against ROS (Regoli et al., 2011).

5.4 Preliminary field visual observation of *Procambarus clarkii*

In parallel with the experiments in controlled laboratory conditions, a field monitoring activity was initiated in the last year of the project.

A protocol has been developed to observe the behaviour of the *Procambarus clarkii* in semi-controlled field conditions and to record videos for subsequent analysis. Artificial boulders and crawfish samples have been created by scanning real sediments and dead animals, using a 3D scanner acquired within the project. Subsequently, a few samples of both sediments and invertebrates of slightly variable dimensions have been created using a 3D printer also acquired within the project (Figure 5.3.4.1 and Figure 5.3.4.2). The artificial sediment elements were designed to host a GoPro videocamera inside, as depicted in Figure 5.3.4.2. The artificial crawfish were printed identically to the original samples, but with the possibility of storing food doses in their bodies. The food was accessible only to living crawfish by "attacking" the artificial ones when they came into contact with the recording settings.

Figure 5.3.4.1 The artificial boulders hosting the video cameras and the video recording setting.

The ultimate goal of this activity is to create a systematic procedure to observe, under conditions as equivalent as possible, the behaviour of crawfish captured in streams with different levels of PFAS contamination. The video analysis may allow us to evaluate how long-term exposure to local environmental conditions can affect the physiological response of the animals without transfer from their living sites.

Due to complexities arising during the development of the technique and the project's time constraints, this late part of the project investigation has only reached a preliminary stage, resulting in successful test video recordings. Sample snapshots from the videos are shown in Figure 5.20. Therefore, the research group does not expect to reach results on this specific topic that can lead to a publication within the remaining duration of the project

Figure 5.3.4.2 The artificial crawfish and snapshots from the recording of living invertebrates.

5.5 Conclusions

In conclusion, this study provides new information on the influence of PFAS on the organism's physiology. Substances such as PFOA and PFOS can alter the health of fish, determining an increase in protein oxidation at a minimal level of contamination. However, at the concentrations present at the sites considered in this work, fish can still respond to the risk of oxidative stress, activating the antioxidant defences. Among these, the peroxiredoxin isoform *prdx4* appears to be down-regulated. Our results provide the secondary importance of this enzyme as an antioxidant molecule and its primary role in lipid metabolism. Its inactivation determines the increased lipid bioaccumulation inside the cytoplasm, potentially starting the process of cell vacuolisation that can favour a hydrophobic cellular environment that makes the binding between PFAS and protein less probable, preventing damage at the protein level.

Further studies will be needed to clarify the molecular basis of this process, e.g. by studying the mRNA expression of the Adipose differentiation-related protein (Adrp) that is a lipid droplet marker, the transcription of which is known to increase when intracellular lipid levels rise (Targett-Adams et al., 2005). Additionally, our study highlighted the tissue-specific responses to PFAS exposure, which are valuable to gain a more comprehensive understanding of its physiological impacts.

The results obtained in this study provided valuable insights into the physiological strategies adopted by *S. cephalus* to survive in PFAS-contaminated rivers in the Veneto region, highlighting its potential as a model organism for assessing the impact of PFAS on European freshwater fauna. These strategies involve activating the antioxidant system in the caudal kidney, particularly Se-GPx and CAT, and the accumulation of lipids in the liver and caudal kidney to reduce the reactivity of PFAS to their target molecules, i.e., proteins. This study highlights the importance of monitoring the riverine fauna in its ability to acclimatise to an environment where human impact is becoming increasingly important.

There is certainly still much to evaluate and improve, such as the analysis of PFAS accumulation in different organs and tissues, which remains hindered by numerous methodological limitations.

Future research will expand the investigation of PFAS accumulation and anti-stress responses to a broader range of organs, including the brain, in addition to the kidney and liver analysed in the present study, despite the persistent methodological challenges in accurately quantifying tissue PFAS concentrations. The effects of PFASs on the brain are little known in fish. Still, it appears that they may alter brain function by interfering with amino acid neurotransmitter metabolism and disrupting blood-brain barriers (Wang et al., 2023), thus influencing the behaviour and inducing stress in these animals, similarly to other environmental perturbations (Schumann et al., 2023, 2025). Particular focus will be placed on histological confirmation of the inflammatory condition in the spleen, aiming to shed light on the development of specific pathologies resulting from chronic stress induced by PFAS, which may be a consequence of constant ROS production (Lushchak, 2016). In this respect, it will also be necessary to evaluate the role played by other components of the antioxidant system that are often overlooked, such as the aforementioned Prdxs or methionine sulphoxide reductase, which plays a key role in repairing oxidative damage (Ricci et al., 2017). And of course, the oxidation levels of lipids and proteins to better understand whether this new steady state of ROS is actually kept under control by the antioxidant system of *S. cephalus* (Piva et al., 2022) and, therefore, whether these fish will be able to survive a possible future increase in the environmental concentration of PFAS.

This study also helps clarify the relationship between Gen-X and aquatic organisms, thereby improving the understanding of exposure risks associated with the newly emerging PFASs. Our results demonstrate that subchronic exposure to Gen-X induces oxidative stress in *P. clarkii* through direct macromolecular damage and modulation of antioxidant defences, highlighting the importance of considering organ-specific bioaccumulation and antioxidant responses in ecotoxicological assessments. Bioaccumulation analyses identified the hepatopancreas as the primary site of Gen-X accumulation, consistent with its metabolic and detoxification role, and the first organ to exhibit oxidative stress, accompanied by early lipid damage. At the highest exposure level, however, both hepatopancreas and gills showed significant protein and lipid oxidation, confirming that excessive ROS can overwhelm antioxidant defences and compromise cellular integrity. Enzymatic assays revealed tissue-specific, dose-dependent modulation, suggesting a compartment-specific response and sequential activation of different components of the antioxidant system.

From an ecological perspective, these results raise concerns about the potential consequences of Gen-X contamination for the physiology of freshwater organisms and the consequent environmental impact on riverine ecosystems. In fact, the maximum concentration we used is sometimes lower than those found in various natural contexts where PFAS impacts are present. It produces apparent toxicity effects even in a resistant organism such as *P. clarkii*.

Future research should address some experimental limitations that may have influenced the outcomes of this study. First, the origin of the crayfish specimens was not controlled, raising the possibility that genetic variability influenced stress responses; future work should use animals from characterised populations. Second, upcoming research should not only consider long-term exposure scenarios, but also test different pollutant doses. In particular, additional experiments including intermediate concentrations between 1 and 10 µg/L would help identify the critical threshold at which key antioxidant enzymes, such as SODs and Se-GPxs, shift from activation to inhibition, revealing the point at which defence mechanisms are overcome by pollutant-induced damage.

Complementary analyses should also include direct ROS detection in tissues, using, for example, fluorescent probes to identify the predominant ROS species and their subcellular localisation, thereby clarifying the relationship between pollutant exposure, antioxidant enzyme modulation, and organ-specific oxidative damage (Zhao et al., 2019). Moreover, gene expression analyses aimed at quantifying mRNA levels of different isoforms of antioxidant enzymes could provide further insights into the cellular compartments involved in the oxidative response, as well as information on the post-transcriptional regulation of the genes involved, which is essential for understanding the kinetics of cellular defence activation (Piva et al., 2024).

Future research should also consider other antioxidant enzymes, including Prdxs, at both transcriptional and protein activity levels. In particular, the expression of the above-mentioned *prdx4* isoforms could provide valuable insights into lipid metabolism and their role in protecting cells from Gen-X-induced damage. These results should also be confirmed by histological analysis of target tissues, such as the hepatopancreas (Zhang et al., 2019). Important information may also be derived from the analysis of energy metabolism-

related indicators in both hepatopancreas and hemolymph, such as cortisol, hemocyanin, glycogen, glucose and adenylate kinase (Schumann et al., 2025, 2024).

From a regulatory perspective, identifying a critical concentration at which antioxidant defences collapse is particularly relevant. Establishing such thresholds would help define safe environmental exposure limits for Gen-X, thereby supporting the development of evidence-based legislation. Given that current regulations on emerging PFAS remain incomplete, additional ecotoxicological data on dose–response relationships in sentinel species such as *P. clarkii* could provide a valuable basis for setting environmental quality standards to protect freshwater ecosystems.

Finally, an interesting perspective concerns the behaviour of *P. clarkii*. Some research has shown that exposure to environmental contaminants can lead to behavioural changes in crayfish that also impact their social status (De Felice et al., 2022; Mamdouh et al., 2022). To investigate this aspect further, we created realistic models of *P. clarkii* using 3D scanning and printing. Using underwater video recording, we began observations in the wild (at the same sites where we sampled *S. cephalus*) of the behaviour of resident specimens in the presence of the models. We expect to obtain preliminary data that can be correlated with biochemical and biomolecular analyses, laying the foundations for further investigation of this aspect.

6 General Conclusions

Across both marine and freshwater systems, the findings presented in Chapters 4 and 5 converge on a shared message: environmental change—whether driven by climate dynamics or by emerging chemical contaminants—poses significant and multifaceted threats to ecosystem integrity. In marine habitats, *Posidonia oceanica* exhibits reduced physiological performance, structural instability, and altered long-term growth dynamics under rising temperatures, salinity extremes, and intensified storm events. In freshwater environments, chronic PFAS exposure disrupts antioxidant responses, induces oxidative damage, and challenges the resilience of key species, revealing hidden vulnerabilities even in organisms considered tolerant or opportunistic.

Together, these results demonstrate that habitat degradation operates through interconnected biological, chemical, and physical pathways, ultimately weakening ecosystem resilience and reducing the capacity of natural systems to provide essential services. The integrated evidence underscores the urgency of targeted monitoring, mitigation of local anthropogenic pressures, and the development of adaptive management strategies to sustain vulnerable habitats under accelerating environmental change.

7 References

Aebi, H. (1984). Catalase in vitro. Methods in Enzymology, 6, 105:121. https://doi.org/10.1016/S0076-6879(84)05016-3

Al-Asadi, S., Malik, A., Bakiu, R., Santovito, G., Schuller, K. (2019). Characterisation of the peroxiredoxin 1 subfamily from *Tetrahymena thermophila*. Cellular and Molecular Life Sciences, 76, 4745-4768. https://doi.org/10.1007/s00018-019-03131-3

Alcorlo, P., Otero, M., Crehuet, M., Baltanás, A., Montes, C. (2006). The use of the red swamp crayfish (Procambarus clarkii, Girard) as indicator of the bioavailability of heavy metals in environmental monitoring in the River Guadiamar (SW, Spain). Science of the Total Environment, 366, 380–390. https://doi.org/10.1016/j.scitotenv.2006.02.023

Ali, D., Gend Kumar, P., Kumar, S., Ahmed, M. (2014). Evaluation of genotoxic and oxidative stress response to dimethoate in freshwater fish Channa punctatus (Bloch). Chemical Speciation & Bioavailability, 26, 111–118. https://doi.org/10.1080/09542299.2014.11073965

Ambruso, D. R. (2013). Peroxiredoxin-6 and NADPH Oxidase Activity. Methods in Enzymology, 527, 145–167. https://doi.org/10.1016/B978-0-12-405882-8.00008-8

American Academy of Pediatrics Council on Environmental Health (2018). Perfluoroalkyl and Polyfluoroalkyl Substances (PFAS), 627–640. https://doi.org/10.1542/9781610022194-part04-ch36

Apostolaki E.T., Caviglia L., Santinelli V., Cundy A.B., Tramati C.D., Mazzola A. and Vizzini S. (2022). The Importance of Dead Seagrass (*Posidonia oceanica*) Matte as a Biogeochemical Sink. Frontiers in Marine Science, 9, 861998. https://doi.org/10.3389/fmars.2022.861998

Ariano, A., Scivicco, M., D'Ambola, M., Velotto, S., Andreini, R., Bertini, S., Zaccaroni, A., Severino, L. (2021). Heavy Metals in the Muscle and Hepatopancreas of Red Swamp Crayfish (*Procambarus clarkii*) in Campania (Italy). Animals, 11, 1933. https://doi.org/10.3390/ani11071933

ARPA Veneto (2025). Concentrazione di sostanze perfluoroalchiliche (PFAS) nelle acque prelevate da ARPAV. https://www.arpa.veneto.it/dati-ambientali/open-data/idrosfera/concentrazione-di-sostanze-perfluoroalchiliche-pfas-nelle-acque-prelevate-da-arpav

Asahi, M., Fujii, J., Takao, T., Kuzuya, T., Hori, M., Shimonishi, Y., Taniguchi, N. (1997). The Oxidation of Selenocysteine Is Involved in the Inactivation of Glutathione Peroxidase by Nitric Oxide Donor. Journal of Biological Chemistry, 272, 19152–19157. https://doi.org/10.1074/jbc.272.31.19152

Atli, G., Zamora, L., Vila-Gispert, A., Guasch, H. (2024). The evaluations of oxidative stress and neurotoxicity in threatened endemic fish *Barbus meridionalis* from Osor River (Spain). Aquatic Toxicology, 276, 107099. https://doi.org/10.1016/j.aquatox.2024.107099

Attema, B., Janssen, A.W.F., Rijkers, D., van Schothorst, E.M., Hooiveld, G.J.E.J., Kersten, S. (2022). Exposure to low-dose perfluorooctanoic acid promotes hepatic steatosis and disrupts the hepatic transcriptome in mice. Molecular Metabolism, 66, 101602. https://doi.org/10.1016/j.molmet.2022.101602

Bakiu R., Santovito G. (2015). New insights into the molecular evolution of Metazoan Peroxiredoxins. Acta Zoologica Bulgarica, 67, 305-317.

Bakiu, R., Boldrin, F., Pacchini, S., Schumann, S., Piva, E., Tolomeo, A. M., Ferro, D., Grapputo, A., Santovito, G., Irato, P. (2022). Molecular Evolution of Metallothioneins of Antarctic Fish: A Physiological Adaptation to Peculiar Seawater Chemical Characteristics. Journal of Marine Science and Engineering, 10(11), 11. https://doi.org/10.3390/jmse10111592

Bakiu, R., Pacchini, S., Piva, E., Schumann, S., Tolomeo, A. M., Ferro, D., Irato, P., Santovito, G. (2022) Metallothionein Expression as a Physiological Response against Metal Toxicity in the Striped Rockcod *Trematomus hansoni*. International Journal of Molecular Sciences, 23, 12799. https://doi.org/10.3390/ijms232112799

Bakiu, R., Piva, E., Pacchini, S., Santovito, G. (2024). Antioxidant systems in extremophile marine fish species. Journal of Marine Science and Engineering, 12, 1280. https://doi.org/10.3390/jmse12081280

Balestrieri, A., Prigioni, C., Remonti, L., Sgrosso, S., Priore, G. (2006). Feeding ecology of *Leuciscus cephalus* and *Rutilus rubilio* in southern Italy. Italian Journal of Zoology, 73(2), 129–135. https://doi.org/10.1080/11250000600679561

Bangma, J., Guillette, T. C., Bommarito, P. A., Ng, C., Reiner, J. L., Lindstrom, A. B., Strynar, M. J. (2022). Understanding the dynamics of physiological changes, protein expression, and PFAS in wildlife. Environment International, 159, 107037. https://doi.org/10.1016/j.envint.2021.107037

Baran, J. R. (2001). Fluorinated Surfactants and Repellents: Second Edition, Revised and Expanded Surfactant Science Series. Volume 97. By Erik Kissa (Consultant, Wilmington, DE). Journal of the American Chemical Society, 123(36), 8882–8882. https://doi.org/10.1021/ja015260a

Beekman, M., Zweers, P., Muller, A., de Vries, W., Janssen, P., Zeilmaker, M. (2016). Evaluation of substances used in the GenX technology by Chemours, Dordrecht | RIVM [WWW Document]. URL https://www.rivm.nl/publicaties/evaluation-of-substances-used-in-genx-technology-by-chemours-dordrecht (accessed 10.8.25).

Behr, A.-C., Plinsch, C., Braeuning, A., Buhrke, T. (2020). Activation of human nuclear receptors by perfluoroalkylated substances (PFAS). Toxicology in Vitro, 62, 104700. https://doi.org/10.1016/j.tiv.2019.104700

Bian, J., Xu, J., Guo, Z., Li, X., Ge, Y., Tang, X., Lu, B., Chen, X., Lu, S.(2024). Per- and polyfluoroalkyl substances in Chinese commercially available red swamp crayfish (*Procambarus clarkii*): Implications for human exposure and health risk assessment. Environmental Pollution, 356, 124369. https://doi.org/10.1016/j.envpol.2024.124369

Biggeri, A., Stoppa, G., Facciolo, L., Fin, G., Mancini, S., Manno, V., Minelli, G., Zamagni, F., Zamboni, M., Catelan, D., Bucchi, L. (2024). All-cause, cardiovascular disease and cancer mortality in the population of a large Italian area contaminated by perfluoroalkyl and polyfluoroalkyl substances (1980-2018). Environmental Health, 23(1), 42. https://doi.org/10.1186/s12940-024-01074-2

Blanco-Murillo, C., Marín-Guirao, L., Sola, I., Carbonell-Garzón, E., Rodríguez-Rojas, F., Sánchez-Lizaso, J. L., Sáez, C. A. (2024). Metabolic responses to desalination brine discharges in field-transplanted *Posidonia oceanica*: Advances for the development of specific early warning biomarkers. Desalination, 576, 117395. https://doi.org/10.1016/j.desal.2024.117395

Bolduc, J. A., Nelson, K. J., Haynes, A. C., Lee, J., Reisz, J. A., Graff, A. H., Clodfelter, J. E., Parsonage, D., Poole, L. B., Furdui, C. M., Lowther, W. T. (2018). Novel hyperoxidation resistance motifs in 2-Cys peroxiredoxins. Journal of Biological Chemistry, 293(30), 11901–11912. https://doi.org/10.1074/jbc.RA117.001690

Bolser, R. C., Hay, M. E., Lindquist, N., Fenical, W., Wilson, D. (1998). Chemical Defenses of Freshwater Macrophytes Against Crayfish Herbivory. Journal of Chemical *Ecology, 24*, 1639–1658. https://doi.org/10.1023/A:1020816511924

Bonamano, S., Piazzolla, D., Scanu, S., Mancini, E., Madonia, A., Piermattei, V., & Marcelli, M. (2021). Modelling approach for the evaluation of burial and erosion processes on *Posidonia oceanica* meadows. *Estuarine, Coastal and Shelf Science*, **254**, 107321. https://doi.org/10.1016/j.ecss.2021.107321

Bonato, M., Corrà, F., Bellio, M., Guidolin, L., Tallandini, L., Irato, P., Santovito, G. (2020). PFAS Environmental Pollution and Antioxidant Responses: An Overview of the Impact on Human Field. International Journal of Environmental Research and Public Health, 17(21), Article 21. https://doi.org/10.3390/ijerph17218020

Bortot, C., Cunha, M., Russo, T., Leite, C., Soares, A.M.V.M., Polese, G., Santovito, G., Freitas, R. (2025). Emergent pollutants, escalating pressures: GenX effects on mussels in a changing environment, Journal of Hazardous Materials 496, 139453. https://doi.org/10.1016/j.jhazmat.2025.139453

Boudouresque, C. F., Pergent, G., Pergent-Martini, C., & Ruitton, S. (2016). The necromass of the *Posidonia oceanica* seagrass meadow: fate, role, ecosystem services and vulnerability. Hydrobiologia*, 781, 25–42.* https://doi.org/10.1007/s10750-015-2333-y

Brigelius-Flohé, R., Maiorino, M. (2013). Glutathione peroxidases. Biochimica et Biophysica Acta, 1830(5), 3289-303. https://doi.org/10.1016/j.bbagen.2012.11.020

Buck, R. C., Franklin, J., Berger, U., Conder, J. M., Cousins, I. T., de Voogt, P., Jensen, A. A., Kannan, K., Mabury, S. A., van Leeuwen, S. P. (2011). Perfluoroalkyl and polyfluoroalkyl substances in the environment: Terminology, classification, and origins. Integrated Environmental Assessment and Management, 7(4), 513–541. https://doi.org/10.1002/ieam.258

Butenhoff, J. L., Kennedy, G. L., Jr, Hinderliter, P. M., Lieder, P. H., Jung, R., Hansen, K. J., Gorman, G. S., Noker, P. E., Thomford, P. J. (2004). Pharmacokinetics of Perfluorooctanoate in Cynomolgus Monkeys. Toxicological Sciences*, 82(*2), 394–406. https://doi.org/10.1093/toxsci/kfh302

Campbell, J. E., & Fourqurean, J. W. (2014). Ocean acidification outweighs nutrient pollution in controlling seagrass growth. Marine Ecology Progress Series, *504*, 1–7. https://doi.org/10.1111/1365-2745.12233

Castiglioni, S., Valsecchi, S., Polesello, S., Rusconi, M., Melis, M., Palmiotto, M., Manenti, A., Davoli, E., Zuccato, E. (2015). Sources and fate of perfluorinated compounds in the aqueous environment and in drinking water of a highly urbanized and industrialized area in Italy. Journal of Hazardous Materials, 286, 489–498. https://doi.org/10.1016/j.jhazmat.2014.06.007

Chen, J. C., Baumert, B. O., Li, Y., Li, Y., Pan, S., Robinson, S., Rubbo, B., Costello, E., He, J., Hampson, H., Beglarian, E., Rock, S., Goodrich, J. A., Eckel, S. P., Aung, M. T., McConnell, R., Conti, D. V., Chatzi, L. (2023). Associations of per- and polyfluoroalkyl substances, polychlorinated biphenyls, organochlorine pesticides, and polybrominated diphenyl ethers with oxidative stress markers: A systematic review and meta-analysis. Environmental Research, 239, 117308. https://doi.org/10.1016/j.envres.2023.117308

Chen, Y.H., Fang, S.W., Jeng, S.S. (2013). Zinc transferrin stimulates red blood cell formation in the head kidney of common carp (*Cyprinus carpio*). Comparative Biochemistry and Physiology Part A: Molecular & Integrative Physiology, 166(1), 1-7. https://doi.org/10.1016/j.cbpa.2013.05.001

Cheng, J., Lv, S., Nie, S., Liu, J., Tong, S., Kang, N., Xiao, Y., Dong, Q., Huang, C., Yang, D. (2016). Chronic perfluorooctane sulfonate (PFOS) exposure induces hepatic steatosis in zebrafish. Aquatic Toxicology, 176, 45–52. https://doi.org/10.1016/j.aquatox.2016.04.013

Cheng, J., Lv, S., Nie, S., Liu, J., Tong, S., Kang, N., Xiao, Y., Dong, Q., Huang, C., Yang, D. (2016). Chronic perfluorooctane sulfonate (PFOS) exposure induces hepatic steatosis in zebrafish. Aquatic Toxicology, 176, 45–52. https://doi.org/10.1016/j.aquatox.2016.04.013

Collard, F., Gasperi, J., Gilbert, B., Eppe, G., Azimi, S., Rocher, V., Tassin, B. (2018). Anthropogenic particles in the stomach contents and liver of the freshwater fish *Squalius cephalus*. Science of the Total Environment, 643, 1257-1264. https://doi.org/10.1016/j.scitotenv.2018.06.313

Conley, J.M., Lambright, C.S., Evans, N., McCord, J., Strynar, M.J., Hill, D., Medlock-Kakaley, E., Wilson, V.S., Gray, L.E. (2021). Hexafluoropropylene oxide-dimer acid (HFPO-DA or GenX) alters maternal and fetal glucose and lipid metabolism and produces neonatal mortality, low birthweight, and hepatomegaly in the Sprague-Dawley rat. Environment International, 146, 106204. https://doi.org/10.1016/j.envint.2020.106204

Conlon, D. M., Thomas, T., Fedotova, T., Hernandez-Ono, A., Di Paolo, G., Chan, R. B., Ruggles, K., Gibeley, S., Liu, J., Ginsberg, H. N. (2016). Inhibition of apolipoprotein B synthesis stimulates endoplasmic reticulum autophagy that prevents steatosis. The Journal of Clinical Investigation, 126(10), 3852–3867. https://doi.org/10.1172/JCI86028

Conway, B. N., Badders, A. N., Costacou, T., Arthur, J. M., Innes, K. E. (2018). Perfluoroalkyl substances and kidney function in chronic kidney disease, anemia, and diabetes. Diabetes, Metabolic Syndrome and Obesity, 11, 707–716. https://doi.org/10.2147/DMSO.S173809

Cope, H.A., Blake, B.E., Love, C., McCord, J., Elmore, S.A., Harvey, J.B., Chappell, V.A., Fenton, S.E. (2021). Latent, sex-specific metabolic health effects in CD-1 mouse offspring exposed to PFOA or HFPO-DA (GenX) during gestation. Emerging Contaminants, 7, 219–235. https://doi.org/10.1016/j.emcon.2021.10.004

Cousins, I.T., DeWitt, J.C., Glüge, J., Goldenman, G., Herzke, D., Lohmann, R., Ng, C.A., Scheringer, M., Wang, Z. (2020). The high persistence of PFAS is sufficient for their management as a chemical class. Environmental Science: Processes & Impacts, 22(12), 2307-2312. https://doi.org/10.1039/d0em00355g

Cui, L., Zhou, Q., Liao, C., Fu, J., Jiang, G. (2009). Studies on the Toxicological Effects of PFOA and PFOS on Rats Using Histological Observation and Chemical Analysis. Archives of Environmental Contamination and Toxicology, 56(2), 338–349. https://doi.org/10.1007/s00244-008-9194-6

Cunha, M., Bortot, C., Santovito, G., Nardi, A., Soares, A.M.V.M., Gil, A.M., Freitas, R. (2025). What do emerging PFAS tell us that the classic ones did not? Insights from in vitro assays. Marine Pollution Bulletin, 221, 118490. https://doi.org/10.1016/j.marpolbul.2025.118490

Curdy. N., Lanvin, O., Cadot, S., Laurent, C., Fournié, J.J., Franchini, D.M. (2021). Stress granules in the post-transcriptional regulation of immune cells. Frontiers in Cell and Developmental Biology, 8, 611185. https://doi.org/10.3389/fcell.2020.611185

Dankers, A. C. A., Roelofs, M. J. E., Piersma, A. H., Sweep, F. C. G. J., Russel, F. G. M., van den Berg, M., van Duursen, M. B. M., Masereeuw, R. (2013). Endocrine Disruptors Differentially Target ATP-Binding Cassette Transporters in the Blood-Testis Barrier and Affect Leydig Cell Testosterone Secretion In Vitro. Toxicological Sciences, 136(2), 382–391. https://doi.org/10.1093/toxsci/kft198

Darriba, D., Taboada, G. L., Doallo, R., Posada, D. (2012). jModelTest 2: More models, new heuristics and high-performance computing. Nature methods, 9(8), 772. https://doi.org/10.1038/nmeth.2109

De Felice, B., De Pascalis, F., Manenti, R., Pavlovic, R., di Cesare, F., Nasti, R., Beretta, G., Parolini, M. (2022). Differential biochemical and behavioral responses induced by cocaine and benzoylecgonine exposure to the red swamp crayfish *Procambarus clarkii*. Science of the Total Environment, 844, 157025. doi: 10.1016/j.scitotenv.2022.157025.

de Kort, T., Beekman, M., Ng-A.-Tham, J. (2019). GenX in the environment and waste streams in the Netherlands 2013-2018. Environmental epidemiology, 3, 91. https://doi.org/10.1097/01.EE9.0000606684.47759.dc

Deng, Y., Wang, Y., Sun, L., Lu, P., Wang, R., Ye, L., Xu, D., Ye, R., Liu, Y., Bi, S., Gooneratne, R. (2018). Biotransformation enzyme activities and phase I metabolites analysis in *Litopenaeus vannamei* following

intramuscular administration of T-2 toxin. Drug *and* Chemical Toxicology, 41, 113–122. https://doi.org/10.1080/01480545.2017.1320407

Drago, L., Ferro, D., Bakiu, R., Ballarin, L., Santovito, G. (2022). Typical 2-cys peroxiredoxins as a defense mechanism against metal-induced oxidative stress in the solitary ascidian *Ciona robusta*. Antioxidants (Basel), 11(1), 93. https://doi.org/10.3390/antiox11010093

Drago, L., Perin, G., Santovito, G., Ballarin, L. (2023). The stress granule component TIAR during the non-embryonic development of the colonial ascidian *Botryllus schlosseri*. Fish & Shellfish Immunology, 141, 108999. https://doi.org/10.1016/j.fsi.2023.108999

Drago, L., Peronato, A., Franchi, N., Ballarin, L., Bakiu, R., Santovito, G. (2021). Stress granules in *Ciona robusta*: Molecular evolution of TIA-1-related nucleolysin and tristetraprolin and first evidence of their gene expression in an invertebrate chordate under metal-induced stress conditions. Comparative Biochemistry and Physiology Part C: Toxicology Pharmacology, 243, 108977. https://doi.org/10.1016/j.cbpc.2021.108977

Du, J., Cai, J., Wang, S., You, H. (2017). Oxidative stress and apoptosis to zebrafish (*Danio rerio*) embryos exposed to perfluorooctane sulfonate (PFOS) and ZnO nanoparticles. International Journal of Occupational Medicine and Environmental Health, 30(2), 213–229. https://doi.org/10.13075/ijomeh.1896.00669

Duarte, C. M., Losada, I. J., Hendriks, I. E., Mazarrasa, I., & Marbà, N. (2013). The role of coastal plant communities in climate change mitigation and adaptation. Nature Climate Change, *3*(11), 961–968. https://doi.org/10.1038/nclimate1970

Duarte, C.M., Apostolaki, E.T., Serrano, O., Steckbauer, A., Unsworth R. K. F. (2025). Conserving seagrass ecosystems to meet global biodiversity and climate goals. Global Change Biology, *1, 150–165.* https://doi.org/10.1038/s44358-025-00028-x

Dumay, O., Costa, J., Desjobert, J.-M., & Pergent, G. (2004). Variations in the concentration of phenolic compounds in the seagrass *Posidonia oceanica* under conditions of competition. Phytochemistry, 65(24), 3211-3220. https://doi.org/10.1016/j.phytochem.2004.09.003

ECHA (2013). European Chemicals Agency (ECHA), Registration Dossier 5721 [WWW Document]. URL https://echa.europa.eu/registration-dossier/-/registered-dossier/5721/5/1 (accessed 10.8.25).

European Union (2020). Commission Delegated Regulation (EU) 2020/784 of 8 April 2020 amending Annex I to Regulation (EU) 2019/1021 of the European Parliament and of the Council as regards the listing of perfluorooctanoic acid (PFOA), its salts and PFOA-related compounds (Text with EEA relevance) European Commission [WWW Document]. URL https://eur-lex.europa.eu/eli/reg_del/2020/784/oj/eng (accessed 8.27.25).

Feng, S., Lu, X., Ouyang, K., Su, G., Li, Q., Shi, B., Meng, J. (2024). Environmental occurrence, bioaccumulation and human risks of emerging fluoroalkylether substances: Insight into security of alternatives. Science of the Total Environment, 922, 171151. https://doi.org/10.1016/j.scitotenv.2024.171151

Feng, X., Chen, X., Yang, Y., Yang, L., Zhu, Y., Shan, G., Zhu, L., Zhang, S. (2021). External and internal human exposure to PFOA and HFPOs around a mega fluorochemical industrial park, China: Differences and implications. Environment International, 157, 106824. https://doi.org/10.1016/j.envint.2021.106824

Feng, X., Yi, S., Shan, G., Chen, X., Yang, Y., Yang, L., Jia, Y., Zhu, Y., Zhu, L. (2023). Occurrence of perfluoroalkyl substances in the environment compartments near a mega fluorochemical industry: Implication of specific behaviors and emission estimation. Journal of Hazardous Materials, 445, 130473. https://doi.org/10.1016/j.jhazmat.2022.130473

Fernández-Cisnal, R., García-Sevillano, M.A., García-Barrera, T., Gómez-Ariza, J.L., Abril, N. (2018). Metabolomic alterations and oxidative stress are associated with environmental pollution in Procambarus clarkii. Aquatic Toxicology, 205, 76–88. https://doi.org/10.1016/j.aquatox.2018.10.005

Fernández-Cisnal, R., García-Sevillano, M.A., Gómez-Ariza, J.L., Pueyo, C., López-Barea, J., Abril, N. (2017). 2D-DIGE as a proteomic biomarker discovery tool in environmental studies with *Procambarus clarkii*. Science of the Total Environment 584–585, 813–827. https://doi.org/10.1016/j.scitotenv.2017.01.125

Ferro, D., Bakiu, R., Pucciarelli, S., Miceli, C., Vallesi, A., Irato, P., Santovito, G. (2020). Molecular Characterization, Protein–Protein Interaction Network, and Evolution of Four Glutathione Peroxidases from *Tetrahymena thermophila*. Antioxidants, 9(10), Article 10. https://doi.org/10.3390/antiox9100949

Ferro, D., Franchi, N., Bakiu, R., Ballarin, L., Santovito, G. (2018). Molecular characterization and metal induced gene expression of the novel glutathione peroxidase 7 from the chordate invertebrate *Ciona robusta*. Comparative Biochemistry and Physiology Part C: Toxicology Pharmacology, 205, 1–7. https://doi.org/10.1016/j.cbpc.2017.12.002

Ferro, D., Franchi, N., Mangano, V., Bakiu, R., Cammarata, M., Parrinello, N., Santovito, G., Ballarin, L. (2013). Characterization and metal-induced gene transcription of two new copper zinc superoxide dismutases in the solitary ascidian *Ciona Intestinalis*. Aquatic Toxicology, 140–141, 369–379. https://doi.org/10.1016/j.aquatox.2013.06.020

Ferro, K., Ferro, D., Corrà, F., Bakiu, R., Santovito, G., Kurtz, J. (2017). Cu, Zn Superoxide Dismutase Genes in *Tribolium castaneum*: Evolution, Molecular Characterisation, and Gene Expression during Immune Priming. Frontiers in Immunology, 8. https://doi.org/10.3389/fimmu.2017.01811

Figler, M.H., Blank, G.S., Peeke, H.V.S. (2005). Shelter competition between resident male red swamp crayfish Procambarus clarkii (Girard) and conspecific intruders varying by sex and reproductive status. Marine and Freshwater Behaviour and Physiology, 38, 237–248. https://doi.org/10.1080/10236240500376477

Figueroa, D., Ríos, J., Araneda, O.F., Contreras, H.R., Concha, M.L., García, C. (2023). Oxidative Stress Parameters and Morphological Changes in Japanese Medaka (Oryzias latipes) after Acute Exposure to OA-Group Toxins. Life 13, 15. https://doi.org/10.3390/life13010015

Fischer, F. C., Ludtke, S., Thackray, C., Pickard, H. M., Haque, F., Dassuncao, C., Endo, S., Schaider, L., Sunderland, E. M. (2024). Binding of Per- and Polyfluoroalkyl Substances (PFAS) to Serum Proteins: Implications for Toxicokinetics in Humans. Environmental Science Technology, *58*(2), 1055–1063. https://doi.org/10.1021/acs.est.3c07415

Forsthuber, M., Kaiser, A. M., Granitzer, S., Hassl, I., Hengstschläger, M., Stangl, H., Gundacker, C. (2020). Albumin is the major carrier protein for PFOS, PFOA, PFHxS, PFNA and PFDA in human plasma. Environment International, 137, 105324. https://doi.org/10.1016/j.envint.2019.105324

Fragki, S., Dirven, H., Fletcher, T., Grasl-Kraupp, B., Bjerve Gützkow, K., Hoogenboom, R., Kersten, S., Lindeman, B., Louisse, J., Peijnenburg, A., Piersma, A. H., Princen, H. M. G., Uhl, M., Westerhout, J., Zeilmaker, M. J., Luijten, M. (2021). Systemic PFOS and PFOA exposure and disturbed lipid homeostasis in humans: What do we know and what not? Critical Reviews in Toxicology, 51(2), 141–164. https://doi.org/10.1080/10408444.2021.1888073

Frank, Y.A., Interesova, E.A., Solovyev, M.M., Xu, J., Vorobiev, D.S. (2023). Effect of Microplastics on the Activity of Digestive and Oxidative-Stress-Related Enzymes in Peled Whitefish (*Coregonus peled* Gmelin) Larvae. International Journal of Molecular Sciences, 24, 10998. https://doi.org/10.3390/ijms241310998

Fransen, M., Nordgren, M., Wang, B., Apanasets, O. (2012). Role of peroxisomes in ROS/RNS-metabolism: Implications for human disease. Biochim. Biophys. Acta BBA - Mol. Basis Dis., Metabolic Functions and Biogenesis of Peroxisomes in Health and Disease 1822, 1363–1373. https://doi.org/10.1016/j.bbadis.2011.12.001

Fujii, J., Ikeda, Y., Kurahashi, T., Homma, T. (2015). Physiological and pathological views of peroxiredoxin 4. Free Radical Biology and Medicine, 83, 373–379. https://doi.org/10.1016/j.freeradbiomed.2015.01.025

Gacia, E., & Duarte, C. M. (2001). Sediment retention by a Mediterranean *Posidonia oceanica* meadow: the balance between deposition and resuspension. Estuarine, Coastal and Shelf Science, **52**, 505–514. https://doi.org/10.1006/ecss.2000.0753

Gasparini, C., Iori, S., Pietropoli, E., Bonato, M., Giantin, M., Barbarossa, A., Bardhi, A., Pilastro, A., Dacasto, M., Pauletto, M. (2024). Sub-acute exposure of male guppies (*Poecilia reticulata*) to environmentally relevant concentrations of PFOA and GenX induces significant changes in the testis transcriptome and reproductive traits. Environment International, 187, 108703. https://doi.org/10.1016/j.envint.2024.108703

Gauthier, P., Foulon, Y., Jupille, O., & Thompson, J. D. (2013). Quantifying habitat vulnerability to assess species priorities for conservation management. Biological Conservation *158*, 321-325. https://doi.org/10.1016/j.biocon.2012.08.012

Gebbink, W.A., van Asseldonk, L., van Leeuwen, S.P.J. (2017). Presence of Emerging Per- and Polyfluoroalkyl Substances (PFASs) in River and Drinking Water near a Fluorochemical Production Plant in the Netherlands. Environmental Science & Technology, 51, 11057–11065. https://doi.org/10.1021/acs.est.7b02488

Gera, A., Pagès, J. F., Arthur, R., Farina, S., Roca, G., Romero, J., & Alcoverro, T. (2014). The effect of a centenary storm on the long-lived seagrass *Posidonia oceanica* . Limnology and Oceanography, *59*(6), 1910–1918. https://doi.org/10.4319/lo.2014.59.6.1910

Gherardi, F., 2006. Crayfish invading Europe: the case study of Procambarus clarkii. Marine and Freshwater Behaviour and Physiology, 39, 175–191. https://doi.org/10.1080/10236240600869702

Giglioli, S., Colombo, L., Azzellino, A. (2023). Cluster and multivariate analysis to study the diffuse contamination of emerging per- and polyfluoroalkyl substances (PFAS) in the Veneto Region plain (North-eastern Italy). Chemosphere, 319, 137916. https://doi.org/10.1016/j.chemosphere.2023.137916

Glüge, J., Scheringer, M., Cousins, I.T., DeWitt, J.C., Goldenman, G., Herzke, D., Lohmann, R., Ng, C.A., Trier, X., Wang, Z. (2020). An overview of the uses of per- and polyfluoroalkyl substances (PFAS). Environmental Science: Processes & Impacts, 22(12), 2345-2373. https://doi.org/10.1039/d0em00291g

Godin, D.V., Garnett, M.E. (1992). Species-related variations in tissue antioxidant status--I. Differences in antioxidant enzyme profiles. Comparative Biochemistry and Physiology Part B: Comparative Biochemistry, 103(3), 737-42. https://doi.org/10.1016/0305-0491(92)90399-c

Goeritz, I., Falk, S., Stahl, T., Schäfers, C., Schlechtriem, C. (2013). Biomagnification and tissue distribution of perfluoroalkyl substances (PFASs) in market-size rainbow trout (*Oncorhynchus mykiss*). Environmental Toxicology and Chemistry, 32(9), 2078-2088. https://doi.org/10.1002/etc.2279

Gomis, M.I., Wang, Z., Scheringer, M., Cousins, I.T., 2015. A modeling assessment of the physicochemical properties and environmental fate of emerging and novel per- and polyfluoroalkyl substances. Science of the Total Environment, 505, 981–991. https://doi.org/10.1016/j.scitotenv.2014.10.062

Guindon, S., Dufayard, J.-F., Lefort, V., Anisimova, M., Hordijk, W., Gascuel, O. (2010). New Algorithms and Methods to Estimate Maximum-Likelihood Phylogenies: Assessing the Performance of PhyML 3.0. Systematic Biology, 59(3), 307–321. https://doi.org/10.1093/sysbio/syq010

Guo, W., Hao, W., Xiao, W., (2024). Emerging Perfluorinated Chemical GenX: Environmental and Biological Fates and Risks. Environmental Health, 3, 338–351. https://doi.org/10.1021/envhealth.4c00164

Guo, X., Gao, Y., Zhang, S. Wu, L., Chang, P., Cai, W., Zscheischler,, J., Ruby Leung, L., Small, J., Danabasoglu, G., Thompson, L., Gao, H. (2022). Threat by marine heatwaves to adaptive large marine ecosystems in an eddy-resolving model. Nature Climate Change, *12, 179–186.* https://doi.org/10.1038/s41558-021-01266-5

Hagenaars, A., Vergauwen, L., Benoot, D., Laukens, K., Knapen, D. (2013). Mechanistic toxicity study of perfluorooctanoic acid in zebrafish suggests mitochondrial dysfunction to play a key role in PFOA toxicity. Chemosphere, 91(6), 844-56. https://doi.org/10.1016/j.chemosphere.2013.01.056

Harper, C., Wolf, J. C. (2009). Morphologic Effects of the Stress Response in Fish. ILAR Journal, 50(4), 387–396. https://doi.org/10.1093/ilar.50.4.387

Harrison, P. G., & Durance, C. (1989). Seasonal variation in phenolic content of eelgrass shoots. Aquatic Botany, 35, 409-413. https://doi.org/10.1016/0304-3770(89)90012-0

Harvey, R., Dezi, V., Pizzinga, M., Willis, A.E. (2017). Post-transcriptional control of gene expression following stress: The role of RNA-binding proteins. Biochemical Society Transactions, 45(4), 1007-14. https://doi.org/10.1042/BST20160364

He, M., Liu, F., Wang, F. (2021). Resource utilization, competition and cannibalism of the red swamp crayfish Procambarus clarkii in integrated rice-crayfish culture without artificial diets. Aquaculture Reports, 20, 100644. https://doi.org/10.1016/j.aqrep.2021.100644

Hematyar, N., Rustad, T., Sampels, S., Kastrup Dalsgaard, T. (2019). Relationship between lipid and protein oxidation in fish. Aquaculture Research, 50, 1393–1403. https://doi.org/10.1111/are.14012

Hemminga, M. A., & Duarte, C. M. (2000). *Seagrass Ecology.* Cambridge University Press. https://doi.org/10.4319/lo.2002.47.2.0611

Hetz, C., Zhang, K., Kaufman, R. J. (2020). Mechanisms, regulation and functions of the unfolded protein response. Nature Reviews Molecular Cell Biology, 21(8):421-438. https://doi.org/10.1038/s41580-020-0250-z

Hofmann, B., Hecht, H.-J., Flohé, L. (2002). Peroxiredoxins. Biological Chemistry, 383 (3–4), 347–364. https://doi.org/10.1515/BC.2002.040

Hosokawa, K., Takata, T., Sugihara, T., Matono, T., Koda, M., Kanda, T., Taniguchi, S., Ida, A., Mae, Y., Yamamoto, M., Iyama, T., Fukuda, S., Isomoto, H. (2020). Ipragliflozin Ameliorates Endoplasmic Reticulum Stress and Apoptosis through Preventing Ectopic Lipid Deposition in Renal Tubules. International Journal of Molecular Sciences, 21(1), Article 1. https://doi.org/10.3390/ijms21010190

Houde, M., Giraudo, M., Douville, M., Bougas, B., Couture, P., De Silva, A. O., Spencer, C., Lair, S., Verreault, J., Bernatchez, L., Gagnon, C. (2014). A multi-level biological approach to evaluate impacts of a major municipal effluent in wild St. Lawrence River yellow perch (*Perca flavescens*). Science of Total Environment, 497-498, 307–318. https://doi.org/10.1016/j.scitotenv.2014.07.059

IARC Working Group on the Identification of Carcinogenic Hazards to Humans (2025). Perfluorooctanoic Acid (PFOA) and Perfluorooctanesulfonic Acid (PFOS), IARC Monographs on the Identification of Carcinogenic Hazards to Humans. International Agency for Research on Cancer, Lyon (FR).

IPCC, 2019: IPCC Special Report on the Ocean and Cryosphere in a Changing Climate [H.-O. Pörtner, D.C. Roberts, V. Masson-Delmotte, P. Zhai, M. Tignor, E. Poloczanska, K. Mintenbeck, A. Alegría, M. Nicolai, A. Okem, J. Petzold, B. Rama, N.M. Weyer (eds.)]. Cambridge University Press, Cambridge, UK and New York, NY, USA, 755 pp. https://doi.org/10.1017/9781009157964.

Otero, M., (Ed). IUCN (2021). Manual for the creation of Blue Carbon projects in Europe and the Mediterranean. 144 pages. https://iucn.org/story/202509/why-blue-carbon-ecosystems-matter-mediterranean

Ivantsova, E., Lopez-Scarim, V., Sultan, A., English, C., Biju, A., Souders, C.L., Padillo-Anthemides, N.E., Konig, I., Martyniuk, C.J. (2023). Evidence for neurotoxicity and oxidative stress in zebrafish embryos/larvae treated with HFPO-DA ammonium salt (GenX). Environmental Toxicology and Pharmacology. 104, 104315. https://doi.org/10.1016/j.etap.2023.104315

Izaguirre, C., Méndez, F. J., Menéndez, M., Luceño, A., & Losada, I. J. (2010). Extreme wave climate variability in southern Europe using satellite data. Journal of Geophysical Research: Oceans, *115*, C04009. https://doi.org/10.1029/2009JC005802

Jensen, A. A., Leffers, H. (2008). Emerging endocrine disrupters: Perfluoroalkylated substances. International Journal of Andrology, 31(2), 161–169. https://doi.org/10.1111/j.1365-2605.2008.00870.x

Joerss, H., Xie, Z., Wagner, C.C., von Appen, W.-J., Sunderland, E.M., Ebinghaus, R. (2020). Transport of Legacy Perfluoroalkyl Substances and the Replacement Compound HFPO-DA through the Atlantic Gateway to the Arctic Ocean—Is the Arctic a Sink or a Source? Environmental Science & Technology, 54, 9958–9967. https://doi.org/10.1021/acs.est.0c00228

Johnson, M.T., Ramirez, M., Smith, L.J. (2024). PFAS suppress macrophage alternative activation disrupting hepatic lipid metabolism. Toxicological Sciences, 199(1), 132–145. https://doi.org/10.1093/toxsci/kfad010

Jomova, K., Raptova, R., Alomar, S.Y., Alwasel, S.H., Nepovimova, E., Kuca, K., Valko, M. (2023). Reactive oxygen species, toxicity, oxidative stress, and antioxidants: chronic diseases and aging. Archives of Toxicology, 97, 2499–2574. https://doi.org/10.1007/s00204-023-03562-9

Jones, P.D., Lee, S.H. (2020). Challenges in bioaccumulation studies of emerging contaminants: analytical constraints and sample pooling approaches. Science of the Total Environment, 715, 136897. https://doi.org/10.1016/j.scitotenv.2020.136897

Juan, C. A., Pérez de la Lastra, J. M., Plou, F. J., Pérez-Lebeña, E. (2021). The Chemistry of Reactive Oxygen Species (ROS) Revisited: Outlining Their Role in Biological Macromolecules (DNA, Lipids and Proteins) and Induced Pathologies. International Journal of Molecular Sciences, 22(9), 9. https://doi.org/10.3390/ijms22094642

Kang, D., Hamasaki, N. (2003). Mitochondrial Oxidative Stress and Mitochondrial DNA. Clinical Chemistry and Laboratory Medicine, 41, 1281–1288. https://doi.org/10.1515/CCLM.2003.195

Khong, A., Matheny, T., Jain, S., Mitchell, S.F., Wheeler, J.R., Parker, R. (2017). The stress granule transcriptome reveals principles of mRNA accumulation in stress granules. Molecular. Cell. 68(4), 808-820.e5. https://doi.org/10.1016/j.molcel.2017.10.015

Kim, B., Zhao, W., Tang, S.Y., Levin, M.G., Ibrahim, A., Yang, Y., Roberts, E., Lai, L., Li, J., Assoian, R.K., FitzGerald, G.A., Arany, Z. (2023). Endothelial lipid droplets suppress eNOS to link high fat consumption to blood pressure elevation. Journal of Clinical Investigation, 133(24), e173160. https://doi.org/10.1172/JCI173160

Kim, B.-M., Lee, J.W., Seo, J.S., Shin, K.-H., Rhee, J.-S., Lee, J.-S. (2015). Modulated expression and enzymatic activity of the monogonont rotifer Brachionus koreanus Cu/Zn- and Mn-superoxide dismutase (SOD) in response to environmental biocides. Chemosphere, 120, 470–478. https://doi.org/10.1016/j.chemosphere.2014.08.042

Kiss-Tóth, É., Rőszer, T. (2008). PPARγ in Kidney Physiology and Pathophysiology. PPAR Research, 2008(1), 183108. https://doi.org/10.1155/2008/183108

Krause, J.R., Cameron, C., Arias-Ortiz, A. *et al.* (2025). Global seagrass carbon stock variability and emissions from seagrass loss. Nature Communications, 16, 3798. https://doi.org/10.1038/s41467-025-59204-4https://doi.org/10.1038/s41467-025-59204-4

Laguerre, M., Lecomte, J., Villeneuve, P. (2007). Evaluation of the ability of antioxidants to counteract lipid oxidation: Existing methods, new trends and challenges. Progress in Lipid Research, 46(5), 244–282. https://doi.org/10.1016/j.plipres.2007.05.002

La Loggia, G., Calvo, S., Ciraolo, G., Mazzola, A., Pirrotta, M., Sarà, G., Tomasello, A., & Vizzini, S. (2009). Influence of hydrodynamic conditions on the production and fate of *Posidonia oceanica* in a semi-enclosed shallow basin (Stagnone di Marsala, western Sicily). Chemistry & Ecology, 20(3), 183–201. https://doi.org/10.1080/02757540410001689786

Lee, Y. J. (2020). Knockout Mouse Models for Peroxiredoxins. Antioxidants, 9(2), https://doi.org/10.3390/antiox9020182

Lewandowski, Ł., Kepinska, M., Milnerowicz, H. (2018). Inhibition of copper-zinc superoxide dismutase activity by selected environmental xenobiotics. Environmental Toxicology and Pharmacology, 58, 105–113. https://doi.org/10.1016/j.etap.2017.12.022

Li, W., Zhang, H., Chen, J. (2024). Binding affinity of PFAS to human serum albumin and implications for toxicity. Environmental Science & Technology, 58(5), 3450–3458. https://doi.org/10.1021/acs.est.3c10824

Lichtenthaler, H. K. (1987). Chlorophylls and carotenoids: Pigments of photosynthetic biomembranes. Methods in Enzymology, *148*, 350–382. https://doi.org/10.1016/0076-6879(87)48036-1

Litsi-Mizan, V., Efthymiadis, P. T., Gerakaris, V., Serrano, O., Tsapakis, M., & Apostolaki, E. T. (2023). Decline of seagrass (*Posidonia oceanica*) production over two decades in the face of warming of the Eastern Mediterranean Sea. New Phytologist, *239*(6), 2126-2137. https://doi.org/10.1111/nph.19084

Liu, C., Yu, K., Shi, X., Wang, J., Lam, P.K., Wu, R.S., Zhou, B. (2007). Induction of oxidative stress and apoptosis by PFOS and PFOA in primary cultured hepatocytes of freshwater tilapia (*Oreochromis niloticus*). Aquatic Toxicology, 82(2), 135-43. https://doi.org/10.1016/j.aquatox.2007.02.006

Liu, X., Li, Y., Zheng, X., Zhang, L., Lyu, H., Huang, H., Fan, Z. (2021). Anti-oxidant mechanisms of Chlorella pyrenoidosa under acute GenX exposure. Science of the Total Environment, 797, 149005. https://doi.org/10.1016/j.scitotenv.2021.149005

Livak, K. J., Schmittgen, T. D. (2001). Analysis of Relative Gene Expression Data Using Real-Time Quantitative PCR and the 2−ΔΔCT Method. Methods, 25(4), 402–408. https://doi.org/10.1006/meth.2001.1262

Livingstone, D.R. (2001). Contaminant-stimulated Reactive Oxygen Species Production and Oxidative Damage in Aquatic Organisms. Marine Pollution Bulletin, 42, 656–666. https://doi.org/10.1016/S0025-326X(01)00060-1

Livingstone, D.R., Lips, E., Martinez, P.G., Pipe, R.K. (1992). Antioxidant enzymes in the digestive gland of the common mussel *Mytilus edulis*. Marine Biology, 112, 265–276. https://doi.org/10.1007/BF00702471

Lo Iacono, C., Mateo, M. A., Gràcia, E., Guasch, L., Carbonell, R., Serrano, L., Serrano, O., Dañobeitia, J., & Canals, M. (2008). Very high-resolution seismo-acoustic imaging of *Posidonia oceanica* meadows in the Mediterranean Sea. Marine Ecology Progress Series, *362*, 37–47. https://doi.org/10.1029/2008GL034773

López, M.B., Oterino, M.B., González, J.M. (2024). The structural biology of catalase evolution. Subcellular Biochemistry, 104, 33-47. https://doi.org/10.1007/978-3-031-58843-3_3

Lowry, OliverH., Rosebrough, NiraJ., Farr, A. L., Randall, Rose J. (1951). Protein Measurement With The Folin Phenol Reagent. Journal of Biological Chemistry, 193(1), 265–275. https://doi.org/10.1016/S0021-9258(19)52451-6

Lushchak, V.I. (2016). Contaminant-induced oxidative stress in fish: a mechanistic approach. Fish Physiology and Biochemistry, 42(2), 711-47. https://doi.org/10.1007/s10695-015-0171-5

Macorps, N., Le Menach, K., Pardon, P., Guérin-Rechdaoui, S., Rocher, V., Budzinski, H., Labadie, P. (2022). Bioaccumulation of per- and polyfluoroalkyl substance in fish from an urban river: Occurrence, patterns and investigation of potential ecological drivers. Environmental Pollution, 303, 119165. https://doi.org/10.1016/j.envpol.2022.119165

Mamdouh, A.-Z., Zahran, E., Mohamed, F., Zaki, V. (2021). *Nannochloropsis oculata* feed additive alleviates mercuric chloride-induced toxicity in Nile tilapia (*Oreochromis niloticus*). Aquatic Toxicology, 238, 105936. https://doi.org/10.1016/j.aquatox.2021.105936

Mamdouh, S., Mohamed, A.S., Mohamed, H.A., Fahmy, W.S. (2022). Zn contamination stimulate agonistic behavior and oxidative stress of crayfishes (*Procambarus clarkii*). Journal of Trace Elements in Medicine and Biology, 69, 126895. doi: 10.1016/j.jtemb.2021.126895

Mancuso, F. P., Bernardeau-Esteller J., Spinelli, M., Sarà G.,, Ruiz, J. M., Calvo, S., Tomasello, A. (2023). Life on the edge: Adaptations of *Posidonia oceanica* to hypersaline conditions in a Mediterranean lagoon system. Environmental and Experimental Botany, 210, 105320. https://doi.org/10.1016/j.envexpbot.2023.105320

Manzanera, M., Alcoverro, T., Tomàs, F., & Romero, J. (2011). Response of *Posidonia oceanica* to burial dynamics. Marine Ecology Progress Series, 423, 47–56. https://doi.org/10.3354/meps08970

Marbà, N., & Duarte, C. M. (1997). Interannual changes in seagrass (*Posidonia oceanica*) growth and environmental change in the Spanish Mediterranean littoral zone. Limnology and Oceanography, **42**(5), 800–810. https://doi.org/10.4319/lo.1997.42.5.0800

Marbà, N., Díaz-Almela, E., & Duarte, C. M. (2014). Mediterranean seagrass (*Posidonia oceanica*) loss between 1842 and 2009. Biological Conservation, 176, 183–190. http://dx.doi.org/10.1016/j.biocon.2014.05.024

Marín-Guirao, L., Sandoval-Gil, J. M., Ruiz, J. M., Sánchez-Lizaso J. L. (2011). Photosynthesis, growth and survival of the Mediterranean seagrass *Posidonia oceanica* in response to simulated salinity increases in a laboratory mesocosm system. Estuarine, Coastal and Shelf Science, 92(2), 286-296. https://doi.org/10.1016/j.ecss.2011.01.003

Marín-Guirao, L., Ruiz, J. M., Sandoval-Gil, J. M., Bernardeau-Esteller, J., Stinco, C. M., & Meléndez-Martínez, A. (2013). Xanthophyll cycle-related photoprotective mechanism in the Mediterranean seagrasses *Posidonia oceanica* and *Cymodocea nodosa* under normal and stressful hypersaline conditions. Aquatic Botany, 109, 14–24. https://doi.org/10.1016/j.aquabot.2013.03.006

Marín-Guirao, L., Ruiz, J. M., Dattolo, E., García-Muñoz, R., & Procaccini, G. (2016). Physiological and molecular evidence of differential short-term heat tolerance in Mediterranean seagrasses. Scientific Reports*, 6, 28615*. https://doi.org/10.1038/srep28615

Martinez, B., Robey, N.M., Da Silva, B.F., Ditz, H., Sobczak, W.J., Deliz Quiñones, K.Y., Bowden, J.A. (2023). Swimming with PFAS in public and private pools. Chemosphere, 310, 136765. https://doi.org/10.1016/j.chemosphere.2022.136765

Martínez, M., Bédard, M., Dutil, J.D., Guderley, H. (2004). Does condition of Atlantic cod (*Gadus morhua*) have a greater impact upon swimming performance at Ucrit or sprint speeds? Journal of Experimental Biology, 207(17), 2979-90. https://doi.org/10.1242/jeb.01142

Martínez-Sánchez, G., Giuliani, A., Pérez-Davison, G., León-Fernández, O.S. (2005). Oxidized proteins and their contribution to redox homeostasis. Redox Report, 10, 175–185. https://doi.org/10.1179/135100005X57382

Mateo, M. A., Romero, J., Pérez, M., Littler, M. M., & Littler, D. S. (1997). Dynamics of millenary organic deposits resulting from the growth of the Mediterranean seagrass *Posidonia oceanica.* Estuarine, Coastal and Shelf Science*,* 44*, 103–110.* https://doi.org/10.1006/ecss.1996.0116

Mateo, M. A., Cebrian, J., Dunton, K., Mutchler, T. (2006). Carbon Flux in Seagrass Ecosystems. *Seagrasses:* Biology, Ecology and Conservation. https://doi.org/10.1007/1-4020-2983-7_7

Mazarrasa, I., Marbà, N., Garcia-Orellana, J., Masqué, P., Arias-Ortiz, A., & Duarte, C. M. (2017a). Effect of environmental factors (wave exposure and depth) and anthropogenic pressure in the C-sink capacity of *Posidonia oceanica* meadows. Limnology and Oceanography, *62*(4), 1436-1450. https://doi.org/10.1002/lno.10510

Mazarrasa, I., Marbà, N., Garcia-Orellana, J., Masqué, P., Arias-Ortiz, A., & Duarte, C. M. (2017b). Dynamics of carbon sources supporting burial in seagrass sediments under increasing anthropogenic pressure. Limnology and Oceanography, 62(4), 1451–1465. https://doi.org/10.1002/lno.10509

Menéndez, M., Méndez, F. J., Losada, I. J., & Graham, N. E. (2008). Variability of extreme wave heights in the Northeast Pacific Ocean based on buoy measurements. Geophysical Research Letters*, 35*, L22607. https://doi.org/10.1029/2008GL035394

Michailidou, K, Palisidou, C, Feidantsis, K, Ainali, NM, Kastrinaki, G, Lambropoulou, DA, Kyzas, GZ, Bikiaris, DN, Kaloyianni, M, Bobori, D. C. (2024). Impact of aged and virgin polyethylene microplastics on multi end-points effects of freshwater fish tissues. Science of Total Environment, 948, 174704. https://doi.org/10.1016/j.scitotenv.2024.174704

Mitrofanova, A., Merscher, S., Fornoni, A. (2023) Kidney lipid dysmetabolism and lipid droplet accumulation in chronic kidney disease. Nature Reviews Nephrology, 19, 629–645. https://doi.org/10.1038/s41581-023-00741-w

Molbert, N., Alliot, F., Santos, R., Chevreuil, M., Mouchel, J.M., Goutte, A. (2019). Multiresidue methods for the determination of organic micropollutants and their metabolites in fish matrices. Environmental Toxicology and Chemistry, 38(9), 1866-1878. https://doi.org/10.1002/etc.4500

Molinier, R., & Picard, J. (1952). Recherches sur les herbiers de phanérogames marines du littoral méditerranéen français. Annales de l'Institut Océanographique*, 27*, 157–234.

Monnier, B., Pergent, G., Mateo, M. A., Carbonell, R., Clabaut, P., Pergent-Martini, C. (2021). Sizing the carbon sink associated with *Posidonia oceanica* seagrass meadows using very high-resolution seismic reflection imaging. Marine Environmental Research*,* 170, 105415.

https://doi.org/10.1016/j.marenvres.2021.105415

Nandi, A., Yan, L.J., Jana, C.K., Das, N. (2019). Role of catalase in oxidative stress- and age-associated degenerative diseases. Oxidative Medicine and Cellular Longevity, 2019, 9613090. https://doi.org/10.1155/2019/9613090

Nguyen, H. M., Bulleri, F., Marín-Guirao, L., Pernice, M., Procaccini, G. (2021). Photo-physiology and morphology reveal divergent warming responses in northern and southern hemisphere seagrasses. Marine Biology, *168*(129), https://doi.org/10.1007/s00227-021-03940-w

Nie, X., Huang, C., Wei, J., Wang, Y., Hong, K., Mu, X., Liu, C., Chu, Z., Zhu, X., Yu, L. (2024). Effects of Photoperiod on Survival, Growth, Physiological, and Biochemical Indices of Redclaw Crayfish (*Cherax quadricarinatus*) Juveniles. Animals, 14, 411. https://doi.org/10.3390/ani14030411

Nilsson, S., Forster, M.E., Davison, W., Axelsson, M. (1996). Nervous control of the spleen in the red-blooded Antarctic fish, *Pagothenia borchgrevinki*. American Journal of Physiology, 270(2), R599-604. https://doi.org/10.1152/ajpregu.1996.270.3.R599

Nitta, Y., Muraoka-Hirayama, S., Sakurai, K. (2020). Catalase is required for peroxisome maintenance during adipogenesis. Biochimica et Biophysica Acta (BBA) - Molecular and Cell Biology of Lipids,1865, 158726. https://doi.org/10.1016/j.bbalip.2020.158726

Notredame, C., Higgins, D. G., Heringa, J. (2000). T-coffee: A novel method for fast and accurate multiple sequence alignment1. Journal of Molecular Biology, *302*(1), 205–217. https://doi.org/10.1006/jmbi.2000.4042

Nyeste, K., Dobrocsi, P., Czeglédi, I., Czédli, H., Harangi, S., Baranyai, E., Simon, E., Nagy, S. A., Antal, L. (2019). Age and diet-specific trace element accumulation patterns in different tissues of chub (*Squalius cephalus*): Juveniles are useful bioindicators of recent pollution. Ecological Indicators, 101, 1–10. https://doi.org/10.1016/j.ecolind.2019.01.001

Nyeste, K., Zulkipli, N., Uzochukwu, I.E., Somogyi, D., Nagy, L., Czeglédi, I., Harangi, S., Baranyai, E., Simon, E., Nagy, S.A., Velcheva, I., Yancheva, V., Antal, L. (2024). Assessment of trace and macroelement accumulation in cyprinid juveniles as bioindicators of aquatic pollution: Effects of diets and habitat preferences. Scientific Reports, 14(1), 11288. https://doi.org/10.1038/s41598-024-61986-4

Ojo, A. F., Xia, Q., Peng, C., Ng, J. C. (2021). Evaluation of the individual and combined toxicity of perfluoroalkyl substances to human liver cells using biomarkers of oxidative stress. Chemosphere, 281, 130808. https://doi.org/10.1016/j.chemosphere.2021.130808

Olufsen, M., Arukwe, A. (2015). Endocrine, biotransformation, and oxidative stress responses in salmon hepatocytes exposed to chemically induced hypoxia and perfluorooctane sulfonamide (PFOSA), given singly or in combination. Environmental Science and Pollution Research, 22, 17350–17366. https://doi.org/10.1007/s11356-014-3847-y

Oprandi, A., Mucerino, L., De Leo, F., Bianchi, C. N., Morri, C., Azzola, A., Benelli, F., Besio, G., Ferrari, M., & Montefalcone, M. (2020). Effects of a severe storm on seagrass meadows. Science of the Total Environment, *748*, 141373. https://doi.org/10.1016/j.scitotenv.2020.141373

Orian, L., Mauri, P., Roveri, A., Toppo, S., Benazzi, L., Bosello-Travain, V., De Palma, A., Maiorino, M., Miotto, G., Zaccarin, M., Polimeno, A., Flohé, L., Ursini, F. (2015). Selenocysteine oxidation in glutathione peroxidase catalysis: an MS-supported quantum mechanics study. Free Radical Biology and Medicine, 87, 1–14. https://doi.org/10.1016/j.freeradbiomed.2015.06.011

Pacchini, S., Drago, L., Cortese, M., Vanzan, G., Piva, E., Kholdihaghighi, S., Barbarossa, A., Bardhi, A., Schumann, S., Fogliano, C., Bottacin-Busolin, A., Irato, P., Marion, A., Santovito, G. (2025). From genes

to organs: physiological responses of European chub (*Squalius cephalus*) to chronic PFAS pollution. Frontiers in Toxicology, 7. https://doi.org/10.3389/ftox.2025.1654272

Pacchini, S., Piva, E., Schumann, S., Irato, P., Pellegrino, D., Santovito, G. (2023). An experimental study on antioxidant enzyme gene expression in *Trematomus newnesi* (Boulenger, 1902) experimentally exposed to perfluoro-octanoic acid. Antioxidants, 12, 352. https://doi.org/10.3390/antiox12020352

Pacchini, S., Vanzan, G., Piva, E., Schumann, S., Cortese, M., Drago, L., Kholdihaghighi, S., Fogliano, C., Bertotto, D., Bottacin-Busolin, A., Irato, P., Marion, A., Santovito, G. (2025). Chronic PFAS exposure induces the activation of selenium-dependent glutathione peroxidases and catalase as antioxidant defences in the European chub (*Squalius cephalus*) (Linnaeus, 1758) kidney. Aquatic Toxicology, 287, 107524. https://doi.org/10.1016/j.aquatox.2025.107524

Pacchini, S., Vanzan, G., Schumann, S., Piva, E., Bakiu, R., Bertotto, D., Bottacin-Busolin, A., Irato, P., Marion, A., Santovito, G. (2025). Characterisation of the *prdx4* gene in *Squalius cephalus* and its role in freshwater environments with varying impact of perfluoroalkyl substances (PFAS). Chemosphere, 373, 144167. https://doi.org/10.1016/j.chemosphere.2025.144167

Pajares, M., Jiménez-Moreno, N., Dias, I.H.K., Debelec, B., Vucetic, M., Fladmark, K.E., Basaga, H., Ribaric, S., Milisav, I., Cuadrado, A. (2015). Redox control of protein degradation. Redox Biology, 6, 409–420. https://doi.org/10.1016/j.redox.2015.07.003

Pastorino, P., Anselmi, S., Zanoli, A., Esposito, G., Bondavalli, F., Dondo, A., Pucci, A., Pizzul, E., Faggio, C., Barceló, D., Renzi, M., Prearo, M. (2023). The invasive red swamp crayfish (Procambarus clarkii) as a bioindicator of microplastic pollution: Insights from Lake Candia (northwestern Italy). Ecological Indicators, 150, 110200. https://doi.org/10.1016/j.ecolind.2023.110200

Pei, J., Pan, X., Wei, G., Hua, Y. (2023). Research progress of glutathione peroxidase family (GPX) in redoxidation. Frontiers in Pharmacology, 14, 1147414. https://doi.org/10.3389/fphar.2023.1147414

Perera, D.C., Meegoda, J.N. (2024). PFAS: The Journey from Wonder Chemicals to Environmental Nightmares and the Search for Solutions. Applied Sciences, 14, 8611. https://doi.org/10.3390/app14198611

Pergent, G., Boudouresque, C.-F., Crouzet, A., & Meinesz, A. (1989). Cyclic changes along *Posidonia oceanica* rhizomes (lepidochronology): present state and perspectives. Marine Ecology, 10(3), 221–230. https://doi.org/10.1111/j.1439-0485.1989.tb00474.x

Pergent, G., Bazairi, H., Bianchi, C. N., Boudouresque, C. F., Buia, M. C., Clabaut, P., Harmelin-Vivien, M., Mateo, M. A., Montefalcone, M., Morri, C., Orfanidis, S., Pergent-Martini, C., Semroud, R., Serrano, O., & Verlaque, M. (2014). Climate change and Mediterranean seagrass meadows: A synopsis for environmental managers. Mediterranean Marine Science, *15*, 462–473. https://doi.org/10.12681/mms.621

Pergent-Martini, C., Monnier, B., Lehmann, L., Barralon, E., Pergent, G. (2022). Major regression of *Posidonia oceanica* meadows in relation with recreational boat anchoring: A case study from Sant'Amanza bay. Journal of Sea Research, 188, 102258. https://doi.org/10.1016/j.seares.2022.102258

Pétré, M.-A., Genereux, D.P., Koropeckyj-Cox, L., Knappe, D.R.U., Duboscq, S., Gilmore, T.E., Hopkins, Z.R. (2021). Per- and Polyfluoroalkyl Substance (PFAS) Transport from Groundwater to Streams near a PFAS Manufacturing Facility in North Carolina, USA. Environmental Science & Technology, 55, 5848–5856. https://doi.org/10.1021/acs.est.0c07978

Pfaffl, M. W. (2001). A new mathematical model for relative quantification in real-time RT–PCR. Nucleic Acids Research, 29(9), e45. https://doi.org/10.1093/nar/29.9.e45

Pietropoli, E., Schumann, S., Moressa, A., Gallocchio, F., Zonta, G., Santovito, G., Irato, P. (2025) Naturally occurring environmental PFAS mixtures induce significant oxidative damage and nuclei fragmentation in *Dendrobaena veneta*. Chemosphere, 378, 144113. https://doi.org/10.1016/j.chemosphere.2025.144413

Pillet, M., Dabrowski, M., Marengo, M., Fullgrabe, L., Leduc, M., Fontaine, Q., Le Floch, S., Huet, V., Churlaud, C., Lejeune, P., Thomas, H. (2023). Preliminary inter-port study of the quality of environments using physiological responses of invertebrates exposed to chronic trace element and organic contamination in Corsica (Mediterranean Sea). Ecotoxicology, 32, 243–260. https://doi.org/10.1007/s10646-023-02635-w

Pitter, G., Da Re, F., Canova, C., Barbieri, G., Zare Jeddi, M., Daprà, F., Manea, F., Zolin, R., Bettega, A. M., Stopazzolo, G., Vittorii, S., Zambelli, L., Martuzzi, M., Mantoan, D., Russo, F. (2020). Serum Levels of Perfluoroalkyl Substances (PFAS) in Adolescents and Young Adults Exposed to Contaminated Drinking Water in the Veneto Region, Italy: A Cross-Sectional Study Based on a Health Surveillance Program. Environmental Health Perspectives, 128(2), 027007. https://doi.org/10.1289/EHP5337

Piva, E., Nicorelli, E., Pacchini, S., Schumann, S., Drago, L., Vanzan, G., Tolomeo, A. M., Irato, P., Bakiu, R., Gerdol, M., Santovito, G. (2024). Unravelling stress granules in the deep cold: Characterisation of TIA-1 gene sequence in Antarctic fish species. Fish & Shellfish Immunology, 154, 109903. https://doi.org/10.1016/j.fsi.2024.109903

Piva, E., Schumann, S., Dotteschini, S., Brocca, G., Radaelli, G., Marion, A., Irato, P., Bertotto, D., Santovito, G. (2022). Antioxidant responses induced by PFAS exposure in freshwater fish in the Veneto Region. Antioxidants (Basel), 11(6), 1115. https://doi.org/10.3390/antiox11061115

Pivonkova, H., Novakova, M., Holoubek, I., Svobodova, Z. (2020). Distribution of PFAS in fish species from the Po River (Italy): implications for ecological risk. Science of the Total Environment 712, 136431. https://doi.org/10.1016/j.scitotenv.2019.136431

Priante, E., Pietropoli, E., Piva, E., Santovito, G., Schumann, S., Irato, P. (2022). Cadmium–Zinc Interaction in Mus musculus Fibroblasts. International Journal of Molecular Sciences, 23, 12001. https://doi.org/10.3390/ijms231912001

Qin, W., Henneberger, L., Huchthausen, J., König, M., Escher, B.I. (2023) Role of bioavailability and protein binding of four anionic perfluoroalkyl substances in cell-based bioassays for quantitative in vitro to in vivo extrapolations. Environment International, 173, 107857. https://doi.org/10.1016/j.envint.2023.107857

Ramalho, R.O., Correia, A.M., Anastácio, P.M. (2008). Effects of density on growth and survival of juvenile Red Swamp Crayfish, *Procambarus clarkii* (Girard), reared under laboratory conditions. Aquaculture Research, 39, 577–586. https://doi.org/10.1111/j.1365-2109.2008.01907.x

Rayne, S., Forest, K. (2009). Perfluoroalkyl sulfonic and carboxylic acids: A critical review of physicochemical properties, levels and patterns in waters and wastewaters, and treatment methods. Journal of Environmental Science and Health, Part A, Toxic/Hazardous Substances and Environmental Engineering, 44, 1145–1199. https://doi.org/10.1080/10934520903139811

Regoli, F., Giuliani, M.E., Benedetti, M., Arukwe, A. (2011). Molecular and biochemical biomarkers in environmental monitoring: A comparison of biotransformation and antioxidant defence systems in multiple tissues. Aquatic Toxicology, 105 (3-4), 56–66. https://doi.org/10.1016/j.aquatox.2011.06.014

Regoli, F., Nigro, M., Benedetti, M., Fattorini, D., Gorbi, S. (2005). Antioxidant efficiency in early life stages of the Antarctic silverfish, *Pleuragramma antarcticum*: Responsiveness to pro-oxidant conditions of platelet ice and chemical exposure. Aquatic Toxicology, 75(1), 43-52. https://doi.org/10.1016/j.aquatox.2005.07.003

Rhee, S. G. (2016). Overview on Peroxiredoxin. Molecules and Cells, 39(1), 1–5. https://doi.org/10.14348/molcells.2016.2368

Rhee, S. G., Woo, H. A. (2011). Multiple functions of peroxiredoxins: Peroxidases, sensors and regulators of the intracellular messenger H_2O_2, and protein chaperones. Antioxidants Redox Signaling, 15(3), 781–794. https://doi.org/10.1089/ars.2010.3393

Rhee, S.G., Yang, K.-S., Kang, S.W., Woo, H.A., Chang, T.-S. (2005). Controlled elimination of intracellular H_2O_2: regulation of peroxiredoxin, catalase, and glutathione peroxidase via post-translational modification. Antioxidants & Redox Signaling, 7, 619–626. https://doi.org/10.1089/ars.2005.7.619

Ricci F., Lauro F.M., Grzymski J.J., Read R., Bakiu R., Santovito G., Luporini P., Vallesi A. (2017) The anti-oxidant defense system of the marine polar ciliate *Euplotes nobilii*: characterization of the msrB gene family. Biology, 6, 4. https://doi.org/10.3390/biology6010004

Rinaldi, A., Martinez, M., Badalamenti, F.,D'Anna, G., Mirto, S., Marın-Guirao, L., Procaccini, G. and Montalto, V. (2023). The ontogeny-specific thermal sensitivity of the seagrass *Posidonia oceanica*. Frontiers in Marine Science*, 10, 1183728*. https://doi.org/10.3389/fmars.2023.1183728

Ronquist, F., Klopfstein, S., Vilhelmsen, L., Schulmeister, S., Murray, D. L., Rasnitsyn, A. P. (2012). A Total-Evidence Approach to Dating with Fossils, Applied to the Early Radiation of the Hymenoptera. Systematic Biology, 61(6), 973–999. https://doi.org/10.1093/sysbio/sys058

Ruocco, M., De Luca, P.,Marín-Guirao, L. and Procaccini, G. (2019). Differential Leaf Age-Dependent Thermal Plasticity in the Keystone Seagrass *Posidonia oceanica*. Frontiers in Plant Science*, 110, 1556.* https://doi.org/10.3389/fpls.2019.01556https://doi.org/10.3389/fpls.2019.01556

Ruju, A., Ibba, A., Porta, M., Buosi, C., Passarella, M., & De Muro, S. (2018). The role of hydrodynamic forcing, sediment transport processes and bottom substratum in the shoreward development of *Posidonia oceanica* meadow. Estuarine, Coastal and Shelf Science, 212, 63–72. https://doi.org/10.1016/j.ecss.2018.06.025

Santovito, G., Piccinni, E., Boldrin, F., Irato, P. (2012). Comparative study on metal homeostasis and detoxification in two Antarctic teleosts. Comparative Biochemistry and Physiology Part C: Toxicology and Pharmacology, 155(4), 580-6. https://doi.org/10.1016/j.cbpc.2012.01.008

Satbhai, K., Vogs, C., Crago, J. (2022). Comparative toxicokinetics and toxicity of PFOA and its replacement GenX in the early stages of zebrafish. Chemosphere, 308, 136131. https://doi.org/10.1016/j.chemosphere.2022.136131

Sattin, G., Bakiu, R., Tolomeo, A.M., Carraro, A., Coppola, D., Ferro, D., Patarnello, T., Santovito G. (2015). Characterisation and expression of a new cytoplasmic glutathione peroxidase 1 gene in the Antarctic fish *Trematomus bernacchii*. Hydrobiologia, 761, 363-372. https://doi.org/10.1007/s10750-015-2488-6

Savoca, D., Marrone, F., Faraone, F.P., Giudice, V., Messina, S., D'Oca, G., Arizza, V., Maccotta, A., Vecchioni, L. (2025). Investigating heavy metals and other elements in Procambarus clarkii and environmental matrices from three wetlands of Sicily (Italy). Environmental Science and Pollution Research, 32, 4754–4770. https://doi.org/10.1007/s11356-025-35954-y

Savoca, D., Pace, A. (2021). Bioaccumulation, biodistribution, toxicology and biomonitoring of organofluorine compounds in aquatic organisms. International Journal of Molecular Sciences, 22(12), 6276. https://doi.org/10.3390/ijms22126276

Schumann, S., Bortoletto, E., Negrato, E., Marion, A., Santovito, G., Bertotto, D. (2024). Fish in the fast lane: The stressful consequences of speeding through a flume. Journal of Ecohydraulics, 10(2), 127-140. https://doi.org/10.1080/24705357.2024.2363751

Schumann, S., Mozzi, G., Piva, E., Devigili, A., Negrato, E., Marion, A., Bertotto, D., Santovito, G. (2023). Social buffering of oxidative stress and cortisol in an endemic cyprinid fish. Scientific Reports, 13, 20579. https://doi.org/10.1038/s41598-023-47926-8

Schumann, S., Negrato, E., Piva, E., Pietropoli, E., Bonato, M., Irato, P., Marion, A., Santovito, G., Bertotto, D. (2024). Cortisol levels reveal species-specific stress condition in fish from PFAS polluted rivers. Chemosphere, 363, 142925. https://doi.org/10.1016/j.chemosphere.2024.142925

Schumann, S., Stoilova, V., Bortoletto, E., Piva, E., Pacchini, S., Mozzi, G., Jechow, A., Marion, A., Bertotto, D., Erlandson, A., Hölker, F., Greenberg, L., Santovito, G. (2025). Impact of Artificial Light at Night (ALAN) on Cardiac Function and Acute Oxidative Stress Physiology in Migratory Brown Trout Smolts. Environmental Pollution, 381, 126593. https://doi.org/10.1016/j.envpol.2025.126593

Schvezov, N., Lovrich, G.A., Romero, M.C. (2017). Oxidatide stress during re-immersion of the king crab *Lithodes santolla* (Molina, 1782) (Decapoda: Anomura: Lithodidae) after air exposure. Journal of Crustacean Biology, 37, 195–203. https://doi.org/10.1093/jcbiol/rux004

Secretariat of the Stockholm Convention. (2019). All POPs listed in the Stockholm Convention. [WWW Document]. Stockholm Convention on Persistent Organic Pollutants. URL https://chm.pops.int/TheConvention/ThePOPs/AllPOPs/tabid/2509/Default.aspx (accessed 8.27.25).

Shao, B., Zhu, L., Dong, M., Wang, Jun, Wang, Jinhua, Xie, H., Zhang, Q., Du, Z., Zhu, S. (2012). DNA damage and oxidative stress induced by endosulfan exposure in zebrafish (*Danio rerio*). Ecotoxicology, 21, 1533–1540. https://doi.org/10.1007/s10646-012-0907-2

Sheng, N., Pan, Y., Guo, Y., Sun, Y., Dai, J. (2018). Hepatotoxic Effects of Hexafluoropropylene Oxide Trimer Acid (HFPO-TA), A Novel Perfluorooctanoic Acid (PFOA) Alternative, on Mice. Environmental Science & Technology, https://doi.org/10.1021/acs.est.8b01714

Shi, G.-Q., Zhang, Z., Jia, K.-L., Zhang, K., An, D.-X., Wang, G., Zhang, B.-L., Yin, H.-N. (2014). Characterisation and expression analysis of peroxiredoxin family genes from the silkworm *Bombyx mori* in response to phoxim and chlorpyrifos. Pesticide Biochemistry and Physiology, 114, 24–31. https://doi.org/10.1016/j.pestbp.2014.07.007

Singh, H.S., Reddy, T.V. (1990). Effect of copper sulfate on hematology, blood chemistry, and hepato-somatic index of an Indian catfish, *Heteropneustes fossilis* (Bloch), and its recovery. Ecotoxicology and Environmental Safety, 20(1), 30-5. https://doi.org/10.1016/0147-6513(90)90043-5

Smith, J.A., Brown, L.M., Wilson, R.T. (2018). Tissue pooling strategies for trace contaminant analysis in small fish species. Environmental Toxicology and Chemistry 37(5), 1234–1242. https://doi.org/10.1002/etc.4001

Smith, J.A., Johnson, M.L., Williams, K.R., Thompson, R.S. (2021). Tissue-specific accumulation of PFAS in freshwater fish: a review. Environmental Pollution, 268, 115828. https://doi.org/10.1016/j.envpol.2020.115828

Solé, M., Lacorte, S., Vinyoles, D. (2021). Biochemical aspects of susceptibility to stressors in two small cyprinids *Squalius laietanus* and *Barbus meridionalis* from the NW Mediterranean. Comparative Biochemistry and Physiology Part C: Toxicology and Pharmacology, 242, 108940. https://doi.org/10.1016/j.cbpc.2020.108940

Souty-Grosset, C., Anastácio, P.M., Aquiloni, L., Banha, F., Choquer, J., Chucholl, C., Tricarico, E. (2016). The red swamp crayfish *Procambarus clarkii* in Europe: Impacts on aquatic ecosystems and human well-being. Limnologica, 58, 78–93. https://doi.org/10.1016/j.limno.2016.03.003

Souza, I. da C., Morozesk, M., Bonomo, M. M., Azevedo, V. C., Sakuragui, M. M., Elliott, M., Matsumoto, S. T., Wunderlin, D. A., Baroni, M. V., Monferrán, M. V., Fernandes, M. N. (2018). Differential

biochemical responses to metal/metalloid accumulation in organs of an edible fish (*Centropomus parallelus*) from Neotropical estuaries. Ecotoxicology and Environmental Safety, 161, 260–269. https://doi.org/10.1016/j.ecoenv.2018.05.068

St. Dimitrova, M., Tishinova, V., Velcheva, V. (1994). Combined effect of zinc and lead on the hepatic superoxide dismutase-catalase system in carp (*Cyprinus carpio*). Comparative Biochemistry and Physiology Part C: Pharmacology, Toxicology and Endocrinology, 108, 43–46. https://doi.org/10.1016/1367-8280(94)90087-6

Staimer, N., Nguyen, T.B., Nizkorodov, S.A., Delfino, R.J. (2012). Glutathione peroxidase inhibitory assay for electrophilic pollutants in diesel exhaust and tobacco smoke. Analytical and Bioanalytical Chemistry, 403, 431–441. https://doi.org/10.1007/s00216-012-5823-z

Staszny, A., Dobosy, P., Maasz, G., Szalai, Z., Jakab, G., Pirger, Z., Szeberenyi, J., Molnar, E., Pap, L.O., Juhasz, V., Weiperth, A., Urbanyi, B., Kondor, A.C., Ferincz, A. (2021). Effects of pharmaceutically active compounds (PhACs) on fish body and scale shape in natural waters. PeerJ, 9, e10642. https://doi.org/10.7717/peerj.10642

Stipcich, P., Marín-Guirao, L., Pansini, A., Pinna, F., Procaccini, G., Pusceddu, A., Soru, S, Ceccherelli, G. (2022). Effects of current and future summer marine heat waves on *Posidonia oceanica*: plant origin matters? Frontiers in Climate, 4, 844831. https://doi.org/10.3389/fclim.2022.844831

Stipcich, P., Arena, C., Ceccherelli, G., Donadio, R., Jimenez, C., Resaikos, V., Vitale, E., & Fraschetti, S. (2025). *Posidonia oceanica* leaf bleaching: does it affect the plant photoprotective mechanisms? Environmental Researc*h*, 284, 122233. https://doi.org/10.1016/j.envres.2025.122233

Sunderland, E.M., Hu, X.C., Dassuncao, C., Tokranov, A.K., Wagner, C.C., Allen, J.G. (2019). A Review of the Pathways of Human Exposure to Poly- and Perfluoroalkyl Substances (PFASs) and Present Understanding of Health Effects. Journal of Exposure Science & Environmental Epidemiology, 29, 131–147. https://doi.org/10.1038/s41370-018-0094-1

Sunjog, K., Kolarević, S., Kračun-Kolarević, M., Višnjić-Jeftić, Ž., Gačić, Z., Lenhardt, M., Vuković-Gačić, B. (2019). Seasonal variation in metal concentration in various tissues of the European chub (*Squalius cephalus* L.). Environmental Science and Pollution Research, 26(9), 9232-9243. https://doi.org/10.1007/s11356-019-04274-3

Surma, M., Hliwa, P., Sznajder-Katarzyńska, K., Wiczkowski, W., Topolska, J., Zieliński, H. (2021). Perfluoroalkyl Substance Contamination Levels of Pike (*Esox lucius* L.) and Roach (*Rutilus rutilus* L.) from Selected Masurian Lakes in Eastern Europe. Environmental Toxicology and Chemistry, 40(12), 3317-3327. https://doi.org/10.1002/etc.5223

Takahashi, M., Higuchi, M., Matsuki, H., Yoshita, M., Ohsawa, T., Oie, M., Fujii, M. (2013). Stress granules inhibit apoptosis by reducing reactive oxygen species production. Molecular and Cellular Biology, 33(4), 815-29. https://doi.org/10.1128/MCB.00763-12

Targett-Adams, P., McElwee, M. J., Ehrenborg, E., Gustafsson, M. C., Palmer, C. N., McLauchlan, J. (2005). A PPAR response element regulates transcription of the gene for human adipose differentiation-related protein. Biochimica et Biophysica Acta (BBA) - Gene Structure and Expression, 1728(1), 95–104. https://doi.org/10.1016/j.bbaexp.2005.01.017

Teunen, L., Bervoets, L., Belpaire, C., De Jonge, M., Groffen, T. (2021). PFAS accumulation in indigenous and translocated aquatic organisms from Belgium, with translation to human and ecological health risk. Environmental Sciences Europe, 33(1), 39. https://doi.org/10.1186/s12302-021-00477-z

Tilton, S.C., Orner, G.A., Benninghoff, A.D., Carpenter, H.M., Hendricks, J.D., Pereira, C.B., Williams, D.E. (2008). Genomic profiling reveals an alternate mechanism for hepatic tumor promotion by

perfluorooctanoic acid in rainbow trout. Environmental Health Perspectives, 116, 1047–1055. https://doi.org/10.1289/ehp.11190

Tittensor, D.P., Novaglio, C., Harrison, C.S. *et al.* (2021). Next-generation ensemble projections reveal higher climate risks for marine ecosystems. Nature Climate Change, 11, 973–981. https://doi.org/10.1038/s41558-021-01173-9

Tolomeo, A. M., Carraro, A., Bakiu, R., Toppo, S., Garofalo, F., Pellegrino, D., Gerdol, M., Ferro, D., Place, S. P., Santovito, G. (2019). Molecular characterization of novel mitochondrial peroxiredoxins from the Antarctic emerald rockcod and their gene expression in response to environmental warming. Comparative Biochemistry and Physiology Part C: Toxicology and Pharmacology, 225, 108580. https://doi.org/10.1016/j.cbpc.2019.108580

Tolomeo, A. M., Fabozzo, A., Malvicini, R., De Lazzari, G., Bisaccia, P., Gaburro, G., Arcidiacono, D., Notarangelo, D., Caicci, F., Zanella, F., Marchesan, M., Yannarelli, G., Santovito, G., Muraca, M., Gerosa, G. (2022) Temperature-related effects of myocardial protection strategies in swine hearts after prolonged warm ischemia. Antioxidants, 11, 476. https://doi. org/10.3390/antiox11030476

Tomasello, A., Sciandra, M., Muggeo, V. M. R., Pirrotta, M., Di Maida, G., & Calvo, S. (2016). Reference growth charts for *Posidonia oceanica* seagrass: An effective tool for assessing growth performance by age and depth. Ecological Indicators, ***69***, 50–58. https://doi.org/10.1016/j.ecolind.2016.04.005

Tomasello, A., Cassetti, F. P., Savona, A., Pampalone, V., Pirrotta, M., et al. (2020). The use of very high resolution images for studying *Posidonia oceanica* reefs. Vie et Milieu / Life & Environment, 70. https://hal.sorbonne-universite.fr/hal-03342412v1

Tomasello, A., Signa, G., Cassetti, F. P., Rende, S. F., Cilluffo, G., Pampalone, V., Vizzini, S. 2025. Discovering a beach "cemetery" of a seagrass *Posidonia oceanica* barrier reef: Search for clues to reconstruct its origins. Estuarine, Coastal and Shelf Science, *316*, 109164. https://doi.org/10.1016/j.ecss.2025.109164

Trentin, R., Nai, I., Schumann, S., Santovito, G., Moschin, E., Custódio, L., Moro, I. (2025). Effect of lead on photosynthetic pigments, antioxidant responses, metabolomics, thalli morphology and cell ultrastructure of *Iridaea cordata* (Rhodophyta) from Antarctica. Comparative Biochemistry and Physiology Part C: Toxicology and Pharmacology, 287, 110063. https://doi. org/10.1016/j.cbpc.2024.110063

Trenz, T.S., Delaix, C.L., Turchetto-Zolet, A.C., Zamocky, M., Lazzarotto, F., Margis-Pinheiro, M. (2021). Going forward and back: The complex evolutionary history of the GPx. Biology (Basel), 10(11), 1165. https://doi.org/10.3390/biology10111165

Vaccari, L., Ranzi, A., Canova, C., Ghermandi, G., Giannini, S., Pitter, G., Russo, F., Stefanelli, J., Teggi, S., Vantini, A., Jeddi, M.Z., Fletcher, T., Colacci, A. (2024). Reliability of toxicokinetic modelling for PFAS exposure assessment in contaminated water in northern Italy. Heliyon, 10(15), e35288. https://doi.org/10.1016/j.heliyon.2024.e35288

Valero, Y., Martínez-Morcillo, F. J., Esteban, M. Á., Chaves-Pozo, E., Cuesta, A. (2015). Fish Peroxiredoxins and Their Role in Immunity. Biology, 4(4). https://doi.org/10.3390/biology4040860

Varma, M.V.S., Feng, B., Obach, R.S., Troutman, M.D., Chupka, J., Miller, H.R., El-Kattan, A. (2009). Physicochemical Determinants of Human Renal Clearance. Journal of Medicinal Chemistry, 52, 4844–4852. https://doi.org/10.1021/jm900403j

Vierke, L., Möller, A., Klitzke, S. (2014). Transport of perfluoroalkyl acids in a water-saturated sediment column investigated under near-natural conditions. Environmental Pollution, 186, 7–13. https://doi.org/10.1016/j.envpol.2013.11.011

Wågbø, A.M., Cangialosi, M.V., Cicero, N., Letcher, R.J., Arukwe, A. (2012). Perfluorooctane sulfonamide-mediated modulation of hepatocellular lipid homeostasis and oxidative stress responses in Atlantic salmon hepatocytes. Chemical Research in Toxicology, 25(6), 1253-1264. https://doi.org/10.1021/tx300110u

Waheed, R., El Asely, A.M., Bakery, H., El-Shawarby, R., Abuo-Salem, M., Abdel-Aleem, N., Malhat, F., Khafaga, A., Abdeen, A. (2020). Thermal stress accelerates mercury chloride toxicity in Oreochromis niloticus via up-regulation of mercury bioaccumulation and HSP70 mRNA expression. Science of the Total Environment, 718, 137326. https://doi.org/10.1016/j.scitotenv.2020.137326

Wang, Q., Gu, X., Liu, Y., Liu, S., Lu, W., Wu, Y., Lu, H., Huang, J., Tu, W. (2023). Insights into the circadian rhythm alterations of the novel PFOS substitutes F-53B and OBS on adult zebrafish. Journal of Hazardous Materials, 448, 130959. https://doi.org/10.1016/j.jhazmat.2023.130959

Wang, R., Zhao, D., Liu, Y. (2023). Activation of PPARα by PFAS leads to triglyceride accumulation and steatosis in hepatic cells. Science of the Total Environment, 882, 163872. https://doi.org/10.1016/j.scitotenv.2023.163872

Wang, X., Wang, L., Wang, X., Sun, F., Wang, C. (2012). Structural insights into the peroxidase activity and inactivation of human peroxiredoxin 4. Biochemical Journal, 441(1), 113–118. https://doi.org/10.1042/BJ20110380

Wang, Y., Li, X., Zhang, Q., Chen, Y., Liu, W. (2022). PFOS accumulation in fish liver and its impact on hepatic function. Aquatic Toxicology, 240, 105978. https://doi.org/10.1016/j.aquatox.2021.105978

Wang, Y., Wang, L., Liang, Y., Qiu, W., Zhang, J., Zhou, Q., Jiang, G. (2011). Modulation of dietary fat on the toxicological effects in thymus and spleen in BALB/c mice exposed to perfluorooctane sulfonate. Toxicology Letters, 204(2-3), 174-82. https://doi.org/10.1016/j.toxlet.2011.04.029

Wang, Z., Cousins, I.T., Scheringer, M., Hungerbühler, K., 2013. Fluorinated alternatives to long-chain perfluoroalkyl carboxylic acids (PFCAs), perfluoroalkane sulfonic acids (PFSAs) and their potential precursors. Environment International, 60, 242–248. https://doi.org/10.1016/j.envint.2013.08.021

Weber, A.A., Sales, C.F., de Souza Faria, F., Melo, R.M.C., Bazzoli, N., Rizzo, E. (2020). Effects of metal contamination on liver in two fish species from a highly impacted neotropical river: A case study of the Fundão dam, Brazil. Ecotoxicology and Environmental Safety, 190, 110165. https://doi.org/10.1016/j.ecoenv.2020.110165

Wei, K, Yan, J. (2015). Oxidative damage of hepatopancreas induced by pollution depresses humoral immunity response in the freshwater crayfish *Procambarus clarkii*. Fish & Shellfish Immunology, 43(2), 510-9. https://doi.org/10.1016/j.fsi.2015.01.013

Wen, J., Li, H., Ottosen, L.D.M., Lundqvist, J., Vergeynst, L. (2023). Comparison of the photocatalytic degradability of PFOA, PFOS and GenX using Fe-zeolite in water. Chemosphere, 344, 140344. https://doi.org/10.1016/j.chemosphere.2023.140344

Widhalm, S., Müller, T., Schmitt, C., Fischer, B. (2024). PFDA induces mitochondrial dysfunction and oxidative stress in aquatic organisms. Aquatic Toxicology, 250, 106123. https://doi.org/10.1016/j.aquatox.2023.106123

Witeska, M. (2013). Erythrocytes in teleost fishes: A review. Zoology and Ecology, 23(4), 275–281. https://doi.org/10.1080/21658005.2013.846963

Witko-Sarsat, V., Friedlander, M., Capeillère-Blandin, C., Nguyen-Khoa, T., Nguyen, A. T., Zingraff, J., Jungers, P., Descamps-Latscha, B. (1996). Advanced oxidation protein products as a novel marker of oxidative stress in uremia. Kidney International, 49(5), 1304–1313. https://doi.org/10.1038/ki.1996.186

Witko-Sarsat, V., Friedlander, M., Khoa, T.N., Capeillère-Blandin, C., Nguyen, A.T., Canteloup, S., Dayer, J.-M., Jungers, P., Drüeke, T., Descamps-Latscha, B. (1998). Advanced Oxidation Protein Products as Novel Mediators of Inflammation and Monocyte Activation in Chronic Renal Failure. Journal of Immunology, 161(5), 2524–2532. https://doi.org/10.4049/jimmunol.161.5.2524

Wolf, J. C., Wolfe, M. J. (2005). A Brief Overview of Nonneoplastic Hepatic Toxicity in Fish. Toxicologic Pathology, 33(1), 75–85. https://doi.org/10.1080/01926230590890187

Woo, S., Denis, V., Won, H., Shin, K., Lee, G., Lee, T.-K., Yum, S. (2013). Expressions of oxidative stress-related genes and antioxidant enzyme activities in *Mytilus galloprovincialis* (Bivalvia, Mollusca) exposed to hypoxia. Zoological Studies, 52, 15. https://doi.org/10.1186/1810-522X-52-15

World Health Organization Regional Office for Europe (2017). Keeping our water clean: the case of water contamination in the Veneto region, Italy. Copenhagen: WHO Europe.

Wu, Y., Deng, M., Jin, Y., Mu, X., He, X., Luu, N.-T., Yang, C., Tu, W. (2019). Uptake and elimination of emerging polyfluoroalkyl substance F-53B in zebrafish larvae: Response of oxidative stress biomarkers. Chemosphere, 215, 182–188. https://doi.org/10.1016/j.chemosphere.2018.10.025

Xiao, F. (2017). Emerging poly- and perfluoroalkyl substances in the aquatic environment: A review of current literature. Water Research, 124, 482–495. https://doi.org/10.1016/j.watres.2017.07.024

Yamada, S., Guo, X. (2018). Peroxiredoxin 4 (PRDX4): Its critical in vivo roles in animal models of metabolic syndrome ranging from atherosclerosis to nonalcoholic fatty liver disease. Pathology International, 68(2), 91–101. https://doi.org/10.1111/pin.12634

Yao, J., Sheng, N., Guo, Y., Yeung, L.W.Y., Dai, J., Pan, Y. (2022). Nontargeted Identification and Temporal Trends of Per- and Polyfluoroalkyl Substances in a Fluorochemical Industrial Zone and Adjacent Taihu Lake. Environmental Science & Technology, 56, 7986–7996. https://doi.org/10.1021/acs.est.2c00891

Yi, S., Chen, P., Yang, L., Zhu, L. (2019). Probing the hepatotoxicity mechanisms of novel chlorinated polyfluoroalkyl sulfonates to zebrafish larvae: Implication of structural specificity. Environment International, 133, 105262. https://doi.org/10.1016/j.envint.2019.105262

Yoo, H., Guruge, K. S., Yamanaka, N., Sato, C., Mikami, O., Miyazaki, S., Yamashita, N., Giesy, J. P. (2009). Depuration kinetics and tissue disposition of PFOA and PFOS in white leghorn chickens (*Gallus gallus*) administered by subcutaneous implantation. Ecotoxicology and Environmental Safety, 72(1), 26–36. https://doi.org/10.1016/j.ecoenv.2007.09.007

Yoo, H.J., Pyo, M.C., Park, Y., Kim, B.Y., Lee, K.-W. (2021). Hexafluoropropylene oxide dimer acid (GenX) exposure induces apoptosis in HepG2 cells. Heliyon, 7, e08272. https://doi.org/10.1016/j.heliyon.2021.e08272

Zenteno-Savín, T., Saldierna, R., Ahuejote-Sandoval, M. (2006). Superoxide radical production in response to environmental hypoxia in cultured shrimp. Comparative Biochemistry and Physiology Part C: Toxicology and Pharmacology, 142, 301–308. https://doi.org/10.1016/j.cbpc.2005.11.001

Zhang, L., Song, Z., Zhou, Y., Zhong, S., Yu, Y., Liu, T., Gao, X., Li, L., Kong, C., Wang, X., He, L., Gan, J. (2023). The Accumulation of Toxic Elements (Pb, Hg, Cd, As, and Cu) in Red Swamp Crayfish (Procambarus clarkii) in Qianjiang and the Associated Risks to Human Health. Toxics, 11, 635. https://doi.org/10.3390/toxics11070635

Zhang, L., Tao, N.-P., Wu, X., Wang, X. (2022). Metabolomics of the hepatopancreas in Chinese mitten crabs (Eriocheir sinensis). Food Research International, 152, 110914. https://doi.org/10.1016/j.foodres.2021.110914

Zhang, Y., Li, Z., Kholodkevich, S., Sharov, A., Feng, Y., Ren, N., Sun, K. (2019). Cadmium-induced oxidative stress, histopathology, and transcriptome changes in the hepatopancreas of freshwater crayfish (*Procambarus clarkii*). Science of the Total Environment, 666, 944–955. https://doi.org/10.1016/j.scitotenv.2019.02.159

Zhao, D., Zhang, X., Li, X., Ru, S., Wang, Y., Yin, J., Liu, D. (2019). Oxidative damage induced by copper in testis of the red swamp crayfish Procambarus clarkii and its underlying mechanisms. Aquatic Toxicology, 207, 120–131. https://doi.org/10.1016/j.aquatox.2018.12.006

Zhao, L., Teng, M., Zhao, X., Li, Y., Sun, J., Zhao, W., Ruan, Y., Leung, K. M. Y., Wu, F. (2023). Insight into the binding model of per- and polyfluoroalkyl substances to proteins and membranes. Environment International, 175, 107951. https://doi.org/10.1016/j.envint.2023.107951

Zheng, G., Eick, S. M., Salamova, A. (2023). Elevated Levels of Ultrashort- and Short-Chain Perfluoroalkyl Acids in US Homes and People. Environmental Science Technology, 57(42), 15782–15793. https://doi.org/10.1021/acs.est.2c06715

Zhong, Y., Shen, L., Ye, X., Zhou, D., He, Y., Zhang, H. (2020). Mechanism of immunosuppression in zebrafish (*Danio rerio*) spleen induced by environmentally relevant concentrations of perfluorooctanoic acid. Chemosphere, 249, 126200. https://doi.org/10.1016/j.chemosphere.2020.126200

Zieman, J. C. (1974). Methods for the study of growth and production of tropical seagrasses. Aquaculture, *4*(2), 139–143.

Zimmermann, R., Eyrisch, S., Ahmad, M., Helms, V. (2011). Protein translocation across the ER membrane. Biochimica et Biophysica Acta (BBA) - Biomembranes, 1808(3), 912–924. https://doi.org/10.1016/j.bbamem.2010.06.015